WIRELESS POWER TRANSFER FOR E-MOBILITY

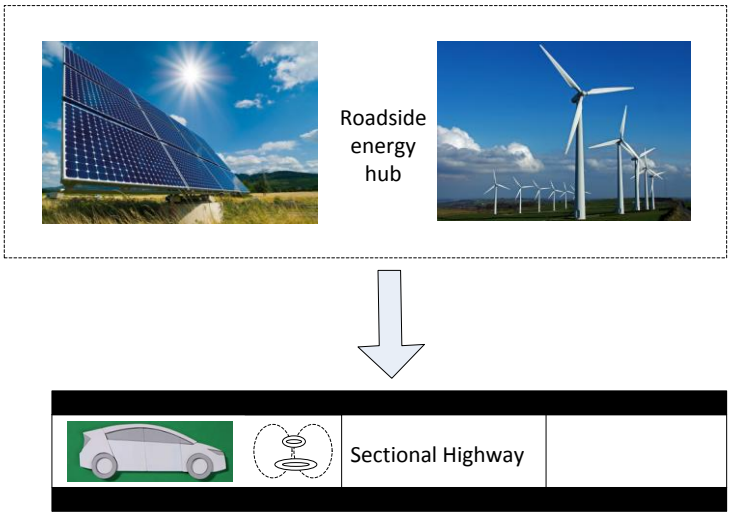

Master of Science Thesis
Venugopal Prasanth
July 2012

DELFT UNIVERSITY OF TECHNOLOGY
FACULTY OF ELECTRICAL ENGINEERING, MATHEMATICS AND COMPUTER SCIENCE
ELECTRICAL POWER PROCESSING

TU Delft

Wireless Power Transfer for E-mobility

July 31, 2011
Delft

Author

Venugopal Prasanth
4119487

Thesis Committee

prof. dr. eng. J.A. Ferreira
prof.dr.ir. P. Bauer
prof.dr. M. Popov

Abstract

Wireless Power Transfer (WPT) is the process of transferring power from one circuit onto another without passing through any manmade conductive elements interconnecting them. Several schemes for wireless power transfer exists – Inductive, Capacitive, Laser, Microwave etc. Of these, Inductive Power Transfer (IPT) is the most popular and is being extensively studied particularly from the last two decades.

The working of an IPT system is comparable to that of an air core transformer with the leakage compensated by means of capacitances. Compensation has been applied to both the primary and secondary of the transformer. This would help boost power transfer as well as make upf operation possible. Literature describes four basic topologies – Series-Series, Series-Parallel, Parallel-Series and Parallel-Parallel depending on the mode of connection of the capacitor to the transformer.

The first part of this thesis is dedicated to an extensive theoretical study of the basic compensation topologies so as to understand their operation and hence aid the design of a generic IPT system depending on the criteria to be optimized. The idea of resonance so developed can also be used to characterize any complex resonant circuit from an engineering approach.

This understanding later evolved into a search for understanding the physics of magnetic fields, inductances etc. The state-of-art for IPT in E-mobility is the powering while driving scenario or dynamic charging. The second part of this thesis is dedicated to enhancing the understanding of the fundamentals of dynamic charging. This scheme is characterized by a major limitation apart from its inherent poor coupling, that being -"Misalignment". Misalignment hampers effective power transfer as the mutual inductance would fall badly as a result of the same.

To tackle the issue of misalignment, modifications can be made to both the secondary as well as the primary of the IPT. Modifications to the secondary in the form of introducing a new set of inductors referred to as "Quadrature Coils" has been studied. Also, a novel primary that could yield potentially higher power transfer, referred to as "Double Lane Model" has been proposed.

Acknowledgements

Academic research on “Wireless Power Transfer for E-mobility” has been carried out at the Delft University of Technology, The Netherlands, in Electrical Power Processing (EPP) group of the Department of Electrical Sustainable Energy. This thesis could not have taken shape without the help and support of many people. I would like to take this opportunity to express my gratitude to all of them.

Firstly, I wish to express my sincere thanks to my supervisor Prof. Pavol Bauer. His faith in my academic abilities and also support during this tough period has to be highlighted. Also, Prof. Ferreira always has been a great motivation for performing research in this field.

I would also like to sincerely acknowledge Swagat Chopra, whose work is a precursor to my work. His tips, suggestion and support formed the initiation of my journey into research life.

I would then like to thank Jayakrishnan Harikumaran (JK ettan) who has been a great colleague and for all his advice both academic and non-academic. Then, George Vereczki (acchaya) with whom I lunched and partied several times. Ellidora Stamati and Vangleis Lanaras (my first student) took pains to read my thesis, my paper and discuss Inductive Power Transfer with me; I wish to acknowledge them for that. Others in my student room including Yating, Ivan etc. are people who have influenced me in many ways. Ilija Peclij took time off to correct my initial PCB designs and Xun Gong helped me use various lab equipments. All PhDs at EPP taught me some lesson in life worth keeping.

I would also like to thank Anoop Jassal, Martin van der geest and Dong Liu for their several discussions and tips particularly in FEM analysis. The lab staff at Delft – Rob Schoevaars and Kasper Zwetsloot is the people without whom many of my experimentation would not have made it to day light. My batch mates – Ananth, Swami, Prasanna, Venkat, Kalyan and Vidya Raju. Also friends, particularly Rijo from my bachelor’s were the greatest moral support I could have asked for particularly in difficult times.

Last but not the least, my family-father, mother and brother who are my inner strength and whom I represent in all walks of my life.

List of abbreviations

1. UPF – Unity Power Factor
2. IPT – Inductive Power Transfer
3. CPT – Capacitive Power Transfer
4. MPT – Microwave Power Transfer
5. LPT – Laser Power Transfer
6. SPS – Space Solar Power Satellites
7. EV – Electric Vehicle
8. OLEV – On-line Electric Vehicle
9. VLF – Very Low Frequency
10. SS – Primary Series, Secondary Series Compensation
11. SP – Primary Series, Secondary Parallel Compensation
12. PS – Primary Parallel, Secondary Series Compensation
13. PP – Primary Parallel, Secondary Parallel Compensation
14. DPF – Displacement Power Factor
15. RPEV – Roadway Powered Electric Vehicle
16. FEM – Finite Element Method
17. EMC – Electromagnetic compatibility
18. THD – Total Harmonic Distortion
19. SiC – Silicon Carbide
20. GaN – Gallium Nitride

List of symbols

1. R_1 – *Primary resistance*
2. L_1– *Primary inductance*
3. R_2 – *Secondary resistance*
4. L_2– *Secondary inductance*
5. C_1– *Primary capacitance*
6. C_2– *Secondary capacitance*
7. R_L– *Load resistance*
8. E_a– *Induced EMF in the primary*
9. E_b– *Induced EMF in the secondary*
10. L_a– *Primary series inductance*
11. L_b– *Secondary series inductance*
12. L_{bh}– *Secondary inductance of the horizontal coil*
13. L_{bv}– *Secondary inductance of the vertical coil*
14. I_p– *Primary current*
15. I_s– *Secondary current*
16. *M– Mutual inductance*
17. k_c– *Current division ratio*
18. *k– Coupling coefficient*
19. *f– Frequency*
20. V_1– *Primary voltage*
21. *w- Angular frequency*
22. w_0– *Resonant angular frequency*
23. *X– Reactance*
24. *Z– Impedance*
25. *P – Power Transferred*
26. *η- Efficiency*
27. l_{mag}*-Magnetic length of the core*
28. l_{core}*-Magnetic core length*
29. Q_2– *Quality factor of the secondary*
30. K_{core}– *Core utilization factor*

List of figures

Figure 1-1 An IPT system for powering an EV 13
Figure 1-2 Electrostatic CPT system 14
Figure 1-3 MPT mode of wireless power transfer 14
Figure 1-4 WEB based on IPT [5] 15
Figure 1-5 The three generations of KAIST OLEV (1G-3G, L-R) [6] 15
Figure 2-1 Flux linkage and leakages in an air cored transformer 19
Figure 2-2 Schematic diagram of a single phase IPT Transformer 19
Figure 2-3 Equivalent circuit of a single phase IPT Transformer 20
Figure 2-4 Circuit resistance as defined as Z_p 20
Figure 2-5 Variation of the current division ratio (k_c) as a function of frequency (f) for different loads (R_L) 22
Figure 2-6 Variation of the current division ratio (k_c) as a function of frequency (f) for different mutual inductances (M) 23
Figure 2-7 Basic compensation topologies (SS, PP, SP and PS) 26
Figure 2-8 Experimental setup of the IPT 36
Figure 2-9 Variation of the SS topology parameters with normalized frequency (w/w_0) 36
Figure 2-10 Variation of the PS topology parameters with normalized frequency (w/w_0) 37
Figure 3-1 Efficiency v/s load resistance and frequency for SS and SP topologies 40
Figure 3-2 SS topology parameters v/s normalized frequency (w/w_0) 42
Figure 3-3 SP topology parameters v/s normalized frequency (w/w_0) 44
Figure 3-4 Frequency tolerance for efficiency and power factor in case of series primary compensation 45
Figure 3-5 Efficiency v/s load resistance and frequency for PS and PP topologies 46
Figure 3-6 PS topology parameters v/s normalized frequency (w/w_0) 48
Figure 3-7 PP topology parameters v/s normalized frequency (w/w_0) 49
Figure 3-8 Frequency tolerance for efficiency and power factor for parallel primary compensation 50
Figure 3-9 Tuning SS compensated transformer by varying primary current (I_p) with normalized frequency (w/w_0) 53
Figure 4-1 Common ferrite shapes 55
Figure 4-2 Dimensions of the E-80 core in mm 56
Figure 4-3 Coil configuration for the primary of a single phase IPT system 57
Figure 4-4 Sinusoidally distributed windings of the primary of a poly-phase IPT system 57
Figure 4-5 Constructed inductors for the experimentation (a and b) 59
Figure 4-6 Variation of the inductance of the primary with number of turns 59
Figure 4-7 Variation of the resistance of the primary with number of turns 60
Figure 4-8 The different types of winding for the pickup 60
Figure 4-9 Study of misalignment at various positions 62

Figure 4-10 The variation in mutual inductance of the horizontal coil as a function of lateral misalignment 63
Figure 4-11 Variation of mutual inductance as a function of longitudinal position 64
Figure 4-12 Orientation of the magnetic fields at the various sections of the inductor 65
Figure 4-13 A symmetrical ended inductor 65
Figure 4-14 The symmetrical ended inductor 65
Figure 4-15 The variation in mutual inductance of the coils (1,2,4 loops) as a function of lateral and longitudinal position 67
Figure 4-16 The variation in mutual inductance as a function of lateral position 68
Figure 4-17 The variation in mutual inductance as a function of longitudinal position 68
Figure 4-18 The variation in mutual inductance of the coils (1,2,4 loops) as a function of lateral and longitudinal position 70
Figure 4-19 Interconnection between the windings of the pickup 71
Figure 4-20 Variation of mutual inductance with lateral position 72
Figure 4-21 Variation of mutual inductance with longitudinal position for the quadrature coil 72
Figure 4-22 The variation in mutual inductance of the quadrature coil as a function of both lateral and longitudinal misalignment 74
Figure 4-23 The variation in efficiency as a function of load resistance and resonant frequency for different turns of inductors (1,2,4) 75
Figure 4-24 The variation in efficiency as a function of load resistance and resonant frequency 76
Figure 5-1 The two dimensional geometry of the primary and the core 78
Figure 5-2 Flux lines for the case where coil currents are in the opposite direction 79
Figure 5-3 Flux lines for the case where coil currents are in the same direction 80
Figure 5-4 Arrangement in case of the replaced core 80
Figure 5-5 Bar diagram representation of the two configurations of inductors for E core 81
Figure 5-6 Double lane model of the IPT system 81
Figure 5-7 Mutual inductance variation as a function of lateral position (L-Opposing currents, R-Unidirectional currents) 82
Figure 5-8 Definition of the core length for the Ecore 83

Contents

Abstract ..... **v**

Acknowledgements ..... **vii**

Contents ..... **ix**

1 INTRODUCTION 12

1.1 Wireless Power Transfer Systems 12

1.2 Classification of wireless power transfer systems 12

1.2.1 Electromagnetic induction 13

1.2.2 Electrostatic induction 13

1.2.3 Far field power transfer 14

1.3 Inductive power transfer applied to electric vehicles –Applications 15

1.4 Research goals and objectives 16

2 ANALYSIS OF IPT AND EFFECTS OF COMPENSATION 18

2.1 Introduction 18

2.2 Single phase IPT equivalent circuit 18

2.2.1 Analysis of a single phase IPT transformer 20

2.3 Need for compensation and its design 24

2.3.1 Analysis of compensation strategies 25

2.3.2 Impedances at resonance 28

2.3.3 Impedance characterization of compensation topologies 35

2.4 Conclusions 37

3 OPTIMIZATION OF COMPENSATION STRATEGIES 38

3.1 Introduction 38

3.2 Efficiency based optimization of compensation strategy 38

3.2.1 Primary series compensation and the selection of optimal resonant frequency 39

3.2.2 Primary parallel compensation and selection of optimal frequency 45

3.2.3 Comparison between the various topologies 50

3.2.4 Tuning of a fixed frequency air cored transformer 51

3.3 Conclusions 53

4 POWERING WHILE DRIVING – STUDY OF MISALIGNMENT 54

4.1 Introduction 54

4.2 IPT for powering while driving 54
4.3 Ferrites and their application in IPT 55
4.4 Choice of the core and the pickup 56
4.5 Track configuration and design of primary 56
4.5.1 Track configuration 56
4.5.2 Design of the tracks 57
4.5.3 Design of the pickup 60
4.6 Study of misalignment and its effect on the power transfer 61
4.6.1 Pickup with horizontal coil and study of lateral misalignment 63
4.6.2 Pickup with horizontal coil and study of longitudinal misalignment 64
4.6.3 Pickup with horizontal coil and combining both horizontal and vertical misalignment 66
4.6.4 Pick up with vertical coil and study of lateral misalignment 67
4.6.5 Pickup with vertical coil and study of longitudinal misalignment 68
4.6.6 Pickup with vertical coil and combining both lateral and longitudinal misalignment 69
4.6.7 Pickup with quadrature coil and study of lateral misalignment 70
4.6.8 Pickup with quadrature coil and study of longitudinal misalignment 72
4.7 Efficiency based optimization of the primary 74
4.7.1 Choice of the primary for efficient power transfer 76
4.8 Conclusion 77
5 MAGNETIC DESIGN OF THE PRIMARY 78
5.1 Introduction 78
5.2 Magnetic design of the IPT system 78
5.3 Two dimensional FEM analysis 79
5.3.1 Replacing the E core with flat core for unidirectional currents 80
5.4 Simulation results from FEM Analysis 80
5.5 Experimental analysis of the inductor with unidirectional currents 81
5.6 Comparison of lateral misalignment 82
5.6.1 Comparison of the two inductor configuration based on core utilization 82
5.7 Conclusion 83
6 CONCLUSIONS AND RECOMMENDATIONS 84
6.1 Conclusions 84

6.2 Recommendations and scope for future work 85
References **87**
Appendix A – Paper I **90**

CHAPTER 1

INTRODUCTION

1.1 Wireless Power Transfer Systems

The history of wireless power transmission dates back to the late 19th century with the prediction that power could be transmitted from one point to another in free space by Maxwell in his "Treatise on Electricity and Magnetism". Heinrich Rudolf Hertz performed experimental validation of Maxwell's equation which was a monumental step in the direction. However, Nikola Tesla's experiments are often considered as being some of the most serious demonstrations of the capability of transferring power wirelessly even with his failed attempts to send power to space [1].

1.2 Classification of wireless power transfer systems

Wireless power transfer systems can be classified into different types depending on various factors. On the basis of the distance from the radiating source, the characteristics of the EM fields change and so are the methods for achieving wireless power transfer. They can be categorized as:

1. Near field
2. Mid field
3. Far field

In case of near field radiation, the boundary between the regions is restricted to one wavelength. In the transition zone, the boundary between the regions is between one to two wavelengths of electromagnetic radiation. In case of far field, the distance between the radiating source and the receiver is more than twice the wavelength of the radiation.

Based on the mode of coupling between the transmitter and the receiver, wireless power transfer techniques can be classified into the following:

1. Electromagnetic induction (Resonant Inductive Power Transfer)
2. Electrostatic induction (Resonant Capacitive Power Transfer)
3. Far field transfer techniques (Laser and Microwave Power Transfer)

1.2.1 Electromagnetic induction

Electromagnetic Inductive Power Transfer (IPT) is a popular technique of transferring power wirelessly over a short range. This technique of transferring power derives its capability from the two fundamental laws of physics: Ampere's law and Faraday's law. The functioning of such IPT systems is based on the changing magnetic field that is created due to alternating currents through a primary that induce a voltage onto a secondary coupled by means of air. In order to improve the efficiency of power transfer, resonant mode coupling of the coils is established by means of capacitive compensation. This technique is one of the most popular for wireless power transfer and has found vast applications including powering consumer devices, biomedical implants, electric mobility, material handling systems, lighting applications and contactless underwater power delivery among many others.

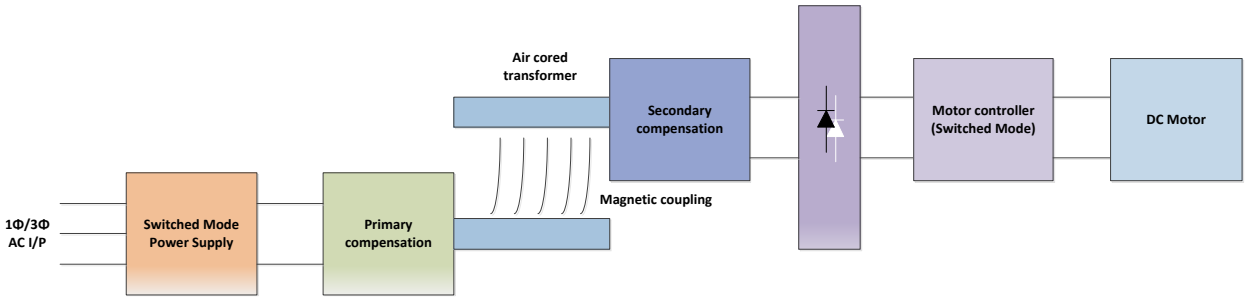

Figure 1-1 An IPT system for powering an EV

1.2.2 Electrostatic induction

Capacitive Power Transfer (CPT) is a novel technique used to transfer power wirelessly between the two electrodes of a capacitor assembly [2]. It is based on the fact that when high frequency ac voltage source is applied to the plates of the capacitor that are placed close to each other, electric fields are formed and displacement current maintains the current continuity. Thus, in this case the energy carrier media is the electric field and hence the dual of IPT. Some of the features that CPT has compared to IPT are [2]:

1. Energy transfer can still continue even on the introduction of a metal barrier as it would result in a structure consisting of two capacitors in series.
2. Most electric fields are confined within the gap between the capacitors and hence EMI radiated and power losses are low.
3. The requirement for bulky and expensive coils doesn't exist and hence, the circuit can be made small.

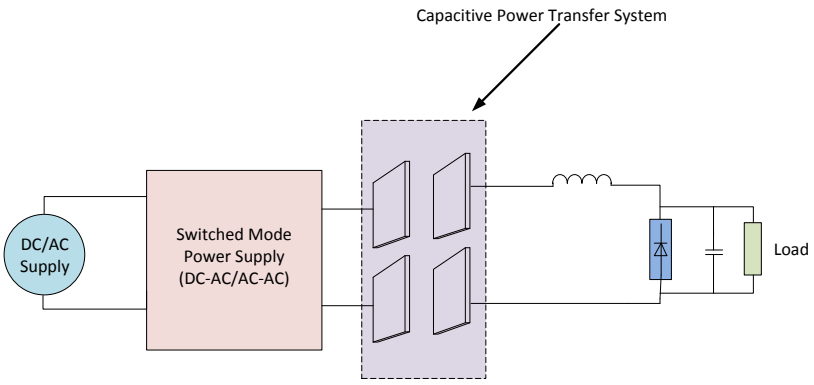

Figure 1-2 Electrostatic CPT system

1.2.3 Far field power transfer

In case of far field power transfer, microwave or laser is used for the transfer of power. In case of Microwave Power Transfer (MPT) systems [3], Space Solar Power Satellites (SPS) are envisaged as an important application and are considered as a travelling energy plant in the Geostationary Earth Orbit (GEO). It consists of three main stages, a collection of PV cells or solar thermal turbine coupled with generator to convert solar energy into electricity. Then, an electrical to microwave conversion stage converts the same into microwaves which are beamed onto the surface of earth by means of gigantic antenna arrays. The receivers on the surface then convert the energy in the form of microwave back to electricity.

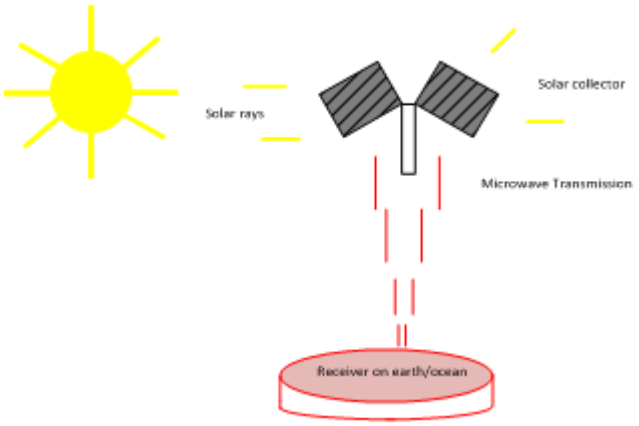

Figure 1-3 MPT mode of wireless power transfer

Laser Power Transfer (LPT) Systems are based on lasers as the energy transport media. Lasers generate phase-coherent electromagnetic radiation by the principle of population inversion and the most commonly used type of lasers are solid state lasers. Direct solar pumping lasers involve the concentration of solar energy before being injected into the laser medium.

1.3 Inductive power transfer applied to electric vehicles – Applications

Inductive power transfer applied to electric vehicles has been proposed over decades with the Partner for Advanced Transit and Highways (PATH) team in California developing a road way powered inductive power transfer EV with the primary and secondary displaced at 7.6 cm's and a power transfer efficiency of 60%. This system was referred to as "Dual Mode Electric Transportation" (DMET) as it considered both batteries as well as powered highways as the energy source of the EV [4]. However, the need to constrain the vehicle movement to ensure adequate power transfer, the low efficiencies of the system and the lack of economic viability were major hurdles that prevented rapid commercialization. Following this, a research group at the University of Auckland, New Zealand also proposed systems for roadway powered magnetically coupled IPT systems. A number of such IPT systems have then been proposed and implemented in electric vehicles notably: Waseda advanced Electric Micro Bus (WEB) of Waseda University, Japan, the three generations of On-Line Electric Vehicle (OLEV) from KAIST University, Korea etc. A comparison of the types of electric vehicles developed is listed in Table 1.

Figure 1-4 WEB based on IPT [5]

Figure 1-5 The three generations of KAIST OLEV (1G-3G, L-R) [6]

Table 1 Specifications of the various IPTs used in Electric Vehicles

Specification of the IPT	WEB	University of Auckland	KAIST 1G OLEV	KAIST 2G OLEV	KAIST 3G OLEV
Power Transferred (kW)	30	2-5 kW	3	6	17
Air gap (cm)	10	10-30	1	17	17
Efficiency (%)	92	85	80	72	71
Weight (kg)	35	variable	10	80	110

1.4 Research goals and objectives

The role that EVs will play in future energy systems has been highlighted particularly with reference to a burning need for a change from fossil fuel based mobility to electric mobility. Several possible strategies for charging EVs including Slow Charging, Fast Charging and Wireless Power Transfer have also been studied in literature.

The main goal of this thesis is to study the effect of resonance in IPT systems and evaluate misalignment in case of powering while driving scenario of IPT. To satisfy these goals, the following objectives are formulated:

- Develop the theory behind IPT and explain the effect of resonance:
  The first part of the work involves the explanation to the working of Inductive Power Transfer systems with a review of design and an extensive theoretical study of the effect of resonance in IPT.
- Explaining the issue of misalignment pertaining to IPT systems:
  The state of art in case of IPT is the powering while driving scenario. The second objective of this thesis is to explain the cause and effect of misalignment in IPT systems. Lab scale models of the distributed inductors were designed, constructed and tested to obtain experimental validation of the issue of misalignment.
- Develop a novel design of inductor so as to counter the issue of misalignment:
  Improvement to the issue of misalignment is achieved traditionally by imposing modifications to the pickup. One such modification is the introduction of quadrature coil. However, in the current work, a novel primary inductor design is looked into.

CHAPTER 2

ANALYSIS OF IPT AND EFFECTS OF COMPENSATION

2.1 Introduction

A Contactless Power Transfer System (IPT) is based on a magnetically coupled transformer that transfers power from a primary winding onto a secondary winding (pick-up) with no physical contact. The principle of operation of such a IPT is based on Faraday's law of electromagnetic induction. This scheme can be compared to that of an air cored transformer that operates at high frequencies (VLF band or more) so as to boost power transfer.

A major problem concerning the IPT system is that of weak coupling caused due to the relatively large leakage unlike the iron cored transformer. This would imply that the efficiency of power transfer would be small and hence, some technique so as to counteract this problem must be evolved. Capacitive compensation of the windings of the IPT is considered so as to nullify this effect by operating the transformer at resonance leading to a boost in efficiency.

In this chapter, the idea of contactless power transfer by means of inductive coupling between the coils of an air cored transformer is evolved. Firstly, analysis of the IPT transformer is undertaken. This is followed by understanding the disadvantages of an air-cored transformer, leading to the idea of compensation of the inductances of the air-core transformer so as to transfer power efficiently. The four basic compensation strategies that are described in literature will be used to understand the idea of resonance and its effect on improving the efficiency of power transfer. Finally, a comparison of the effect of resonance on the efficiency of the air-cored transformer will be considered.

2.2 Single phase IPT equivalent circuit

An IPT transformer is characterized by a primary winding that has a resistance, R_1 and a self-inductance, L_1. Similarly, the secondary coil is characterized by a winding resistance, R_2 and a self-inductance, L_2. When such a primary is excited by a sinusoidal voltage source, V_1 of angular frequency, ω and brought closer to the primary, a part of the primary current is used to set up the mutual flux, $\emptyset_m$ and the rest forms the leakage flux of the primary, $\emptyset_p$. The mutual flux is that part of the flux that links both the primary and secondary and is produced by the combined effect of both the primary current and secondary current. Also, the secondary current is also subjected

to leakage and is represented by the leakage flux of the secondary, $\emptyset_s$. This has been represented diagrammatically in Figure 2-1. Thus, according to the theory of coupled inductors [7], when the primary is excited and the two coils are magnetically coupled, the self-inductance of the primary (L_1) results in a mutual inductance (M) and a series inductance (L_a). Also, the secondary self-inductance results in a series inductance (L_b) and the mutual inductance (M). This can be expressed as:

$$L_1 = L_a + M \tag{1}$$

$$L_2 = L_b + M \tag{2}$$

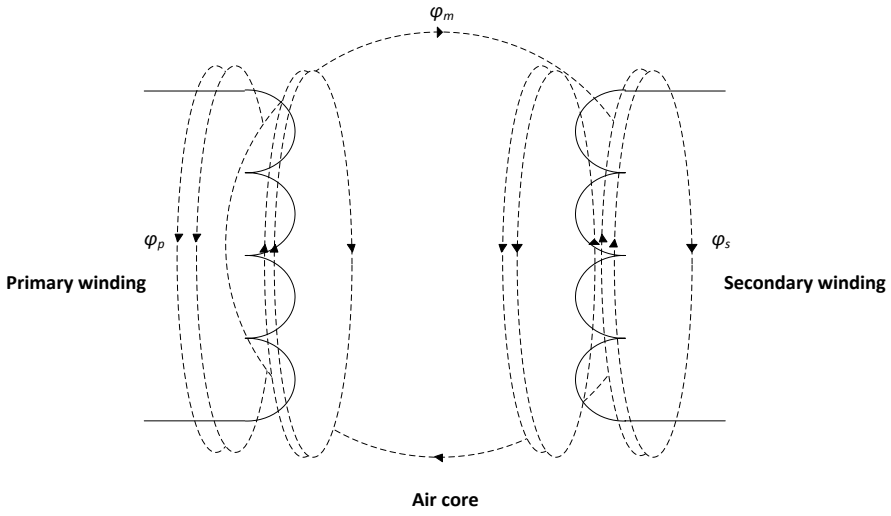

Figure 2-1 Flux linkage and leakages in an air cored transformer

This effect is represented in a schematic diagram for the IPT system which is shown in Figure 2-2 where, I_p and I_s are the primary and secondary currents and the resistance, R_L is the load resistance.

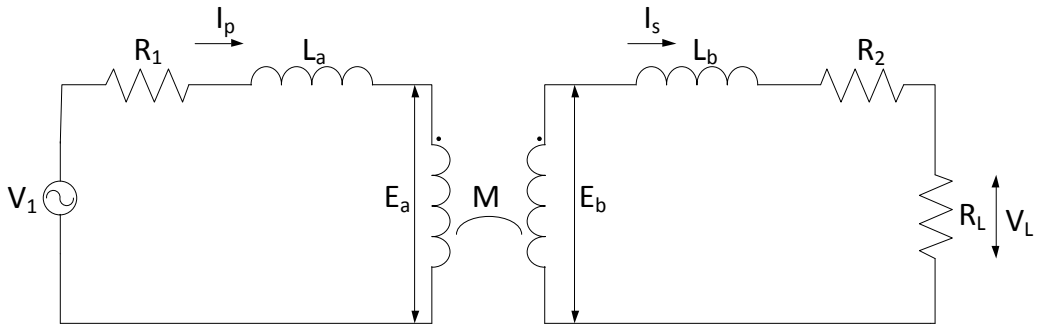

Figure 2-2 Schematic diagram of a single phase IPT Transformer

This schematic can be transformed into an equivalent circuit by making use of the theory of coupled inductors. The resulting equivalent circuit is shown in Figure 2-3.

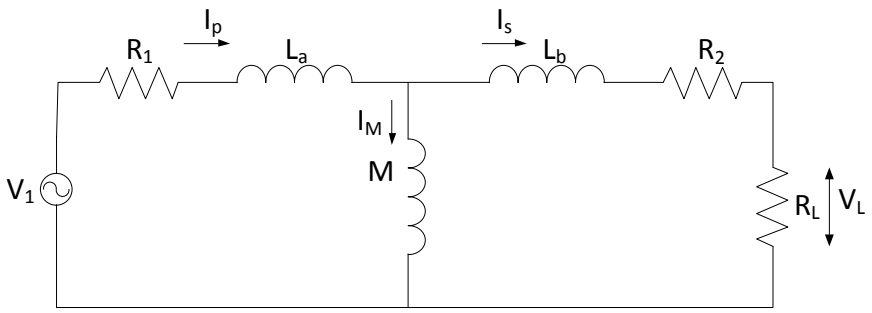

Figure 2-3 Equivalent circuit of a single phase IPT Transformer

It is essential to note that this equivalent circuit needs to be modelled in terms of inductance and not reactance as the air-cored transformer can be operated at any frequency with both fixed frequency control and variable frequency control. This is not the case with 50 Hz or 60 Hz power transformers. Also, the IPT transformer can be modeled by making use of a lumped equivalent circuit provided the length of the primary coil is small compared to the wavelength of the electromagnetic fields associated with the primary source.

2.2.1 Analysis of a single phase IPT transformer

Circuit analysis of the IPT transformer can be used to determine the equivalent impedance of the transformer which can be used to obtain the currents through the various branches. Finally, the current division ratio (k_c) of such a transformer can be obtained and this ratio would give an indirect method of estimating the frequency at which the transformer has to be operated for maximum power to be transferred to the load.

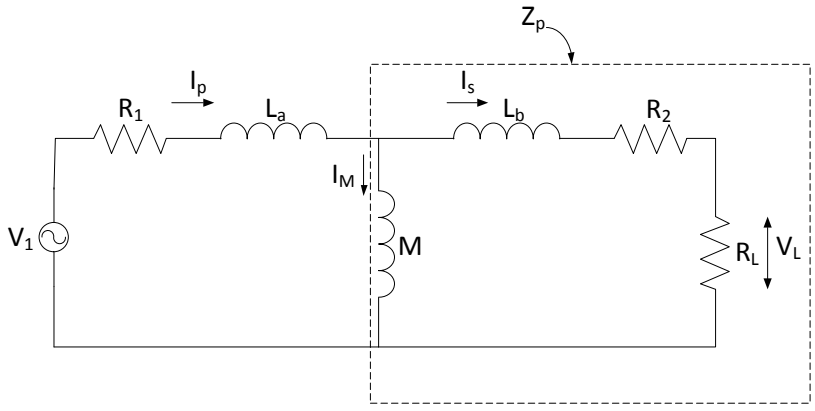

Figure 2-4 Circuit resistance as defined as Z_p

The equivalent resistance of the branch as shown in the dotted box and referred to as Z_p in Figure 2-4 is obtained as follows:

$$Z_p = j\omega M//(j\omega L_b + R_2 + R_L) \tag{3}$$

This on further simplification would yield:

$$Z_p = \left[j\omega M + \left(\frac{\omega^2 M^2}{R_2 + R_L + j\omega(L_b + M)}\right)\right] \tag{4}$$

The equivalent impedance as seen by the source can be expressed as:

$$Z_{eq} = R_1 + j\omega L_a + Z_p \tag{5}$$

Hence,

$$Z_{eq} = \left[R_1 + j\omega(L_a + M) + \left(\frac{\omega^2 M^2}{R_2 + R_L + j\omega(L_b + M)}\right)\right] \tag{6}$$

2.2.1.1 Current division ratio and frequency of operation:

Current division ratio for an air cored transformer would depend not only on the transformer parameters but also on frequency. When the input to the IPT transformer is an ideal voltage source, the primary current can be obtained as:

$$I_p = \left(\frac{V_1}{R_1 + j\omega(L_a + M) + \left(\frac{\omega^2 M^2}{R_2 + R_L + j\omega(L_b + M)}\right)}\right) \tag{7}$$

The secondary current can be related to a primary current as:

$$I_s = I_p \times \left(\frac{j\omega M}{R_2 + R_L + j\omega(L_b + M)}\right) \tag{8}$$

This would further imply that the current division ratio in case of a lossless air-cored transformer would be:

$$k_c = \frac{I_s}{I_p} = \left(\frac{j\omega M}{R_2 + R_L + j\omega(L_b + M)}\right) \tag{9}$$

The above result would imply that the currents in case of an air-cored transformer that is operated at variable frequencies would be related as a function of both the transformer parameters as well as the frequency of operation. Also, the efficiency of operation of the air-cored transformer is given by:

$$\eta = \frac{\mathrm{R_L I_s^2}}{\mathrm{R_L I_s^2 + R_2 I_s^2 + R_1 I_p^2}} \tag{10}$$

A plot between the current division ratio k_c as a function of normalized frequency (w/w_0) for variation in load resistances (R_L) is shown in the Figure 2-5. Also, a plot between the current division ratio k_c as a function of normalized frequency (w/w_0) for variation in mutual inductances (M) is shown in Figure 2-6. In both the plots, the parameters of the air cored transformer are obtained from that in Table 3.

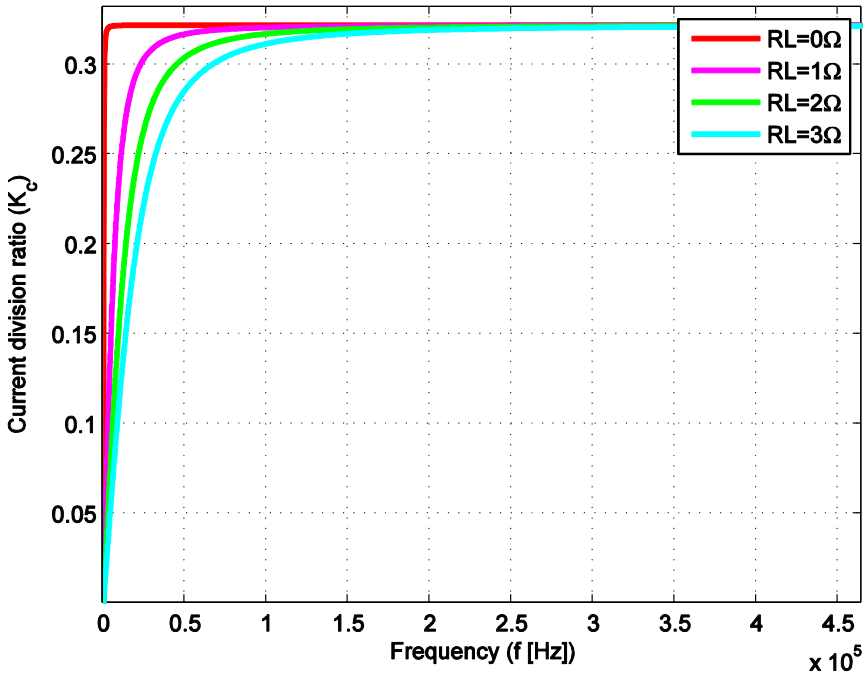

Figure 2-5 Variation of the current division ratio (k_c) as a function of frequency (f) for different loads (R_L)

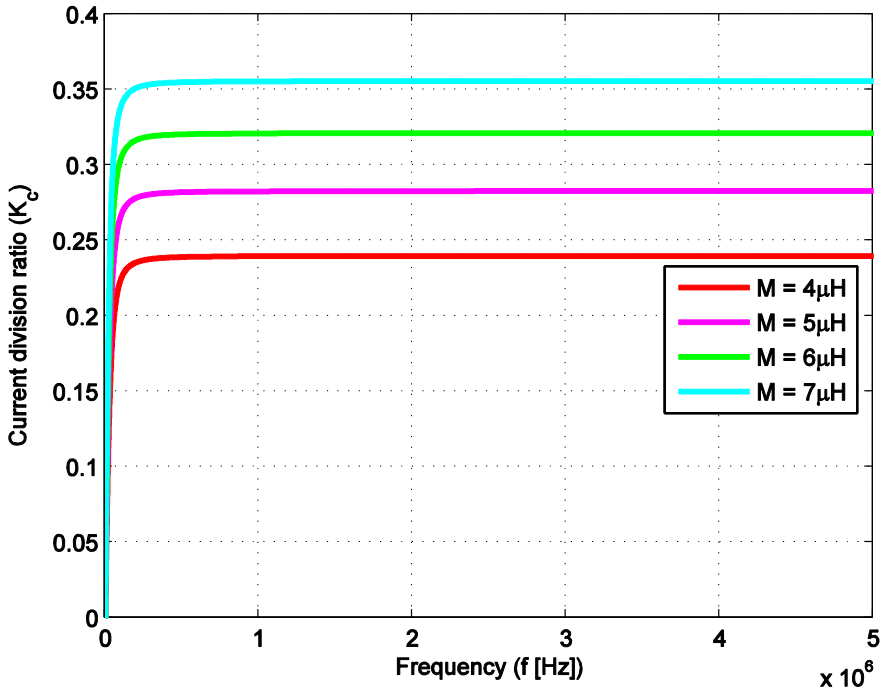

Figure 2-6 Variation of the current division ratio (k_c) as a function of frequency (f) for different mutual inductances (M)

The graphs above indicate that by increasing frequency, the current division ratio keeps increasing up to a certain frequency at which the same begins to saturate. It can be directly observed that the value of K_c so obtained is not equal to unity. This is because of the fact the that the efficiency of an air core transformer is not very high due to the poor coupling (k) and hence the poor mutual inductance (M). Also, the

The value to which the current division ratio saturates can be obtained by considering that:

$$k_c = \left(\frac{j\omega M}{R_2 + R_L + j\omega(L_b + M)}\right) \tag{11}$$

And the condition, If $\omega M >> (R_2 + R_L)$,

$$k_{c(sat)} = \frac{M}{(L_b + M)} \tag{12}$$

This value indicates that for higher frequencies the current division ratio becomes a constant independent of the load and dependent only on the transformer parameters. A typical range of higher frequency for the ratio to be a constant as observed for the constructed air-cored

transformer is in the order of 10's of kHz or more. This would imply that the transformer needs to be operated at frequencies higher than 10 kHz so as to transfer power efficiently.

2.3 Need for compensation and its design

Due to the large leakage inductances associated with both the primary and secondary, an air-cored transformer suffers from poor efficiency. An intelligent method to circumvent this problem is to compensate the reactive currents by using capacitors.

Capacitive compensation has been applied to power systems for reactive power compensation. Both shunt and series compensations are used in power systems, but with different effects. It has been observed that shunt compensation leads to an increase in power transfer capability and a reduction in the reactive voltage drop across the line. In case of series compensation, the maximum power transfer capability of the line is improved due to partial compensation of series inductance and a reduction in load angle resulting in improvement of system stability [8].

This principle of compensation can be utilized in an air-cored transformer and hence, four basic types of compensation strategies can be applied depending upon the capacitor connection to the primary winding and the secondary winding:

1. Series-Series (SS) type
2. Series-Parallel (SP) type
3. Parallel-Series (PS) type
4. Parallel-Parallel (PP) type

However, selection of both the primary and secondary compensation capacitances is based on two different criterions [9, 10]:

1. The secondary capacitance is chosen as the first step. This is done in such a manner so as to compensate the secondary leakage inductance and the mutual inductance. This type of compensation would lead to an improvement in the power transferred to the load.
2. The primary capacitance is then chosen such that it considers the inductance of the entire circuit. In literature, primary capacitances chosen to compensate just the self-inductance of the primary and the inductance of the entire circuit are present. However, it is a better choice to perform compensation for the entire circuit so that the input power factor becomes unity.

Mathematically, the selection of the secondary capacitance can be expressed in terms of the capacitive reactance associated with the capacitor, X_{c2} and the inductive reactance associated with the secondary leakage and the mutual inductance (X_{l2} *and* X_m) as:

$$X_{l2} + X_m = X_{c2} \tag{13}$$

This would further imply that the capacitance of the secondary compensation capacitor (C_2) is related to the resonant angular frequency of the secondary circuit (ω_0) as:

$$C_2 = \frac{1}{\omega_0^2 (L_b + M)} \tag{14}$$

The above relation would remain the same independent of the type of capacitor connection to the secondary. This is followed by the design of the primary circuit compensation capacitance. In this case, since the secondary frequency was fixed as the resonant frequency (ω_0), the primary would also operate at the same frequency as the transformer cannot vary frequency. Further, the imaginary part of the impedance as seen by the entire circuit is made to zero. This would imply that the voltage source in the primary circuit would see only a resistive load and hence results in a unity input power factor.

2.3.1 Analysis of compensation strategies

Mathematical analysis of the various compensation strategies can be performed by applying network equations to the various topologies. Literature is available on the various compensation techniques that consider the system parameters like branch impedances, branch currents, branch voltages, and efficiency among others. However, the selection of a particular compensation topology has been the result of some general understanding of compensation from power systems and some literature on a particular strategy. An optimization technique can be worked out by performing mathematical analysis and considering the parameter to be optimized and its dependence on the various other parameters that can be adapted. Figure 2-7 indicates the various compensation strategies [9, 10]. The analytical expressions that correspond to the various compensation topologies are described in Table 2.

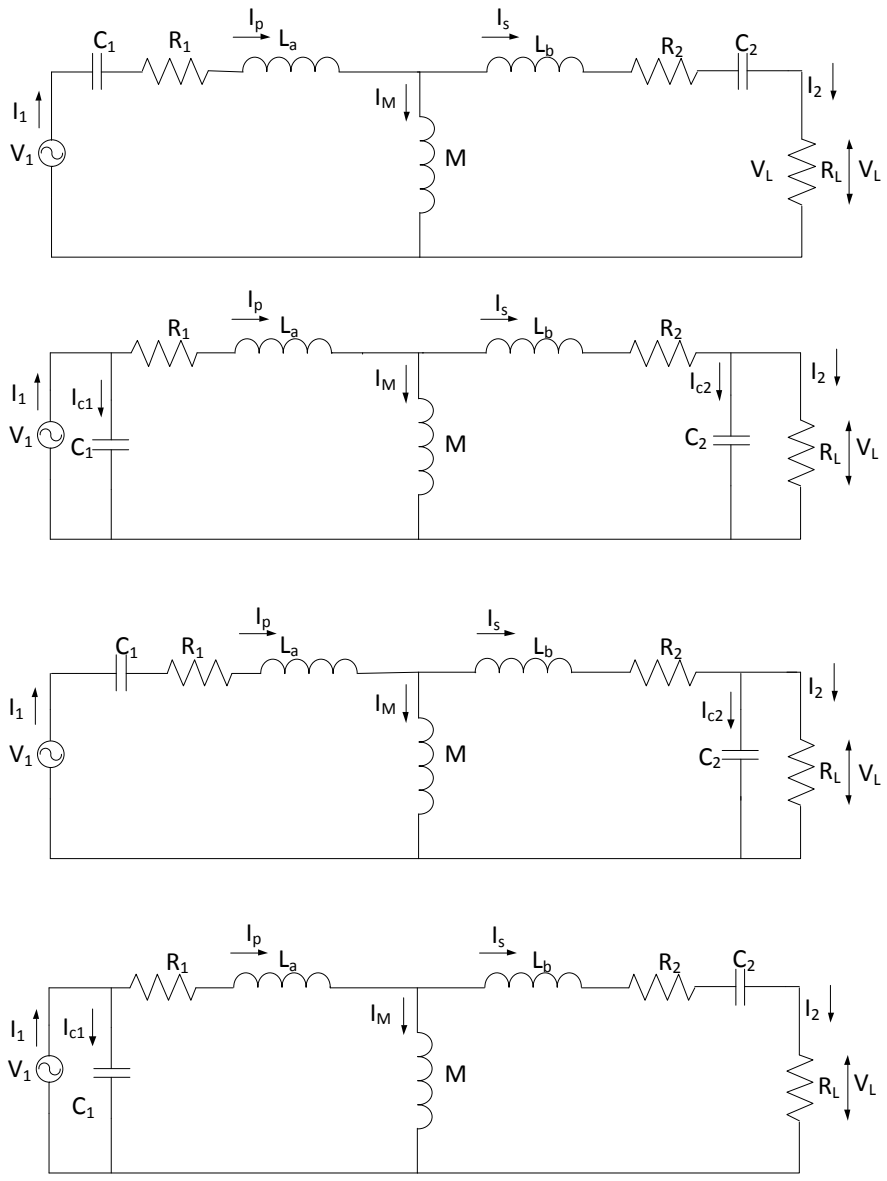

Figure 2-7 Basic compensation topologies (SS, PP, SP and PS)

Table 2. The various compensation topologies and their parameters

Topology	Equivalent circuit impedance (Z_{eq})	Primary compensation capacitance (C_1)
SS type	$Z_{eq(ss)} = \left(\frac{M^2\omega^2}{j\omega(L_b + M) - \frac{j}{\omega C_2} + R_2 + R_L} \right) + j\omega(L_a + M) - \frac{j}{\omega C_1} + R_1$	$C_1 = \frac{1}{\omega_0^2(L_a + M)}$
SP type	$Z_{eq(sp)} = \left(\frac{M^2\omega^2}{j\omega(L_b + M) + R_2 + \frac{R_L}{1 + jR_L C_2\omega}} \right) + j\omega(L_a + M) - \frac{j}{\omega C_1} + R_1$	$C_1 = \frac{1}{\omega_0^2((L_a + M) - (M^2/(L_b + M)))}$
PS type	$Z_{eq(ps)} = \frac{1}{j\omega C_1 + \frac{1}{R_1 + j\omega L_a + \frac{1}{\frac{1}{j\omega M} + \frac{1}{R_2 + R_L + j\left(\omega L_b - \frac{1}{\omega C_2}\right)}}}}$	$C_1 = \frac{(L_a + M)}{\left(\frac{{\omega_0}^2 M^2}{R_L}\right)^2 + \omega_o^2(L_a + M)^2}$
PP type	$Z_{eq(pp)} = \frac{1}{j\omega C_1 + \frac{1}{R_1 + j\omega L_a + \frac{1}{\frac{1}{j\omega M} + \frac{1}{j\omega L_b + R_2 + \frac{1}{j\omega C_2 + \frac{1}{R_L}}}}}}$	$C_1 = \frac{(L_a + M) - (M^2/(L_b + M))}{\left(\frac{M^2 R_L}{(L_b + M)^2}\right)^2 + \omega_0^2\left((L_a + M) - \frac{M^2}{(L_b + M)}\right)^2}$

2.3.2 Impedances at resonance

Operation of a resonant circuit is determined by the impedance the circuit offers at the resonant frequency. This impedance can have different characteristic depending on the type of compensation that has been applied to the circuit. The value of this impedance can be obtained by equating the imaginary part of the complex impedance function of the various topologies to zero at the resonant frequency.

At ($\omega = \omega_0$),

$$Z_{eq(topology,\ \omega=\omega_0)} = Re\left(Z_{eq(topology)}\right) \tag{15}$$

2.3.2.1 SS Topology:

From Table 2, the equivalent impedance of SS topology can be written as:

$$Z_{eq(ss)} = \left(\frac{M^2\omega^2}{j\omega(L_b + M) - \frac{j}{\omega C_2} + R_2 + R_L}\right) + j\omega(L_a + M) - \frac{j}{\omega C_1} + R_1 \tag{16}$$

At ($\omega = \omega_0$),

$$Z_{eq(ss,\ \omega=\omega_0)} = Re\left(Z_{eq(ss)}\right) = \left(\frac{M^2\omega^2}{R_2 + R_L}\right) + R_1 \tag{17}$$

2.3.2.2 SP Topology:

From Table 2, the equivalent impedance of SP topology can be written as:

$$Z_{eq(sp)} = \left(\frac{M^2\omega^2}{j\omega(L_b + M) + R_2 + \frac{R_L}{1 + jR_L C_2\omega}}\right) + j\omega(L_a + M) - \frac{j}{\omega C_1} + R_1 \tag{18}$$

$$Z_{eq(sp)} = \left(\frac{M^2\omega^2}{j\omega(L_b + M) + R_2 + \frac{R_L(1 - jR_L C_2\omega)}{1 + (R_L C_2\omega)^2}}\right) + j\omega(L_a + M) - \frac{j}{\omega C_1} + R_1 \tag{19}$$

Upon further simplification,

$$= \left(\frac{M^2\omega^2}{\left(R_2 + \frac{R_L}{1+(R_L C_2\omega)^2}\right) + j\left(\omega(L_b+M) - \frac{(R_L^2 C_2\omega)}{1+(R_L C_2\omega)^2}\right)} \right) + j\omega(L_a+M) - \frac{j}{\omega C_1} + R_1 \tag{20}$$

$$= \left(\frac{M^2\omega^2\left(R_2 + \frac{R_L}{1+(R_L C_2\omega)^2}\right) - j\left(\omega(L_b+M) - \frac{(R_L^2 C_2\omega)}{1+(R_L C_2\omega)^2}\right)}{\left(R_2 + \frac{R_L}{1+(R_L C_2\omega)^2}\right)^2 + \left(\omega(L_b+M) - \frac{(R_L^2 C_2\omega)}{1+(R_L C_2\omega)^2}\right)^2} \right) + j\omega(L_a+M) - \frac{j}{\omega C_1} + R_1 \tag{21}$$

At ($\omega = \omega_0$),

$$Z_{eq(sp,\ \omega=\omega_0)} = Re\left(Z_{eq(sp)}\right)$$

$$= \left(\frac{M^2\omega^2\left(R_2 + \frac{R_L}{1+(R_L C_2\omega)^2}\right)}{\left(R_2 + \frac{R_L}{1+(R_L C_2\omega)^2}\right)^2 + \left(\omega(L_b+M) - \frac{(R_L^2 C_2\omega)}{1+(R_L C_2\omega)^2}\right)^2} \right) + R_1 \tag{22}$$

2.3.2.3 PS Topology:

From Table 2, the equivalent impedance of PS topology can be written as:

$$Z_{eq(ps)} = \frac{1}{j\omega C_1 + \dfrac{1}{R_1 + j\omega L_a + \dfrac{1}{\dfrac{1}{j\omega M} + \dfrac{1}{R_2 + R_L + j\left(\omega L_b - \dfrac{1}{\omega C_2}\right)}}}} \tag{23}$$

Expanding a part of the main function,

$$\frac{1}{\frac{1}{j\omega M}+\frac{R_2+R_L-j\left(\omega L_b-\frac{1}{\omega C_2}\right)}{(R_2+R_L)^2+\left(\omega L_b-\frac{1}{\omega C_2}\right)^2}}$$

$$=\frac{\frac{(R_2+R_L)}{(R_2+R_L)^2+\left(\omega L_b-\frac{1}{\omega C_2}\right)^2}+j\left(\frac{1}{\omega M}+\frac{\left(\omega L_b-\frac{1}{\omega C_2}\right)}{(R_2+R_L)^2+\left(\omega L_b-\frac{1}{\omega C_2}\right)^2}\right)}{\left(\frac{(R_2+R_L)}{(R_2+R_L)^2+\left(\omega L_b-\frac{1}{\omega C_2}\right)^2}\right)^2+\left(\frac{1}{\omega M}+\frac{\left(\omega L_b-\frac{1}{\omega C_2}\right)}{(R_2+R_L)^2+\left(\omega L_b-\frac{1}{\omega C_2}\right)^2}\right)^2} \quad (24)$$

For simplicity define the constant,

$$k_1=\left[\left(\frac{R_2+R_L}{(R_2+R_L)^2+\left(\omega L_b-\frac{1}{\omega C_2}\right)^2}\right)^2+\left(\frac{1}{\omega M}+\frac{\left(\omega L_b-\frac{1}{\omega C_2}\right)}{(R_2+R_L)^2+\left(\omega L_b-\frac{1}{\omega C_2}\right)^2}\right)^2\right] \quad (25)$$

Now, consider the following terms,

$$\frac{1}{R_1+j\omega L_a+\frac{1}{\frac{1}{j\omega M}+\frac{R_2+R_L-j\left(\omega L_b-\frac{1}{\omega C_2}\right)}{(R_2+R_L)^2+\left(\omega L_b-\frac{1}{\omega C_2}\right)^2}}}$$

$$=\frac{\left(R_1+\frac{\left(\frac{R_2+R_L}{(R_2+R_L)^2+\left(\omega L_b-\frac{1}{\omega C_2}\right)^2}\right)}{k_1}\right)-j\left(\omega L_a+\frac{\frac{1}{\omega M}+\frac{\left(\omega L_b-\frac{1}{\omega C_2}\right)}{(R_2+R_L)^2+\left(\omega L_b-\frac{1}{\omega C_2}\right)^2}}{k_1}\right)}{\left[\left(R_1+\frac{\left(\frac{R_2+R_L}{(R_2+R_L)^2+\left(\omega L_b-\frac{1}{\omega C_2}\right)^2}\right)}{k_1}\right)^2+\left(\omega L_a+\frac{\frac{1}{\omega M}+\frac{\left(\omega L_b-\frac{1}{\omega C_2}\right)}{(R_2+R_L)^2+\left(\omega L_b-\frac{1}{\omega C_2}\right)^2}}{k_1}\right)^2\right]} \quad (26)$$

Again, define the constant,

$$k_2 = \left(R_1 + \frac{\left(\frac{R_2 + R_L}{(R_2 + R_L)^2 + \left(\omega L_b - \frac{1}{\omega C_2}\right)^2} \right)}{k_1} \right)^2 + \left(\omega L_a + \frac{\frac{1}{\omega M} + \frac{\left(\omega L_b - \frac{1}{\omega C_2}\right)}{(R_2 + R_L)^2 + \left(\omega L_b - \frac{1}{\omega C_2}\right)^2}}{k_1} \right)^2 \quad (27A)$$

Finally, it can be obtained that

$$Z_{eq(ps,\ \omega=\omega_0\ )} = Re\left(\frac{1}{j\omega C_1 + \frac{1}{R_1 + j\omega L_a + \frac{1}{\frac{1}{j\omega M} + \frac{R_2 + R_L - j\left(\omega L_b - \frac{1}{\omega C_2}\right)}{(R_2 + R_L)^2 + \left(\omega L_b - \frac{1}{\omega C_2}\right)^2}}}} \right) \quad (27\ B)$$

$$= \frac{k_2\left(R_1 + \frac{R_2 + R_L}{k_1\left((R_2 + R_L)^2 + \left(\omega L_b - \frac{1}{\omega C_2}\right)^2\right)} \right)}{\left(R_1 + \frac{R_2 + R_L}{k_1\left((R_2 + R_L)^2 + \left(\omega L_b - \frac{1}{\omega C_2}\right)^2\right)} \right)^2 + \left(\omega L_a - \omega C_1 + \frac{\left(\omega L_b - \frac{1}{\omega C_2}\right)}{(R_2 + R_L)^2 + \left(\omega L_b - \frac{1}{\omega C_2}\right)^2} \right)^2}$$

2.3.2.4 PP Topology:

From Table 2, the equivalent impedance of PP topology can be written as:

$$Z_{eq(pp)} = \frac{1}{j\omega C_1 + \dfrac{1}{R_1 + j\omega L_a + \dfrac{1}{\dfrac{1}{j\omega M} + \dfrac{1}{j\omega L_b + R_2 + \dfrac{1}{j\omega C_2 + \dfrac{1}{R_L}}}}}}} \tag{27}$$

Now, consider the following terms,

$$\frac{1}{j\omega M} + \frac{1}{j\omega L_b + R_2 + \dfrac{1}{j\omega C_2 + \dfrac{1}{R_L}}} \tag{28}$$

On expanding these terms,

$$\begin{aligned} &\frac{R_2 + \dfrac{\dfrac{1}{R_L}}{\left(\left(\frac{1}{R_L}\right)^2 + (\omega C_2)^2\right)}}{\left(R_2 + \dfrac{\dfrac{1}{R_L}}{\left(\left(\frac{1}{R_L}\right)^2 + (\omega C_2)^2\right)}\right)^2 + \left(\dfrac{\left(\omega L_b - \frac{1}{\omega C_2}\right)}{(R_2 + R_L)^2 + \left(\omega L_b - \frac{1}{\omega C_2}\right)^2}\right)^2} \\ &- j\left(\frac{\left(\omega L_b - \dfrac{\omega C_2}{\left(\frac{1}{R_L}\right)^2 + (\omega C_2)^2}\right)}{\left(R_2 + \dfrac{\dfrac{1}{R_L}}{\left(\left(\frac{1}{R_L}\right)^2 + (\omega C_2)^2\right)}\right)^2 + \left(\dfrac{\left(\omega L_b - \frac{1}{\omega C_2}\right)}{(R_2 + R_L)^2 + \left(\omega L_b - \frac{1}{\omega C_2}\right)^2}\right)^2} + \frac{1}{\omega M}\right) \end{aligned} \tag{29}$$

Define the constant,

$$k_1 = \left(R_2 + \frac{\dfrac{1}{R_L}}{\left(\left(\frac{1}{R_L}\right)^2 + (\omega C_2)^2\right)}\right)^2 + \left(\frac{\left(\omega L_b - \frac{1}{\omega C_2}\right)}{(R_2 + R_L)^2 + \left(\omega L_b - \frac{1}{\omega C_2}\right)^2}\right)^2 \tag{30}$$

Now, consider the following terms

$$\frac{1}{\dfrac{1}{j\omega M} + \dfrac{1}{j\omega L_b + R_2 + \dfrac{1}{j\omega C_2 + \dfrac{1}{R_L}}}} \tag{31}$$

On expanding it can be obtained that

$$\frac{\left(R_2+\frac{\frac{1}{R_L}}{\frac{\left(\left(\frac{1}{R_L}\right)^2+(\omega C_2)^2\right)}{k_1}}\right)+j\left(\frac{\left(\omega L_b-\frac{\omega C_2}{\left(\frac{1}{R_L}\right)^2+(\omega C_2)^2}\right)}{k_1}+\frac{1}{\omega M}\right)}{\left(R_2+\frac{\frac{1}{R_L}}{\frac{\left(\left(\frac{1}{R_L}\right)^2+(\omega C_2)^2\right)}{k_1}}\right)^2+\left(\frac{\left(\omega L_b-\frac{\omega C_2}{\left(\frac{1}{R_L}\right)^2+(\omega C_2)^2}\right)}{k_1}+\frac{1}{\omega M}\right)^2} \tag{32}$$

Once again define the constant,

$$k_2=\left(R_2+\frac{\frac{1}{R_L}}{\frac{\left(\left(\frac{1}{R_L}\right)^2+(\omega C_2)^2\right)}{k_1}}\right)^2+\left(\frac{\left(\omega L_b-\frac{\omega C_2}{\left(\frac{1}{R_L}\right)^2+(\omega C_2)^2}\right)}{k_1}+\frac{1}{\omega M}\right)^2 \tag{33}$$

$$\frac{1}{R_1+j\omega L_a+\frac{1}{\frac{1}{j\omega M}+\frac{1}{j\omega L_b+R_2+\frac{1}{j\omega C_2+\frac{1}{R_L}}}}} \tag{34}$$

$$= \frac{R_1 + \left(\frac{R_2 + \frac{\frac{1}{R_L}}{\left(\frac{1}{R_L}\right)^2 + (\omega C_2)^2}}{k_1 k_2} \right) - j\left(\omega L_a + \frac{1}{k_2}\left(\frac{\omega L_b - \frac{\omega C_2}{\left(\frac{1}{R_L}\right)^2 + (\omega C_2)^2}}{k_1} + \frac{1}{\omega M} \right) \right)}{\left(R_1 + \left(\frac{R_2 + \frac{\frac{1}{R_L}}{\left(\frac{1}{R_L}\right)^2 + (\omega C_2)^2}}{k_1 k_2} \right) \right)^2 + \left(\omega L_a + \frac{1}{k_2}\left(\frac{\omega L_b - \frac{\omega C_2}{\left(\frac{1}{R_L}\right)^2 + (\omega C_2)^2}}{k_1} + \frac{1}{\omega M} \right) \right)^2} \quad (35)$$

Now, define the constant,

$$k_3 = \left(R_1 + \left(\frac{R_2 + \frac{\frac{1}{R_L}}{\left(\frac{1}{R_L}\right)^2 + (\omega C_2)^2}}{k_1 k_2} \right) \right)^2 + \left(\omega L_a + \frac{1}{k_2}\left(\frac{\omega L_b - \frac{\omega C_2}{\left(\frac{1}{R_L}\right)^2 + (\omega C_2)^2}}{k_1} + \frac{1}{\omega M} \right) \right)^2 \quad (36)$$

$$Z_{eq(pp,\ \omega=\omega_0\ )} = Re\left(\frac{1}{j\omega C_1 + \frac{1}{R_1 + j\omega L_a + \frac{1}{\frac{1}{j\omega M} + R_2 + \frac{\frac{1}{R_L}}{\left(\frac{1}{R_L}\right)^2 + (\omega C_2)^2} + j\left(\frac{\omega L_b - \omega C_2}{\left(\frac{1}{R_L}\right)^2 + (\omega C_2)^2} \right)}}} \right) \quad (37)$$

$$\frac{R_1}{k_3}+\frac{R_2}{k_1k_2k_3}+\frac{\frac{1}{R_L}}{\left(\left(\frac{1}{R_L}\right)^2+(\omega C_2)^2\right)(k_1k_2k_3)} = \frac{}{k_4} \tag{38}$$

Where,

$$k_4=\left(\frac{R_1}{k_3}+\frac{R_2}{k_1k_2k_3}+\frac{\frac{1}{R_L}}{\left(\left(\frac{1}{R_L}\right)^2+(\omega C_2)^2\right)(k_1k_2k_3)}\right)^2 + \left(\frac{1}{\omega M(k_2k_3)}+\frac{\omega L_b}{(k_1k_2k_3)}-\frac{\omega C_2}{(k_1k_2k_3)\left(\left(\frac{1}{R_L}\right)^2+(\omega C_2)^2\right)}+\frac{\omega L_a}{k_3}-\omega C_1\right)^2 \tag{39}$$

2.3.3 Impedance characterization of compensation topologies

The constructed air cored transformer with parameters as tabulated in Table 3 and the setup as designed and constructed in Figure 2-8 [10], can be used to simulate the variation in the equivalent impedance *(Z_{eq})*, equivalent reactance *(X_{eq})* and equivalent resistance *(R_{eq})* of the air cored transformer. The compensation capacitance corresponding to all the four basic topologies were obtained from Table 2. The resonant frequency was fixed as 100 kHz and a load of R_L = 4 Ω has been set while carrying out the simulation study.

Table 3 Constructed IPT transformer and its parameters

Physical parameters	Measured values
Leakage inductance of primary	103.4 µH
Leakage inductance of secondary	12.67 µH
Mutual inductance	6.02 µH
DC resistance of primary	0.153 Ω
DC resistance of secondary	0.066 Ω

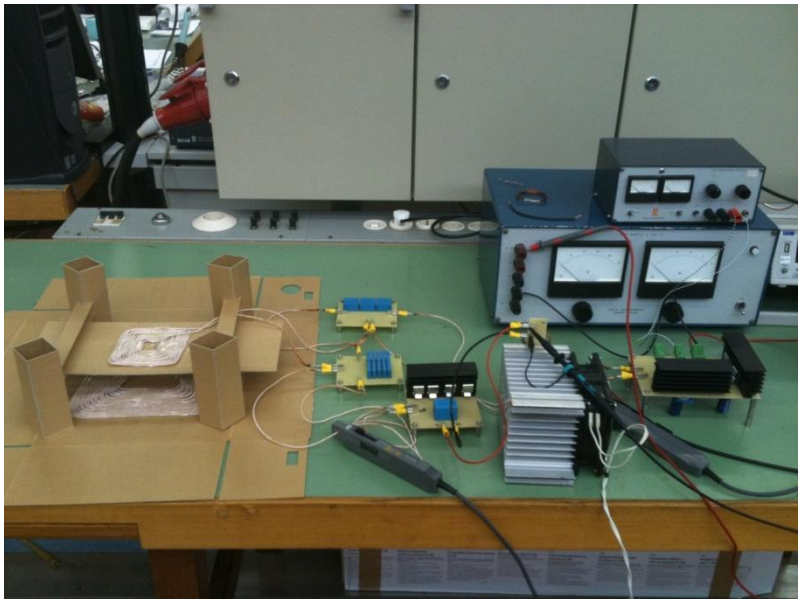

Figure 2-8 Experimental setup of the IPT

2.3.3.1 Primary series compensated topologies – SS and SP topologies

In case of the primary series compensated topologies, the compensated air cored transformer shifts from a capacitive circuit at low frequencies to an inductive circuit at higher frequencies. Resonance occurs at the point where the capacitive and inductive reactance's become equal and cancels each other. A very peculiar feature that can be observed is the fact that the equivalent resistance for all variations in the frequency becomes independent of frequency.

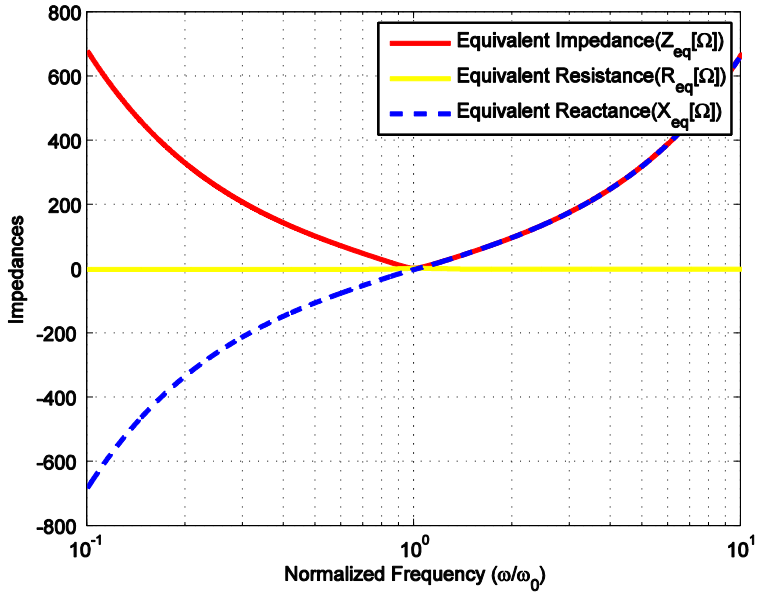

Figure 2-9 Variation of the SS topology parameters with normalized frequency *(w/w₀)*

2.3.3.2 Primary parallel compensated topologies-PS and PP topologies

In case of primary parallel compensated topologies, the compensated air cored transformer shifts from an inductive circuit at lower frequencies to a capacitive circuit at higher frequencies. However, a major difference between the parallel and series compensated topologies is the fact that the equivalent resistance peaks at the frequency of resonance and hence the impedance reaches a peak at the same frequency.

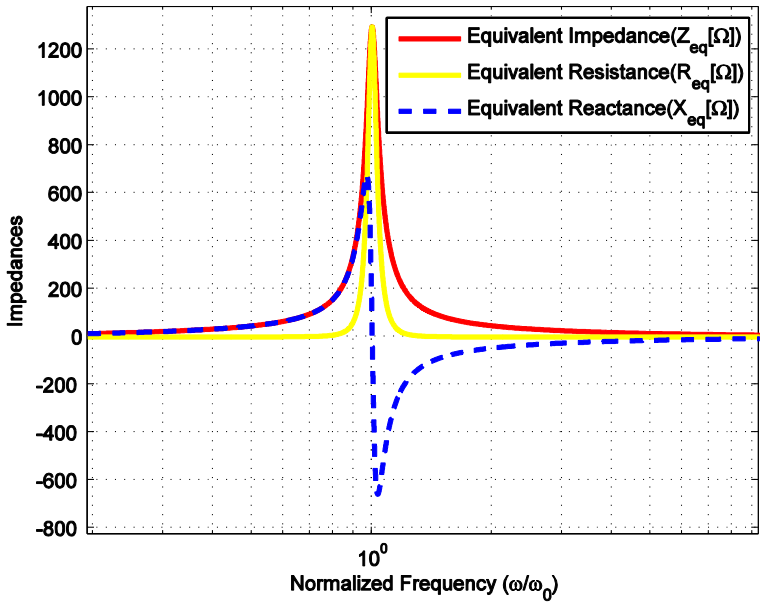

Figure 2-10 Variation of the PS topology parameters with normalized frequency *(w/w₀)*

2.4 Conclusions

In this chapter, the basics of the functioning of the IPT Transformer were considered and the various compensation strategies for the same were explained. In case of the compensated IPT transformer, it was observed that resonance behaves differently in case of both primary series and primary parallel topologies. In case of primary series topologies, it was observed that resonance results in the net impedance of the transformer reaching its minimum. While, in case of primary parallel topologies, it was observed that resonance results in the net impedance reaching its maximum. The impedances of the various circuit topologies at the resonance point were derived and the variation in the resistance, reactance and the impedance of the circuit at various frequencies were explained.

CHAPTER 3

OPTIMIZATION OF COMPENSATION STRATEGIES

3.1 Introduction

Inductive power transfer based on air cored transformers with compensation applied to both the primary and secondary and their characteristics are described in the previous chapter. However, optimization and design of such transformers still remain a major problem considering the various constraints such as the power levels to be transferred, choice of optimal resonant frequency, the operating efficiency of the IPT transformer, the configuration and number of coils to be chosen in the primary and secondary, the constraints with regard to power electronics among other factors. A perfect design of such an air core transformer is not possible, however, it is possible to look into some important parameters assuming that the other factors are maintained a constant. In this case, efficiency is the parameter to be optimized with the coils already designed and power levels fixed. The parameters that are considered to be variable are the frequency and the load.

3.2 Efficiency based optimization of compensation strategy

The previous analysis on the various basic compensation strategies and their design is based on the fact that resonant frequency is well known.

However, this is often not the case and the choice of resonant frequency has to be made. It is observed in the analysis of the previous sections that the efficiency depends on the frequency and the load resistance.

$$\eta = func(f, \mathrm{R_L}) \tag{40}$$

Thus, the choice of the resonant frequency can be made by performing the following steps:

1. Vary the frequency over a range adapting the values of the primary and secondary compensation such that all the frequencies are resonant.
2. Calculate the theoretical load by modelling it as a resistance such that:

$$R = \frac{V^2}{P} \tag{41}$$

3. Choose the resonant frequency that corresponds to the maximum efficiency point for a particular value of load resistance. This step is crucial as the efficiency begins to saturate after a certain frequency. Thus, an optimum can be considered by:

$$\left(\frac{\partial \eta}{\partial f}\right)_{R_L=const} \cong 0 \tag{42}$$

Simulation studies were carried out to explain this selection for all the basic topologies by modelling the network of an IPT system with a fixed leakage and mutual inductance i.e. the case where horizontal movement is constraint or in case of stationary charging. Skin effect that plays a prominent role in case of higher frequencies was also modelled. However, the use of Litz wire can to a large extent downplay this effect and the constructed IPT transformer made use of such windings. The parameters of the constructed IPT transformer are tabulated in Table 3.

3.2.1 Primary series compensation and the selection of optimal resonant frequency

Simulation studies for the series primary compensation was carried out by considering that the input to the transformer was an ideal voltage source and the efficiency was optimized by considering the three dimensional plots corresponding to the variation in efficiency with load and frequency. They are shown in Figure 3-1.

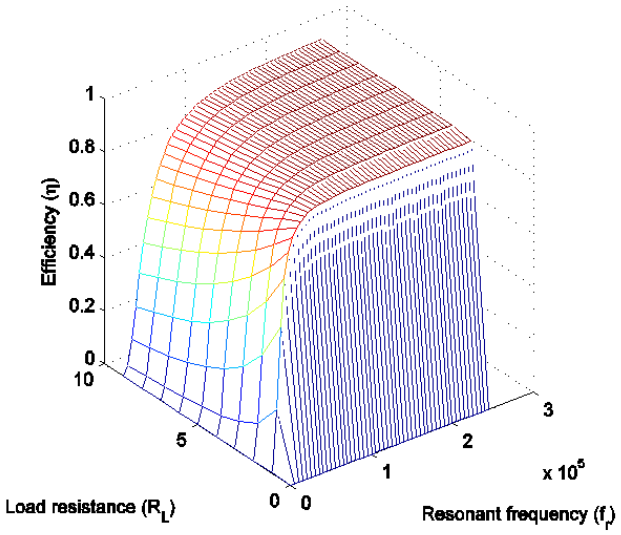

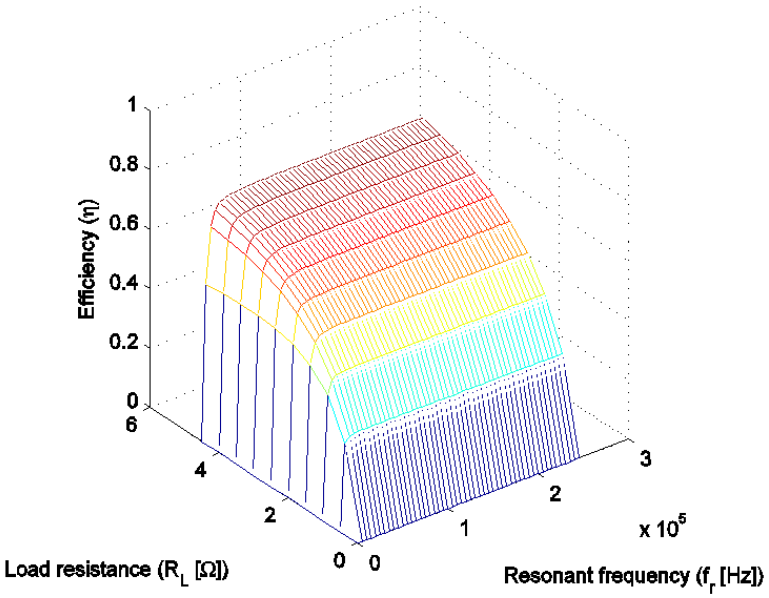

Figure 3-1 Efficiency v/s load resistance and frequency for SS and SP topologies

The plots obtained can be used to identify an optimal frequency corresponding to high efficiency for a particular value of load. Usually, the frequency so selected would be a trade-off between rise in efficiency, the maximum switching frequency of power devices and expense. It was observed that for the designed IPT transformer, the optimal resonant frequency was about 100 kHz. There was not much of a difference in efficiency corresponding to this operating point in case of both of the series compensated topologies.

Once, the optimal resonant frequency is selected from the range of resonant frequencies, the behaviour of the topologies can be simulated by fixing the compensation capacitances of the primary and the secondary corresponding to that resonant frequency and solving the network for a range of operating frequencies.

3.2.1.1 SS topology

In case of SS topology, when the IPT transformer is operated at a resonant frequency of 100 kHz with a fixed primary and secondary compensating capacitance, the variations in various parameters corresponding to a source voltage of 20 V and load resistance R_L of 4 Ω when frequency is varied over a range is shown in Figure 3-2.

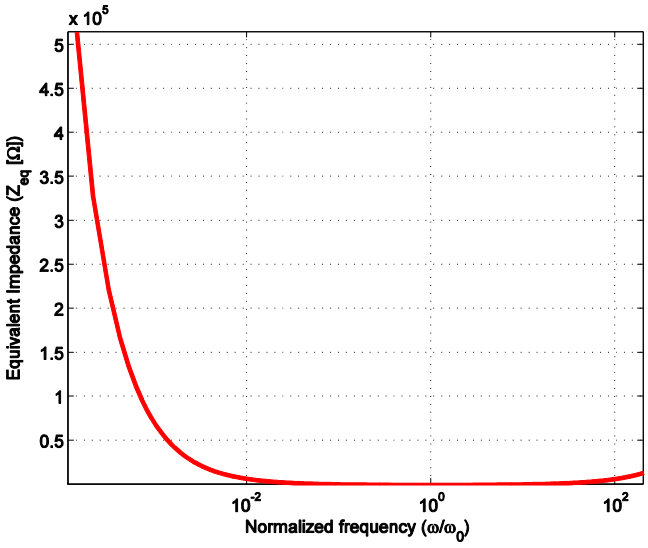
x 10^5
Equivalent Impedance (Z_eq [Ω])
Normalized frequency (ω/ω_0)

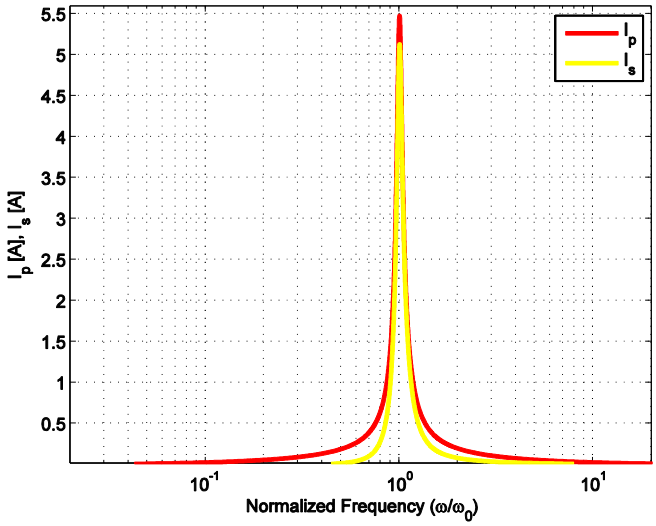
I_p
I_s
I_p [A], I_s [A]
Normalized Frequency (ω/ω_0)

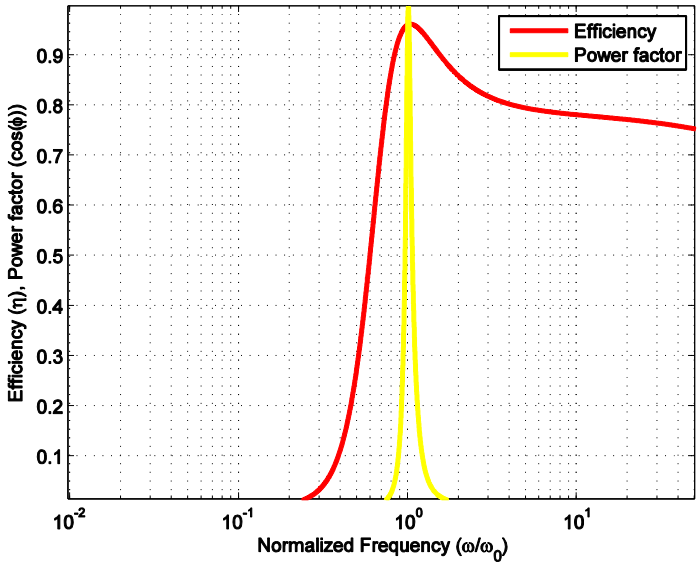
Efficiency
Power factor
Efficiency (η), Power factor (cos(ϕ))
Normalized Frequency (ω/ω_0)

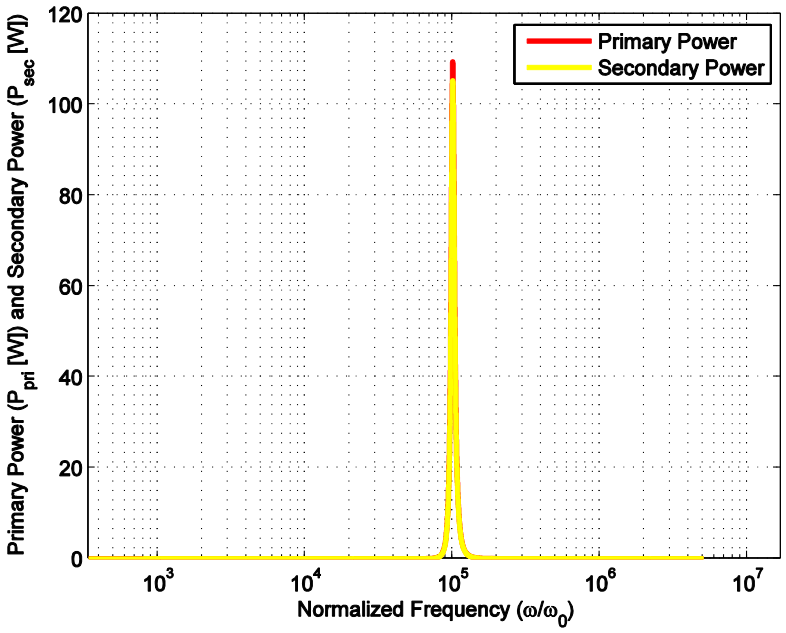

Figure 3-2 SS topology parameters v/s normalized frequency *(w/wₒ)*

It is observed that in case of SS topology, the impedance of the entire circuit reduces to a minimum at the resonant frequency and the same rises gradually as the frequency increases to super-resonant frequencies. This variation in impedance would imply that for a constant primary voltage, the primary current also varies as frequency varies. The primary current would reach a peak at the resonant frequency and the secondary current also shows a similar trend. It can also be observed that the efficiency rises gradually as the frequency increases and reaches its maximum at the resonant frequency and gradually reduces for super-resonant frequencies. This would imply that in terms of variation in efficiency for variable frequency IPT systems, the tolerance for efficiency to super-resonant frequencies is higher than that of sub-resonant frequencies.

3.2.1.2 SP topology

In case of SP topology, the transformer was simulated under the same conditions as in the SS topology case and the various parameters observed have been plotted in Figure 3-3.

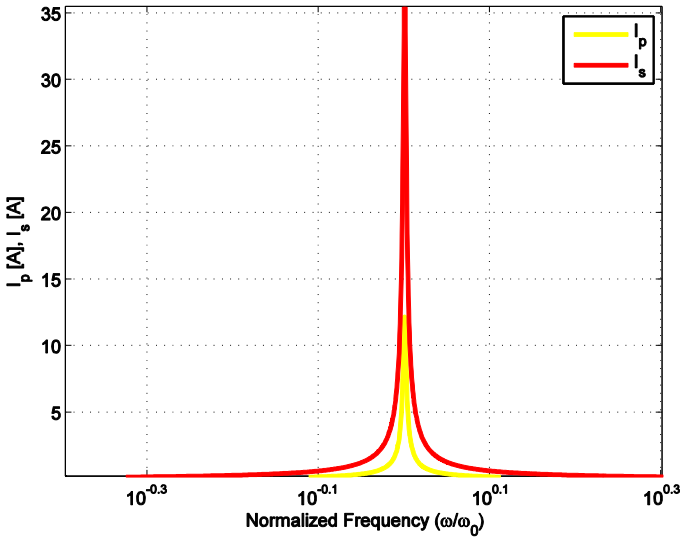
I_p
I_s
I_p [A], I_s [A]
Normalized Frequency (ω/ω_0)

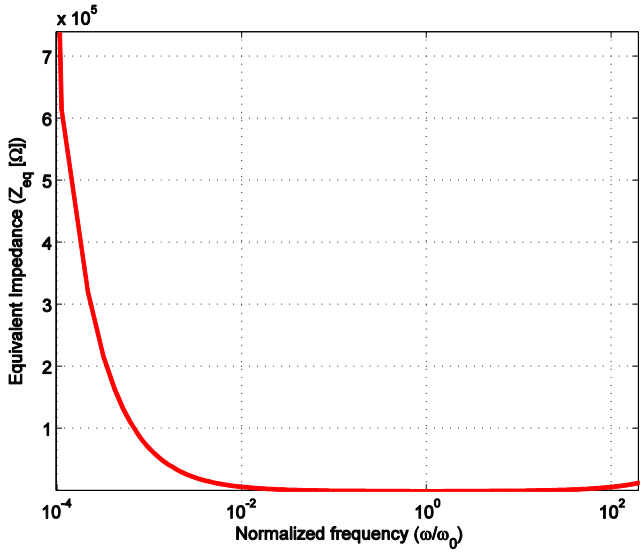
x 10^5
Equivalent Impedance (Z_eq [Ω])
Normalized frequency (ω/ω_0)

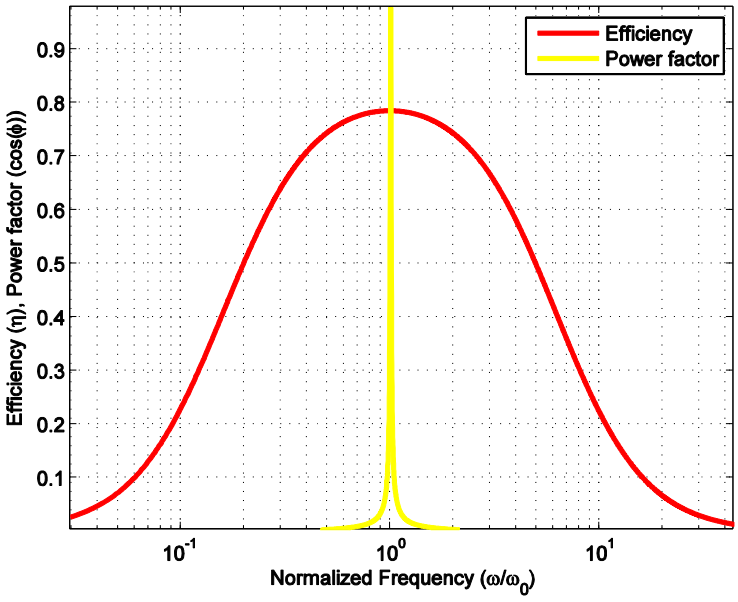
Efficiency
Power factor
Efficiency (η), Power factor (cos(ϕ))
Normalized Frequency (ω/ω_0)

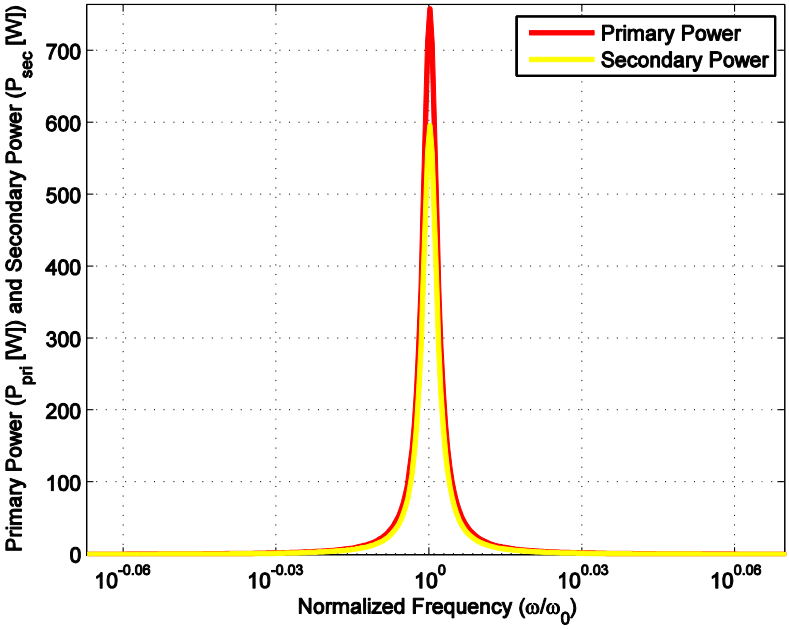

Figure 3-3 SP topology parameters v/s normalized frequency *(w/w₀)*

It is observed that in case of SP topology, the impedance of the entire circuit reduces to a minimum at the resonant frequency and the same rises gradually as the frequency increases to super-resonant frequencies. This variation in impedance is similar to that in case of SS topology. The primary current, the secondary current and efficiency show the same trend as in case of SS topology. A noticeable difference is the fact that the theoretical power levels in case of SP topology are much higher than SS under the same conditions. This happens so because, in case of SP topology, the equivalent circuit impedance at resonant frequency is much lower than that of SS topology.

3.2.1.3 Choice between SS and SP topology

A very important feature that the primary series compensation topologies possess is that the choice of their compensation capacitances is independent of the load which is a desirable property particularly when the loading profile is variable. The choice between the two primary series compensation strategies would in turn depend on various factors such as efficiency and its tolerance to variable frequencies, the desired power levels of operation, power factor and its tolerance to variable frequencies and cost. It can be generally observed that for higher power levels, SP compensation can transfer high powers at low voltage and high current. In case of SS compensation, due to its comparatively large impedance at resonant frequency, the currents drawn at low voltages are not very high and hence high power transfer can take place only at high voltages. In case of variable frequency operations, it is desirable to go for SS topology as it has higher tolerance for power factor when frequency changes. Also, a comparison between efficiency tolerance in case of SS and SP topologies at a particular resonant frequency is shown in Figure 3-4.

It can be observed that the maximum efficiency for SS topology is much higher than that of SP topology. Hence, for fixed frequency systems, it would be better to opt for SS topology. However, frequency tolerance for efficiency is better in case of SS topology over SP topology particularly at super-resonant frequencies. For sub-resonant frequencies, the efficiencies in case of SP topology is higher than that of SS topology.

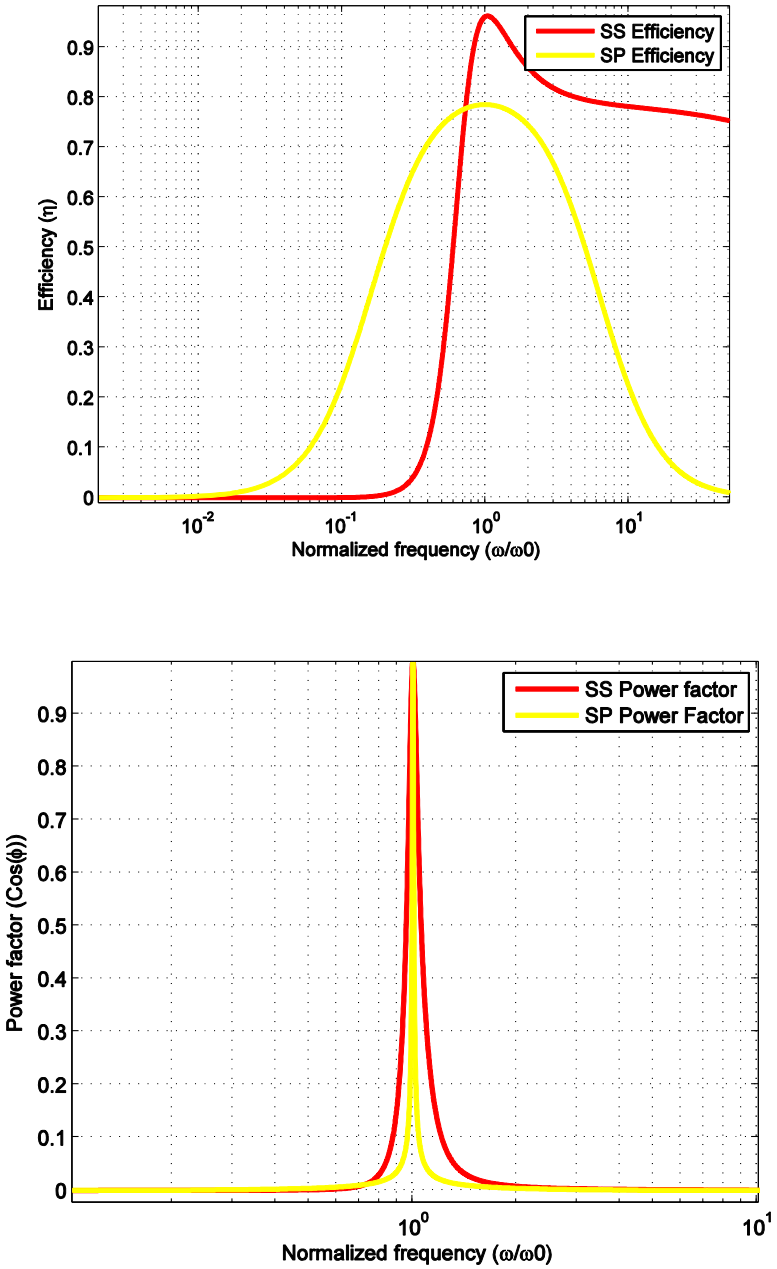

Figure 3-4 Frequency tolerance for efficiency and power factor in case of series primary compensation

3.2.2 Primary parallel compensation and selection of optimal frequency

Simulation studies were carried out for primary parallel compensation assuming that the input to the IPT transformer was an ideal current source. This was done as an ideal voltage source input could never supply a current that could deliver power of required levels. The three dimensional plots corresponding to the variation in efficiency as a function of load resistance and the frequency are shown in Figure 3-5.

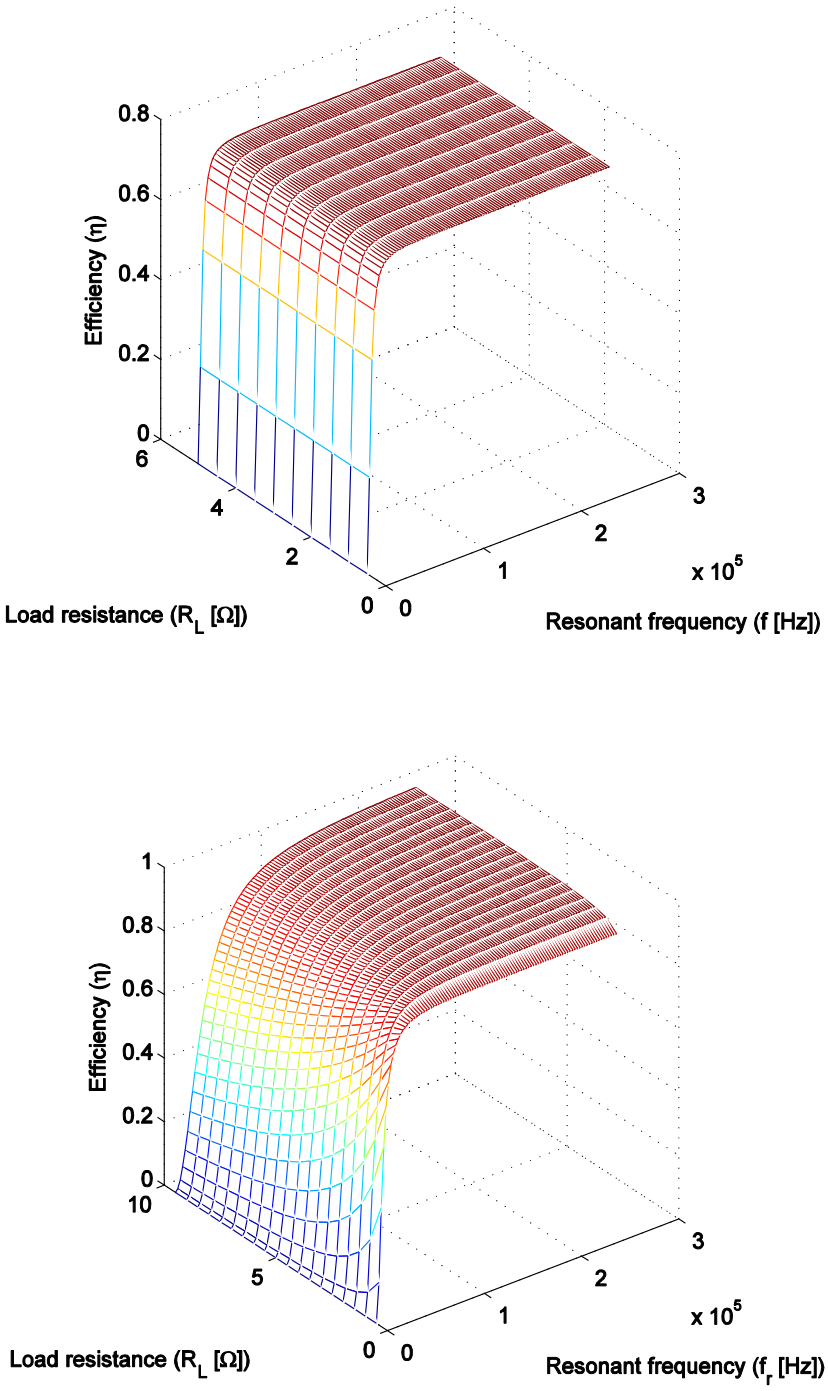

Figure 3-5 Efficiency v/s load resistance and frequency for PS and PP topologies

It was observed that there was a drastic difference in efficiencies between the case of PS and PP topologies. This fact can alone lead to the elimination of the PP topology for efficient power transfer. However, both the topologies were simulated for understanding the phenomena of power transfer.

3.2.2.1 PS topology

The IPT transformer with PS compensation topology was supplied with an ideal current source whose magnitude was chosen as I_p=5A. The resonant frequency was chosen as 100 kHz and the compensation capacitances were fixed corresponding to the resonant frequency and the frequency was varied. Graphs relating the various parameters corresponding to a load of R_L = 4Ω, is shown in Figure 3-6.

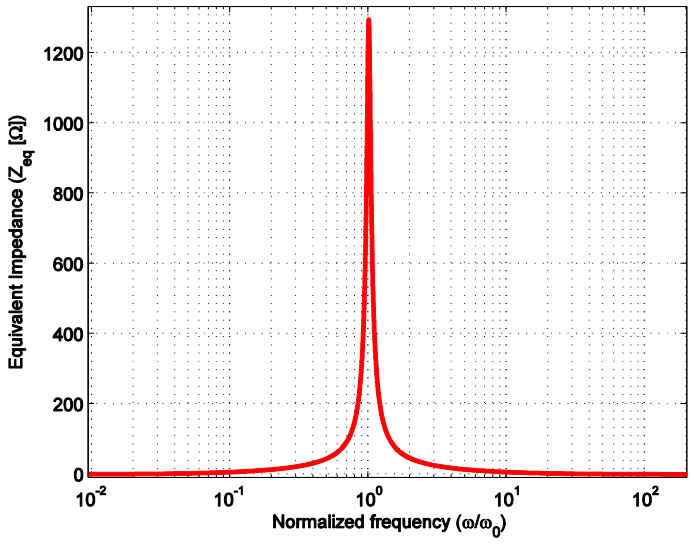

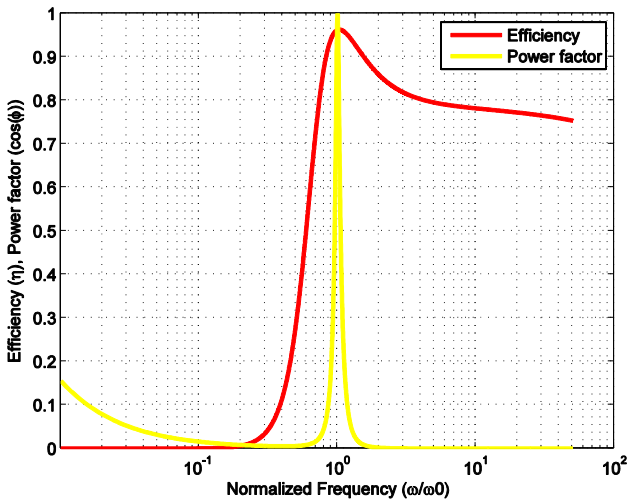

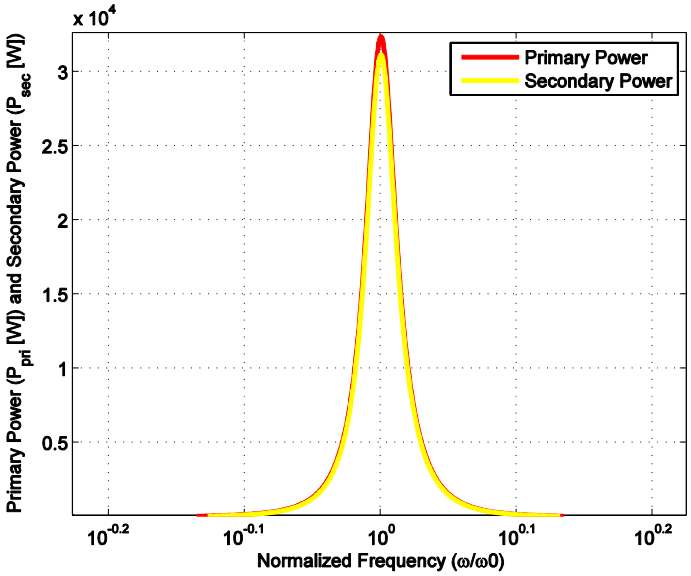

Figure 3-6 PS topology parameters v/s normalized frequency *(w/w₀)*

The fact that the impedance is peaking at the resonant frequency is very characteristic of parallel resonance and hence it can be directly observed that the power transfer can be maximized only by having a current source input. Thus, the input to the IPT transformer is a constant high frequency sinusoidal current. The secondary current as a function of frequency would peak at the resonant frequency, implying that at the resonant frequency there occurs maximum power transfer. Similar to series resonant circuits, it was observed that the frequency tolerance for efficiency was much higher in case of super-resonant frequencies than sub-resonant frequencies.

3.2.2.2 PP topology

The IPT transformer was subjected to the same conditions as in the case of the IPT transformer with PS compensation. The various graphs relating the parameters are shown in Figure 3-7.

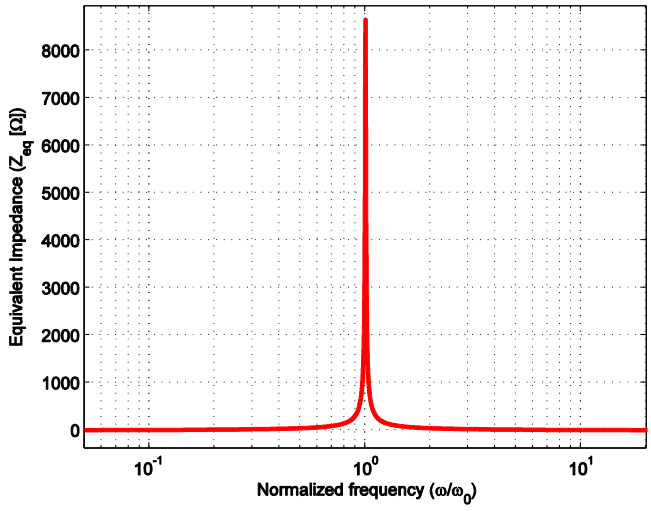

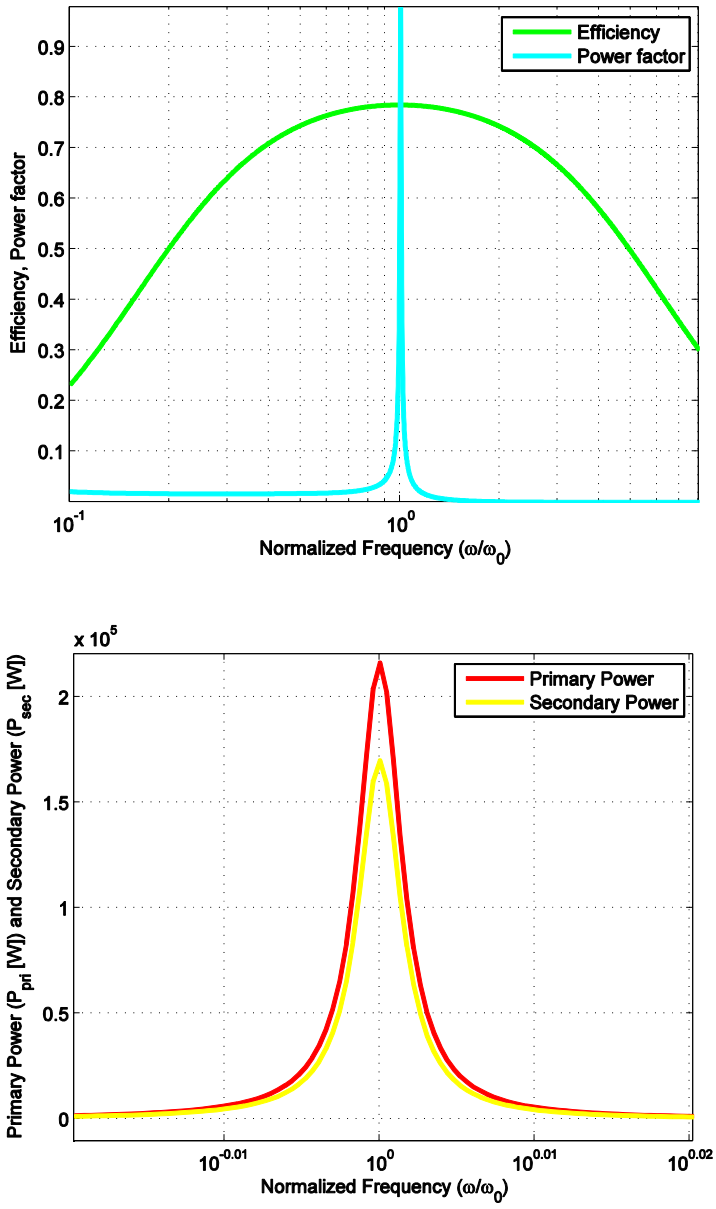

Figure 3-7 PP topology parameters v/s normalized frequency *(w/w₀)*

In case of PP topology, the circuit impedance peaks at the resonant frequency and being fed from a current source, the secondary current also peaks. It was also observed that since the impedance peaks to very high levels, the circuit has higher losses and hence, the efficiency remains poor for the constructed transformer.

3.2.2.2.1 Choice between PS and PP topology

A very unfavourable feature that the primary parallel topologies possess is the fact that the compensation capacitance varies with changing load. Hence, in applications where load changes are drastic, it would be better to prefer series primary compensation. The choice between the two topologies would then depend on a number of factors such as peak efficiency, tolerance of efficiency for variable frequency, tolerance of power factor for

variable frequency and cost. The variations in efficiency and power factor are shown in Figure 3-8. It can be readily observed that peak efficiency for the PS topology is higher than that of the PP topology. Also, the power factor tolerance for PS topology for super-resonant frequencies is much higher than that of PP topology. However, for sub-resonant frequencies, the efficiency of PP topology is higher than that of PS topology. Also, the frequency tolerance for PS topology is much higher than that of PP topology.

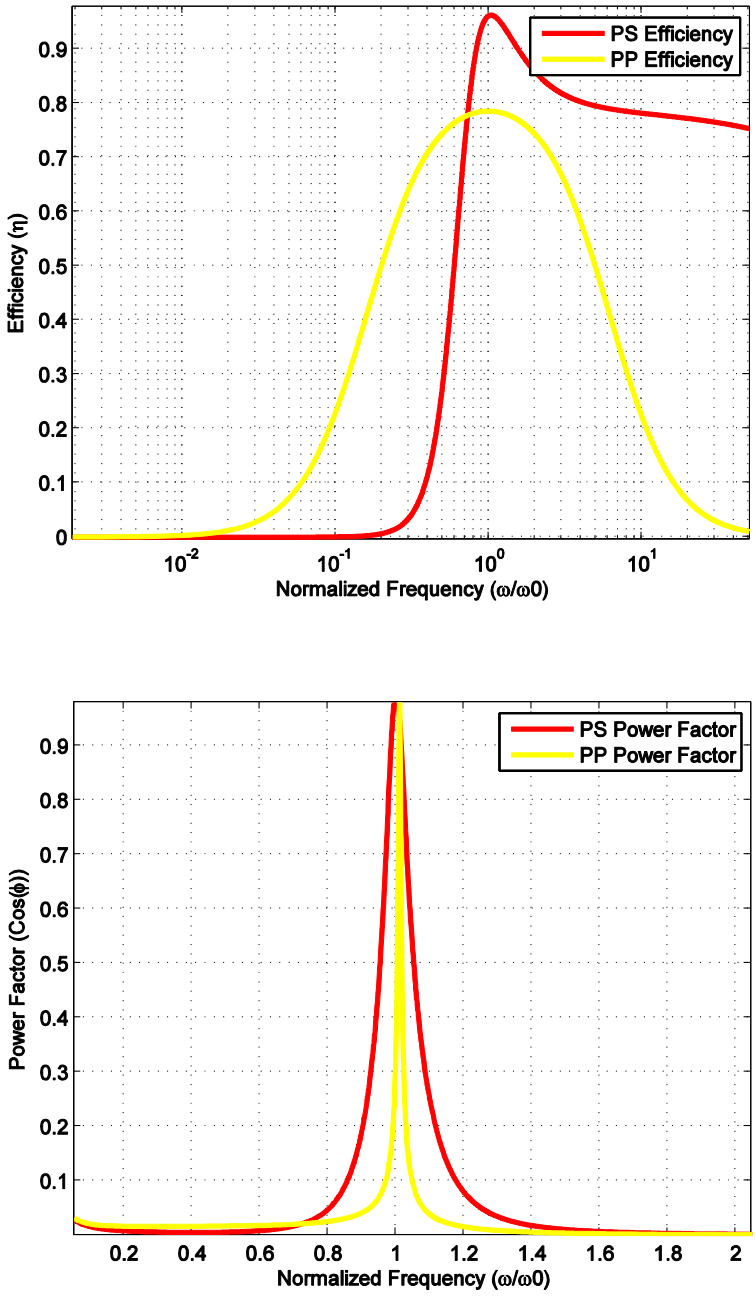

Figure 3-8 Frequency tolerance for efficiency and power factor for parallel primary compensation

3.2.3 Comparison between the various topologies

A comparison of the various characteristics of the compensated air core transformer is tabulated in Table 4.

Table 4 Comparison of the characteristics of the various compensation topologies

Characteristic of the topology	SS Topology	SP Topology	PS Topology	PP Topology
Dependence of the primary compensation capacitance on load	None	None	Dependent	Dependent
Circuit equivalent impedance at resonance	Minimum	Minimum	Maximum	Maximum
Type of ac source to be applied so as to transfer maximum power	Voltage source	Voltage source	Voltage source at high voltage/ Current Source	Voltage source at high voltage/ Current Source
Power transferred at constant source voltage (SS, SP)/ current (PS,PP)	Lower	Higher	Lower	Higher
Peak efficiency	Higher	Lower	Higher	Lower
Tolerance of efficiency to variable frequency	Lower	Higher	Lower	Higher
Tolerance of power factor to variable frequency	Higher	Lower	Higher	Lower

3.2.4 Tuning of a fixed frequency air cored transformer

Inductive power transfer systems based on both series and parallel primary compensation must supply either a constant voltage or a constant current input so as to supply maximum power at the resonant frequency. While testing the air cored transformer for the equivalent circuit parameters, the compensation capacitances are fixed based on the observed leakage and the magnetizing inductances. However, these parameters are subject to changes in the field such as changes in the physical distribution of the primary windings or the presence of materials with very high permeability. It is also likely that the compensation capacitances that are selected are only close to the actual compensation requirement which is further

aggravated by capacitive degradation over periods of time. All these factors result in a circuit resonant frequency that is different from that of the frequency of operation. Such an operation would increase the reactive power loading of the topology and hence reduces the effective power transfer to the load and results in a deviation from upf operation. Under these circumstances, it is essential that we perform tuning of the air cored transformer. Two techniques can be considered for tuning of the air cored transformers.

- Tuning considering the primary voltage/current
- Tuning based on the Displacement Power Factor (DPF)

3.2.4.1 Tuning considering the primary current/voltage

In case of series primary compensation, it was observed in the previous sections that when a constant voltage is fed into the primary, the current peaks at the point of resonance. Hence, a frequency sweep using the inverter can be performed at no load or light load so as to determine the point at which the current shows its maximum and this frequency can be set as the frequency of operation. Any current limiting stage used for constant current control of the output current of the inverter will render this tuning difficult as the current could remain a constant for a range of frequencies. In that case, it is best to select the lowest frequency at which the required current was obtained.

In case of parallel primary compensation, the behaviour of the resonant circuit is to peak the impedance at the point of resonance and hence, such topologies must be supplied with a constant current so as to transfer power effectively. A frequency sweep with the inverter can be performed so as to determine the point at which the input voltage reaches its minima. This is then the operating point of the inverter.

This knowledge of the impedance and its behaviour at resonance can be used to tune the IPT track with a single sensor i.e. either a current or voltage sensor.

3.2.4.2 Tuning based on Displacement Power Factor

Since operating at resonance should result in a unity displacement power factor operation, it is also possible to tune the system by observing both the current and voltage waveforms fed into the primary. For a well-designed compensation strategy, the input current and voltage waveform will be in phase and hence by performing a frequency sweep, it is possible to observe the waveforms and tune the system.

This technique however suffers from the need for having two sensors.

3.2.4.3 Experimental tuning of SS compensated IPT Transformer

In case of SS topology, the constructed IPT transformer whose theoretical frequency of operation was fixed as 100 kHz is subjected to tuning by performing a frequency sweep with

the inverter and the inverter resonant frequency so obtained was 105 kHz. The variation of primary current as a function of frequency for different loads is plotted in Figure 3-9.

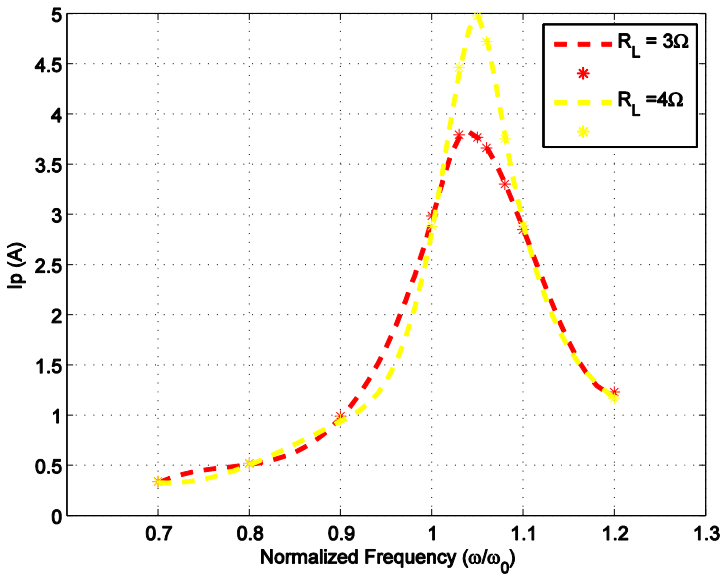

Figure 3-9 Tuning SS compensated transformer by varying primary current (I_P) with normalized frequency *(w/w_o)*

3.3 Conclusions

In this chapter, efficiency was considered as a parameter for the optimization of the various basic compensation topologies and an optimal frequency was selected for the operation of the topologies with maximum efficiency. Also, the operation of the primary series compensated topologies with a voltage source input and the primary parallel compensated topologies with a current source input was analyzed and simulated. A number of factors involved in the choice of the various basic compensation topologies are considered and explained. Tuning of the IPT transformer during non-ideal conditions for varying the resonant frequency is considered for keeping the system in resonance. An open loop testing of the IPT transformer was considered in order to check the feasibility of the technique.

CHAPTER 4

POWERING WHILE DRIVING – STUDY OF MISALIGNMENT

4.1 Introduction

The state of the art in mobility based on inductive power transfer system is the concept of powering while driving or roadway-based inductive power transfer systems. There is an increased effort in developing such technologies owing to the very high cost of energy storage schemes in electric vehicles. The most ideal scenario then would be inductive power transfer based electric vehicles which have tolerance to driving outside the region of power transfer by means of energy storage with a smaller capacity than that in place right now. However, there is a lot of freedom in the configuration of the primary and the secondary of the air-cored transformer so as to transfer power effectively. This chapter focuses on the design and construction of such a system so as to transfer power effectively over an air gap. The designs are then experimentally verified and the concept of misalignment brought into the picture.

4.2 IPT for powering while driving

In case of Roadway Powered Electric Vehicles (RPEVs), the primary of the IPT system is buried under the ground and the secondary of the IPT system is positioned underneath the vehicle. A major problem facing such a configuration as opposed to a configuration for stationary charging is the reduced mutual inductance between the primary and secondary. A reduced coupling as is the case with an air-cored transformer would further plague the problem of power transfer. The transferred power to the secondary, P_2 can be expressed in terms of the primary current I_1, mutual inductance M, quality factor of the secondary Q_2, resonant angular frequency ω_0 and the secondary series inductance L_2 as

$$P_2 = \frac{I_1^2 M^2 Q_2 \omega_0}{L_2} \tag{43}$$

With the use of ferrite cores, the factor $(\frac{M^2}{L_2})$ increases and hence higher power can be transferred even at lower frequencies. This advantage makes the use of ferrites very popular in case of RPEVs.

4.3 Ferrites and their application in IPT

Ferrites are ceramic like compounds which have ferric oxide (α-Fe_2O_3) as their main composition. Magnetite, Fe_3O_4 is a naturally occurring ferrite mineral that has been recognized for its magnetism for over two millennia. The advantages that ferrites have are applicability at higher frequencies, heat resistance, and higher corrosion resistance [20].

The use of ferrites in IPT is imperative because of the inherent low coupling factors obtained without the same in case of powering while driving. Two choices exist while considering ferrite based IPT. They are:

1. Use of ferrites in the primary.
2. Use of ferrite in the secondary/pickup.

Use of ferrite in the secondary/pickup is most often considered as laying tracks with ferrites under the ground would prove extremely expensive. For the pickup, different types of common ferrite shapes are discussed in literature. Some of the most common types of ferrite pickups are:

1. E pickups
2. Planar E pickups
3. I pickup
4. U pickup
5. ETD pickup

The choice of the most suitable pickup will depend on a number of factors including the amount of power to be transferred, the resonant frequency to be considered, the best ferrite shape that can capture the magnetic flux created by the chosen configuration of the primary among many others. A set of most common ferrite shapes that are commonly used in practice is shown in Figure 4-1.

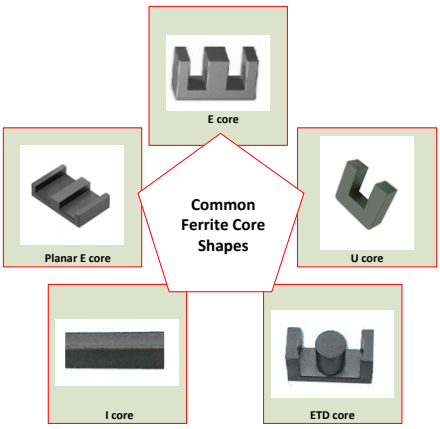

Figure 4-1 Common ferrite shapes

4.4 Choice of the core and the pickup

One of the most commonly used ferrite core for industrial applications is the E core. Such cores are commercially available in various sizes. For ease of experimentation and availability, Ferroxcube E80/38/20 core of the grade 3C90 was chosen. These ferrites can be used up to frequencies of 100 kHz and hence can be used successfully for the VLF range. The dimension of such a core is represented pictorially in Figure 4-2.

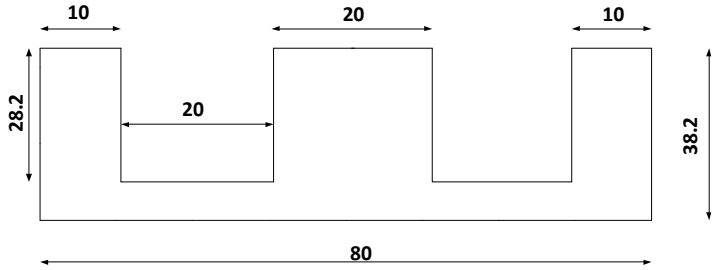

Figure 4-2 Dimensions of the E-80 core in mm

4.5 Track configuration and design of primary

4.5.1 Track configuration

The design of the primary of the IPT is very crucial as it needs to be optimized keeping in mind factors such as cost, efficiency and power transferred. Different configurations for the primary can be considered for IPT. They are:

1. Single phase primary systems
2. Poly phase primary systems

Single phase primary systems are economical and simple. They can be made of a single loop or multiple loops. While in case of single loop, the self and hence the mutual inductance may be low, they have reduced primary resistance compared to loops with multiple turns. Such a configuration of the primary is shown in Figure 4-3.

Poly phase primary systems consist of multiple number of phases that are distributed in such a manner so as to create a region above the primary where the power transfer is a constant. Such a configuration is shown in Figure 4-4.

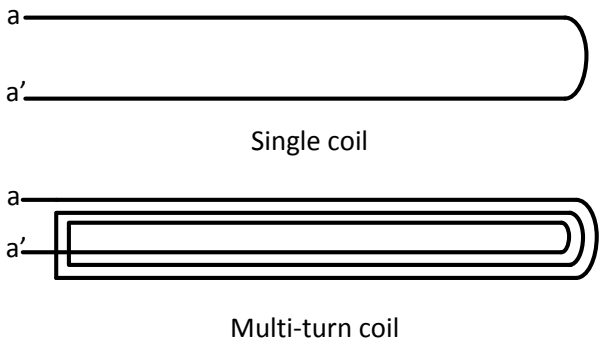

Figure 4-3 Coil configuration for the primary of a single phase IPT system

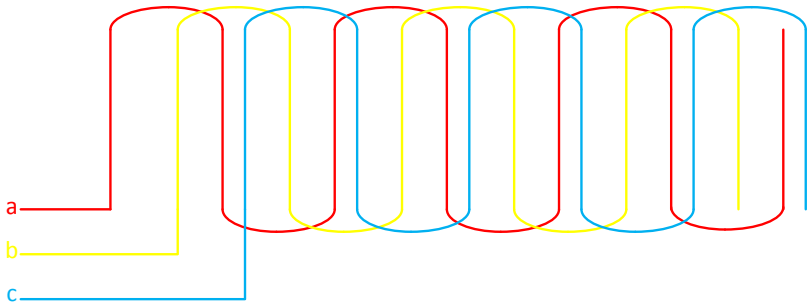

Figure 4-4 Sinusoidally distributed windings of the primary of a poly-phase IPT system

4.5.2 Design of the tracks

In order to create an extensive study of the effect of the primary loop on the power transferred via IPT, four different configurations of the primary were constructed with a single turn, double turn, four turns and five turns. The physical properties of the tracks are tabulated in Table 5.

Table 5 Physical properties of the track that forms the primary

S/No	Property type	Specification of the property
1.	Selected type of wire	Litz wire – 600 (No of strands) × 0.071mm (Dia of each strand)
2.	Type of loops constructed	Rectangular loops with variable number of turns
3.	Length of rectangular loop (m)	1
4.	Width of rectangular loop (cm)	4

The resistances and inductances of the primary are tabulated in Table 6.

Table 6 Resistances and Inductances of the primary loops

S/No.	No. of turns	Inductances (μH)	Resistances(mΩ)
1.	1	2.1	19.7
2.	2	5.6	35
3.	4	18.9	66
4.	5	27.5	81

The constructed inductors are shown in .The variation of the inductances and resistances with the number of turns of the primary coil are represented in Figure 4-6 and Figure 4-7 respectively.

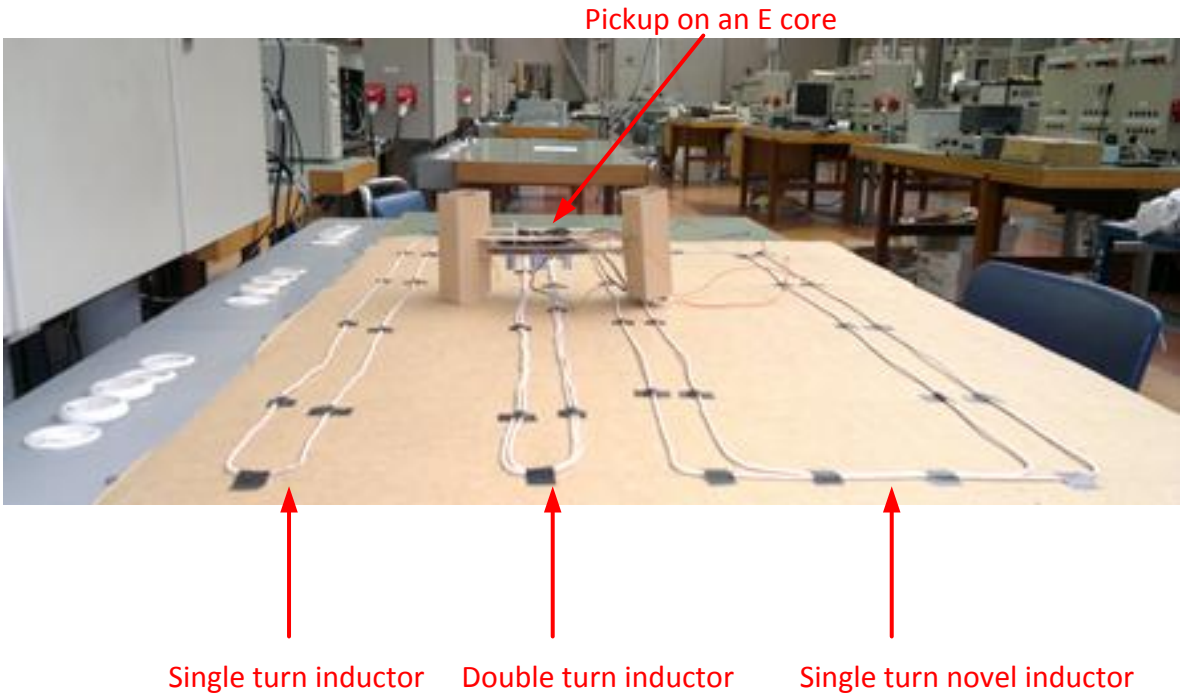

(a)

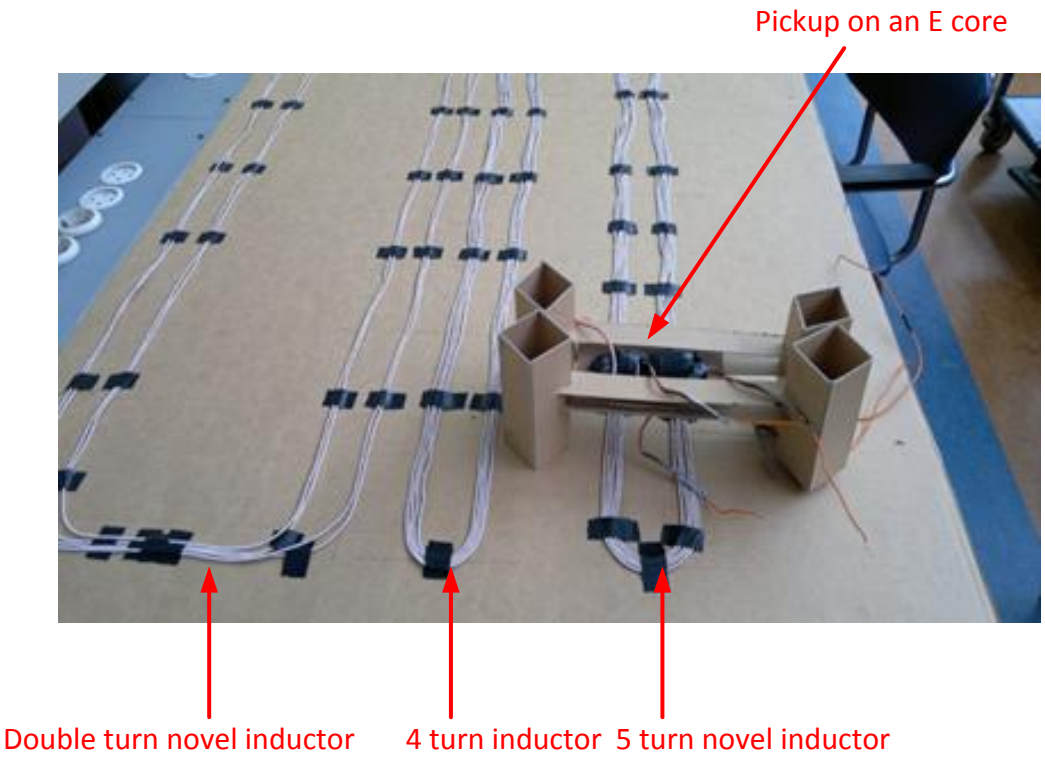

(b)

Figure 4-5 Constructed inductors for the experimentation (a and b)

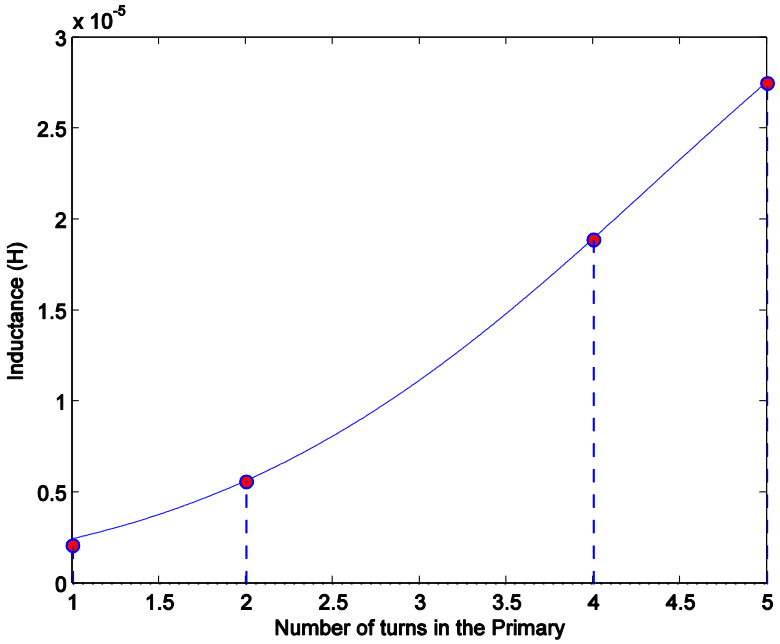

Figure 4-6 Variation of the inductance of the primary with number of turns

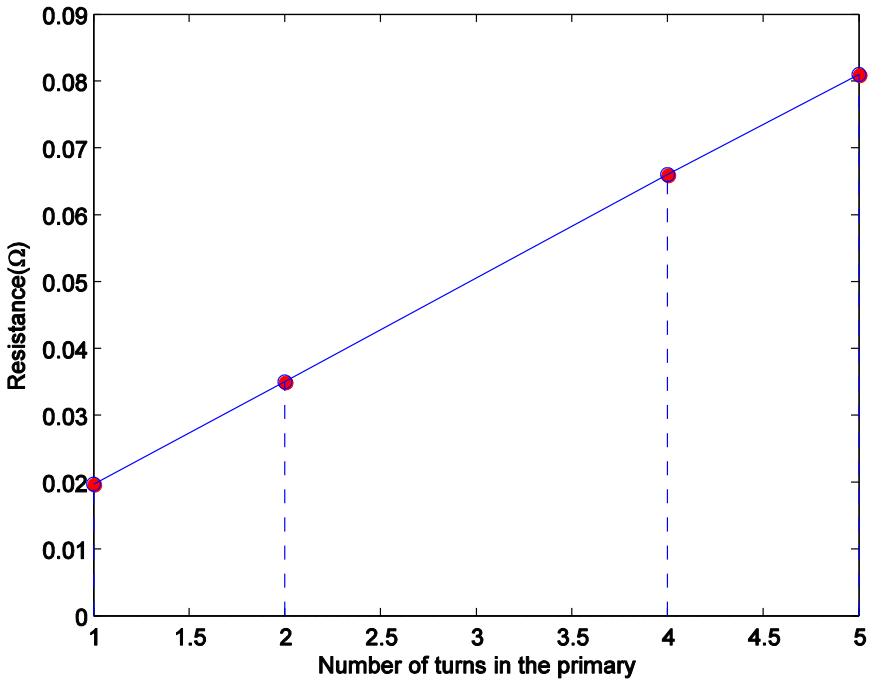

Figure 4-7 Variation of the resistance of the primary with number of turns

The above graphs indicate that while the variation in inductance is exponential with an increase in the number of turns, the variation of resistance is linear with an increase in number of turns.

4.5.3 Design of the pickup

Windings along the horizontal axis and windings along the vertical axis were used. Also, both the windings in the horizontal axis as well as the vertical axis were combined together so as to form the quadrature coils with additive flux distribution.

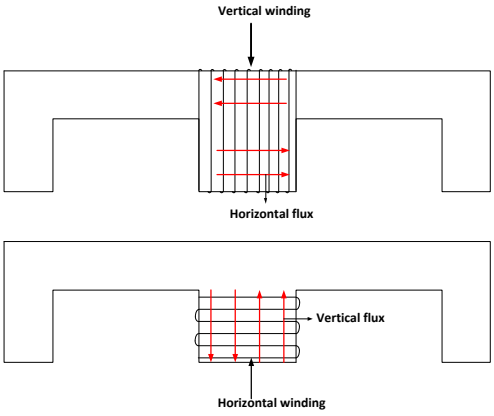

Figure 4-8 The different types of winding for the pickup

The various parameters of the pickup used are tabulated below.

Table 7 Specification of the pickup to be used for the IPT

S/No	Property type	Specification of the property
1.	Type of core selected	Ecore/ E80
2.	Limb used for winding	Central limb
3.	Type of ferrite core	3C90
4.	Distance between the centres of the core (cm)	4

Table 8 Winding specification for the pickup

S/No	Type of winding	No. of turns	Inductance (μH)	Resistances(mΩ)
1.	Horizontal	21 (double layer)	52.5	18.9
2.	Vertical	8	11.6	7.72
3.	Quadrature	11(H)/10(V)	15.55/14.31	11.8/9.65

4.6 Study of misalignment and its effect on the power transfer

Misalignment refers to the displacement of the pickup with respect to the primary leading to reduction in power transfer than that is expected. In order to give maximum freedom to the driver, it is extremely essential to have a constant power transfer across the air gap even when the pick-up is displaced with respect to the primary. Misalignment can be categorised into two:

- Lateral misalignment :

This kind of misalignment takes place when the pickup is displaced laterally with respect to the windings.

- Longitudinal misalignment:

This kind of misalignment takes place when the pickup is close to the terminations of the primary. In literature so far [11], this type of misalignment was ignored as the loops were

assumed to be infinitely long. However, in practical circumstances, the loops will be of finite length and hence, longitudinal misalignment has to be considered.

In this section, the mutual inductance between the primary and the pickup are noted at several displaced positions of the pickup w.r.t the primary. The various positions of the pickup and the primary are indicated in Figure 4-9.

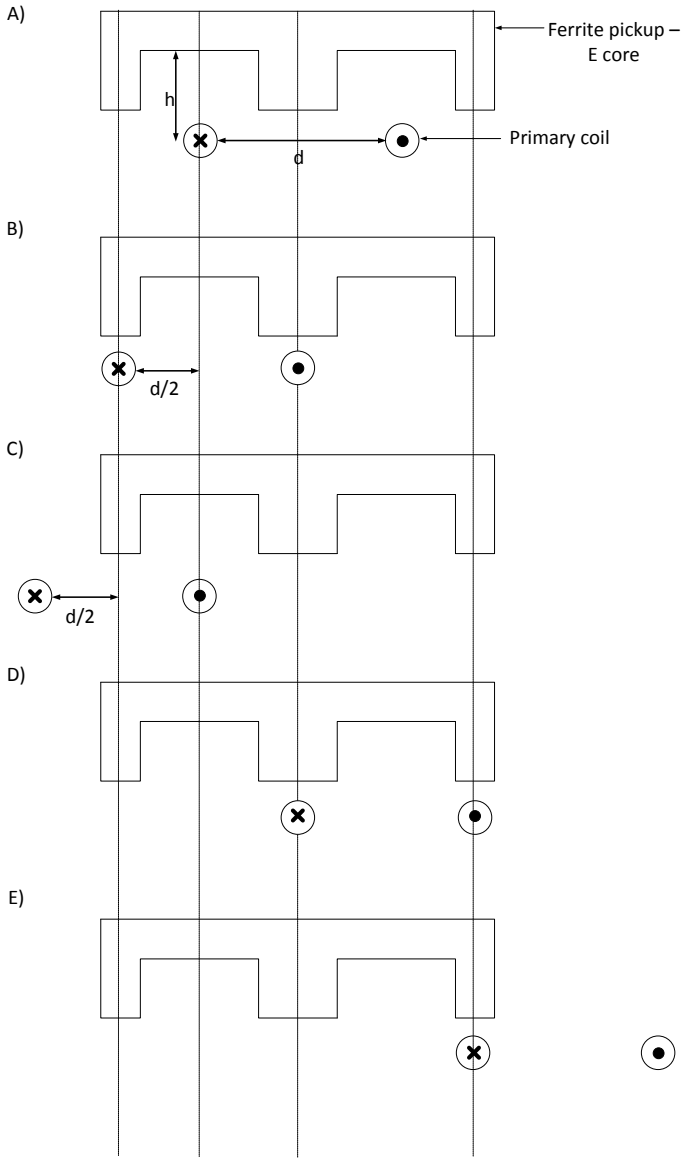

Figure 4-9 Study of misalignment at various positions

The analysis of misalignment was carried out at several points on the primary of the IPT system. The following parameters represent the various dimensions of the IPT system.

Table 9 Parameters of the IPT system

S/No.	Parameter	Value
1.	Height (h)	5 cm
2.	Displacement (d/2)	2 cm
3.	Points in the longitudinal direction	0m, 0.25m, 0.50m, 0.75m, 1m

4.6.1 Pickup with horizontal coil and study of lateral misalignment

Horizontal coils as shown in Figure 4-8 can capture the vertical component of flux. In order to study lateral misalignment, the pickup was displaced as shown in Figure 4-9 and the variation in mutual inductances were noted with the aid of an LCR-meter. The pickup was displaced 2cm from its reference position to two new points along the left as well as the right and the variation in the mutual inductance was measured and the plots were obtained.

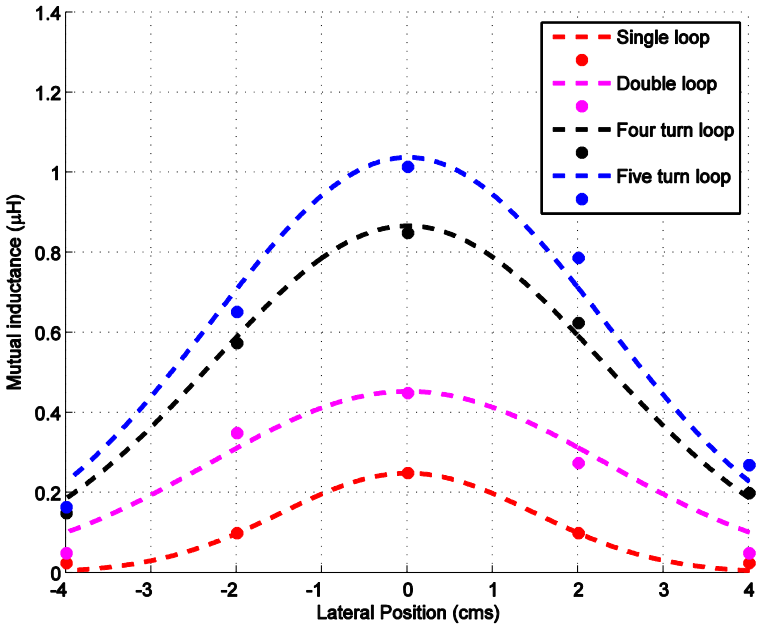

Figure 4-10 The variation in mutual inductance of the horizontal coil as a function of lateral misalignment

The above plot indicates that the variation in mutual inductance and hence the variation in power transferred over the air gap will be in such a manner that the most perfectly aligned point would be as indicated by Figure 4-9 A) with maximum power transferred at that point. Also, if the primary loop with maximum number of turns is selected, it would have much better mutual inductance at all possible points of observation.

4.6.2 Pickup with horizontal coil and study of longitudinal misalignment

In order to study longitudinal misalignment, various points were selected in the primary loop at variable distances from the reference and mutual inductance was plotted as a function of longitudinal distance for the point of perfect alignment as shown in Figure 4-9 A).

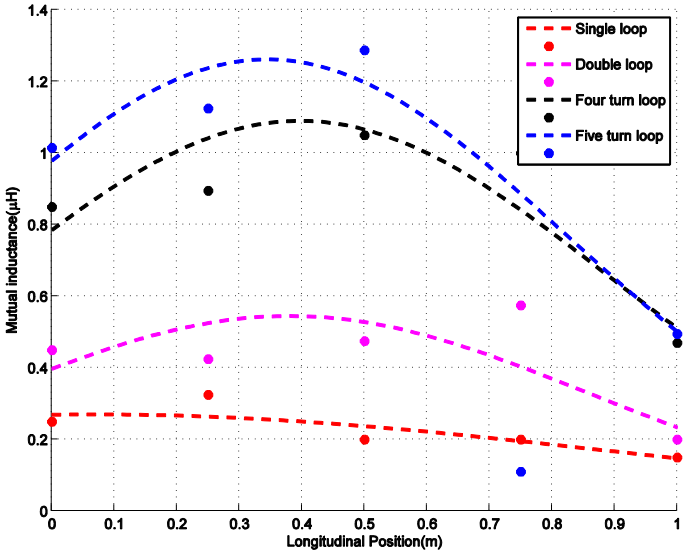

Figure 4-11 Variation of mutual inductance as a function of longitudinal position

In case of longitudinal misalignment, it was observed that the variation in mutual inductance is not as drastic as is the case with lateral misalignment. However, as the number of turns increases, the nature of the variation becomes more drastic. It was also observed that the variation in mutual inductance is most drastic at the extremities of the loop. This effect is referred to as "Edge Effect". An interesting observation is that the mutual inductance at the sending end of the inductor is higher than that of the other extreme end.

4.6.2.1 Edge effect

In order to explain the unsymmetrical nature of mutual inductance as observed at the sending end and the other end of the inductor, it is useful to consider the orientation of the magnetic fields at the two ends.

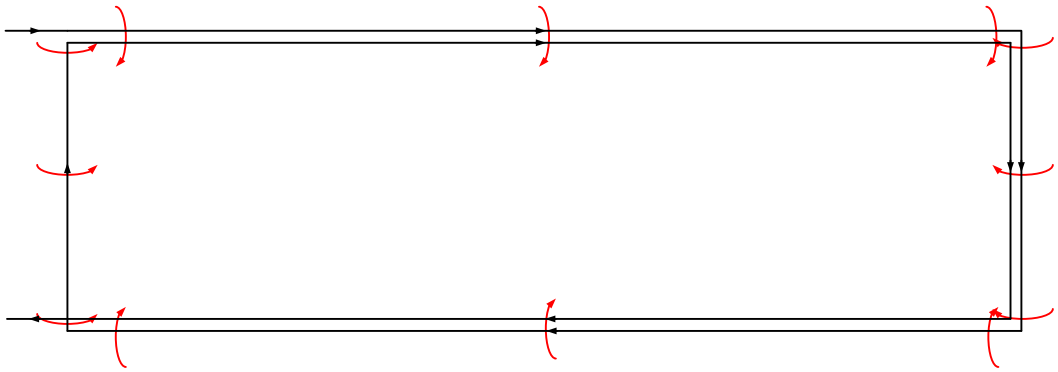

Figure 4-12 Orientation of the magnetic fields at the various sections of the inductor

Two observations that are very apparent are that the magnetic fields that are caused due to the vertical sections of the rectangle have currents that are in opposite directions in either ends. Hence, the resultant magnetic field observed at either ends have different magnitudes due to the additive/subtractive components on either end. Also, the number of vertical sections that contribute to the flux is different in either ends.

In order to eliminate just the possibility of the difference in the number of vertical sections in either ends (Left, 1 and Right, 2), a new inductor design was considered. This is represented in Figure 4-13and is referred to as "Symmetrical ended inductor". This design was constructed on a smaller inductor version and tested for lateral misalignment at either ends. The constructed inductor is shown in Figure 4-14.

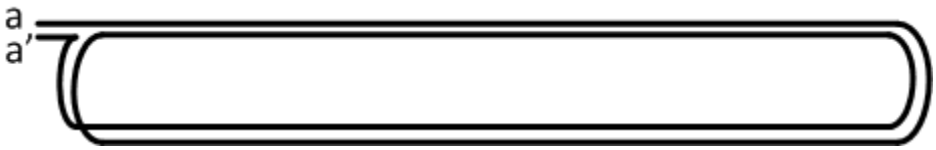

Figure 4-13 A symmetrical ended inductor

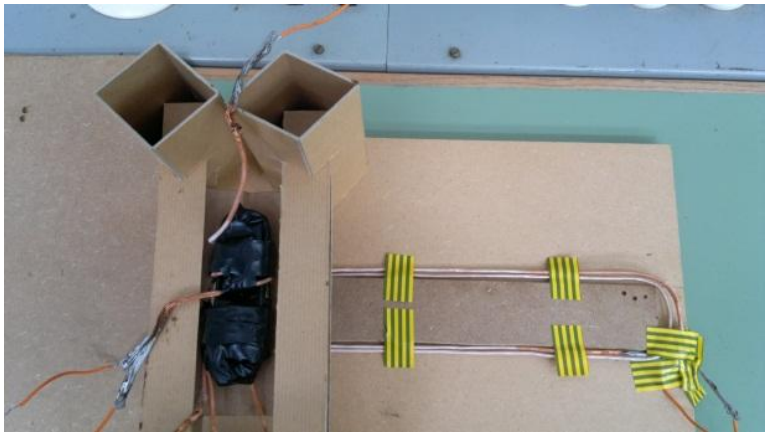

Figure 4-14 The symmetrical ended inductor

4.6.3 Pickup with horizontal coil and combining both horizontal and vertical misalignment

The readings as observed for both lateral and longitudinal misalignment were combined together and the variation in mutual inductances was plotted as a function of both lateral displacement and longitudinal displacement.

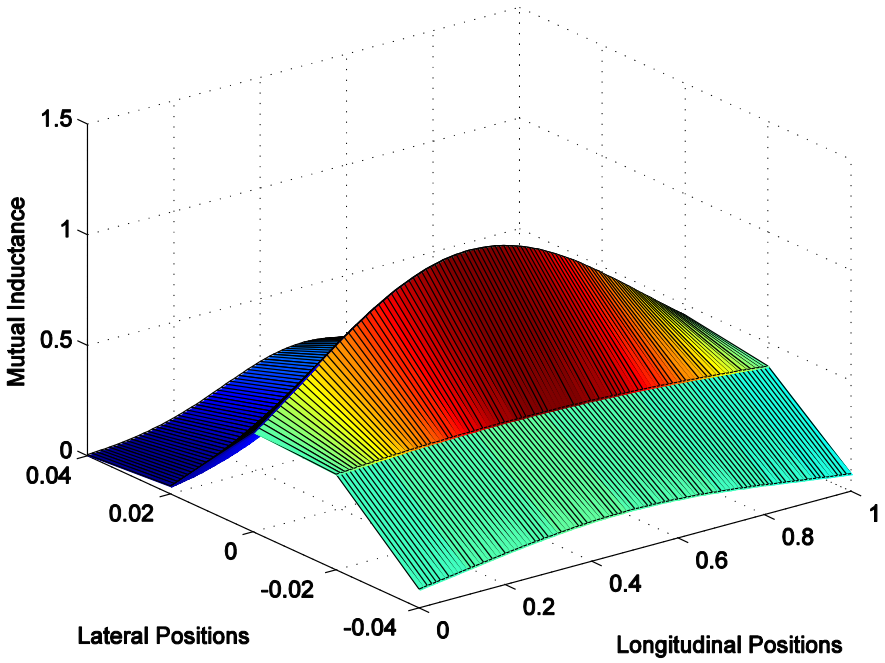

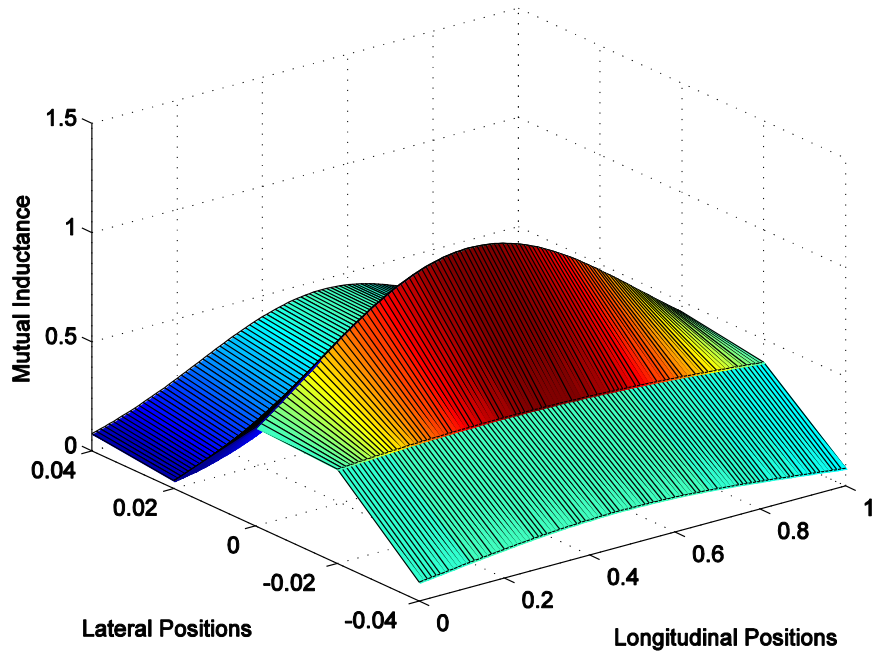

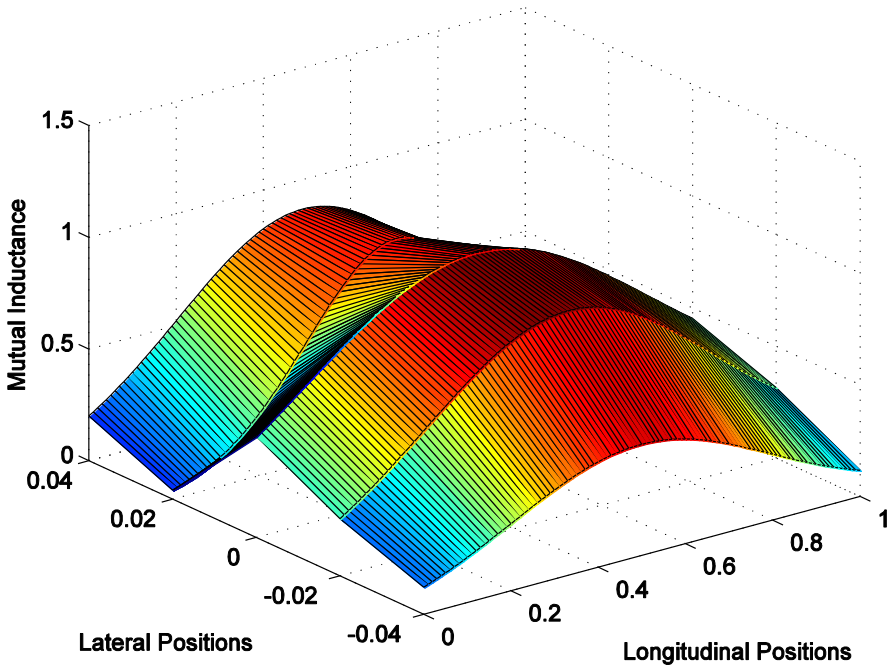

Figure 4-15 The variation in mutual inductance of the coils (1,2,4 loops) as a function of lateral and longitudinal position

It can be directly inferred that the variation in mutual inductance as a function of both lateral and longitudinal position would be bell shaped curves with the variation along the lateral direction much more drastic than that of the longitudinal direction.

4.6.4 Pick up with vertical coil and study of lateral misalignment

In order to capture the horizontal component of flux, vertical coils as shown in Figure 4-8 was used. In order to study lateral misalignment, the pickup was displaced as shown in Figure 4-9 and the variation in mutual inductances was noted with the aid of an LCR-meter. The pickup was displaced as with the study on the horizontal coils and the variation in mutual inductance was studied.

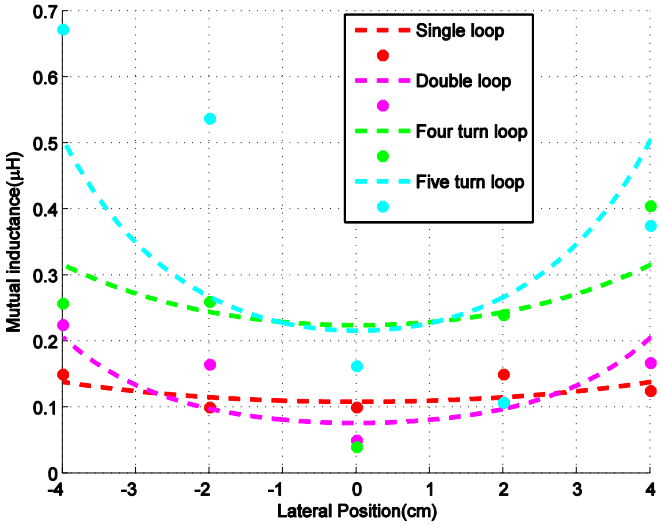

Figure 4-16 The variation in mutual inductance as a function of lateral position

It can be inferred from the variation in mutual inductance that the mutual inductance would have a maximum value at either ends of the inductor with the minima occurring at the point of perfect alignment. This trend is opposite to that observed when the horizontal coils were previously used to capture the vertical flux. This profile would explain the possibility of combing the two coils with additive flux so as to obtain a more flat power profile.

4.6.5 Pickup with vertical coil and study of longitudinal misalignment

In order to study longitudinal misalignment, various points were selected in the primary loop at variable distances from the reference and mutual inductance was plotted as a function of longitudinal distance for the point of perfect alignment as shown in Figure 4-9 A).

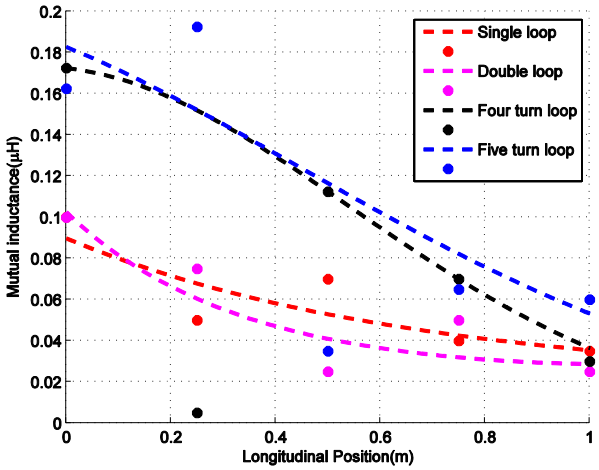

Figure 4-17 The variation in mutual inductance as a function of longitudinal position

In case of variation of mutual inductance as a function of longitudinal position, the variation is more drastic as the number of turns keeps increasing. Also, for the horizontal flux, the variation is more abrupt as the longitudinal position is varied compared to that in case of vertical flux.

4.6.6 Pickup with vertical coil and combining both lateral and longitudinal misalignment

The readings for both lateral and longitudinal misalignment were combined together and the variation in the mutual inductance was plotted as a function of both lateral and longitudinal misalignment.

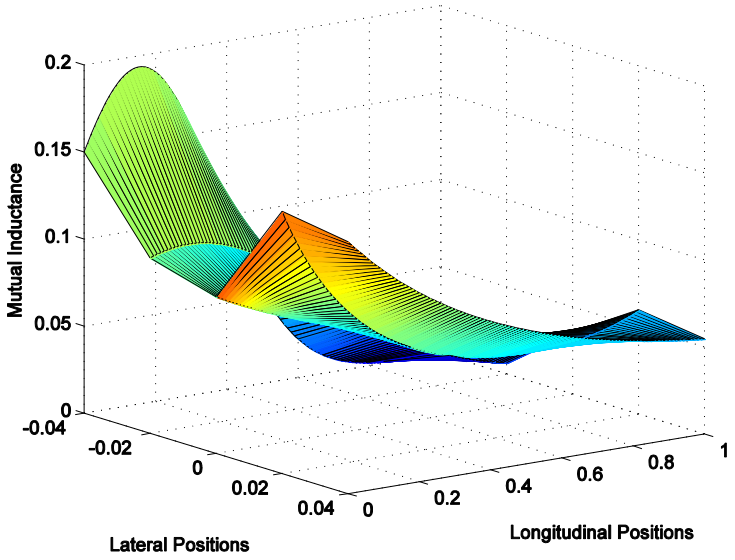

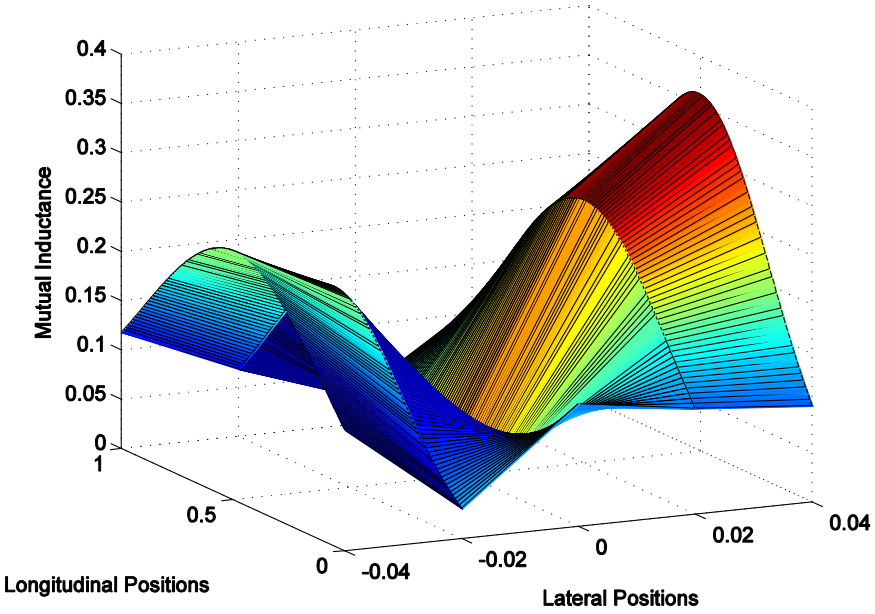

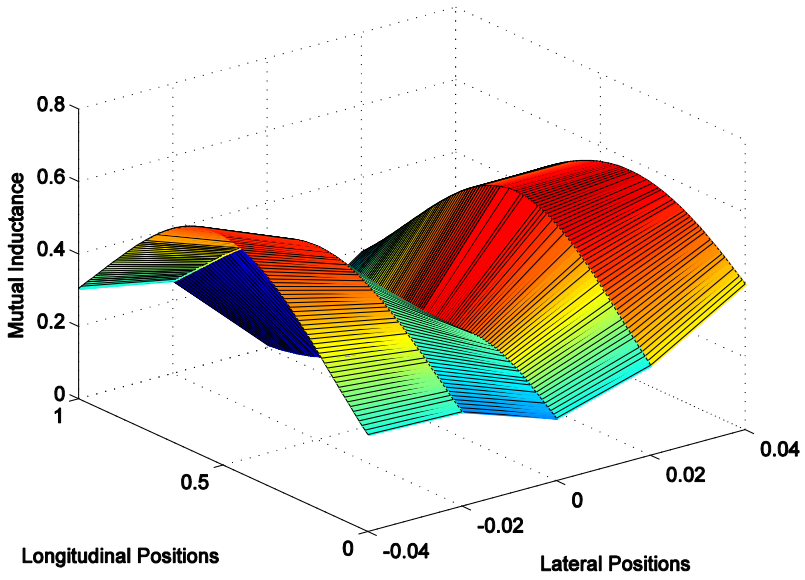

Figure 4-18 The variation in mutual inductance of the coils (1,2,4 loops) as a function of lateral and longitudinal position

It can be directly observed that in the well aligned position, the mutual inductance is the lowest and it has its maximum at the extremes on either side. Also, the mutual inductance rises from a minimum value and reaches a constant till it begins to drop as distance further increases.

4.6.7 Pickup with quadrature coil and study of lateral misalignment

A direct comparison of the variation in mutual inductance of both the horizontal and the vertical coils when subjected to lateral misalignment yields the result that a more flat mutual inductance profile can be obtained by direct flux addition. Thus, a setup was fabricated where the two coils were wound over the central limb of the E core and they could be interconnected either serially or parallel. This forms the secondary/pickup and the mutual inductance between the primary and the secondary can be obtained by interconnecting them suitably. These four choices of interconnection are shown in Figure 4-19.

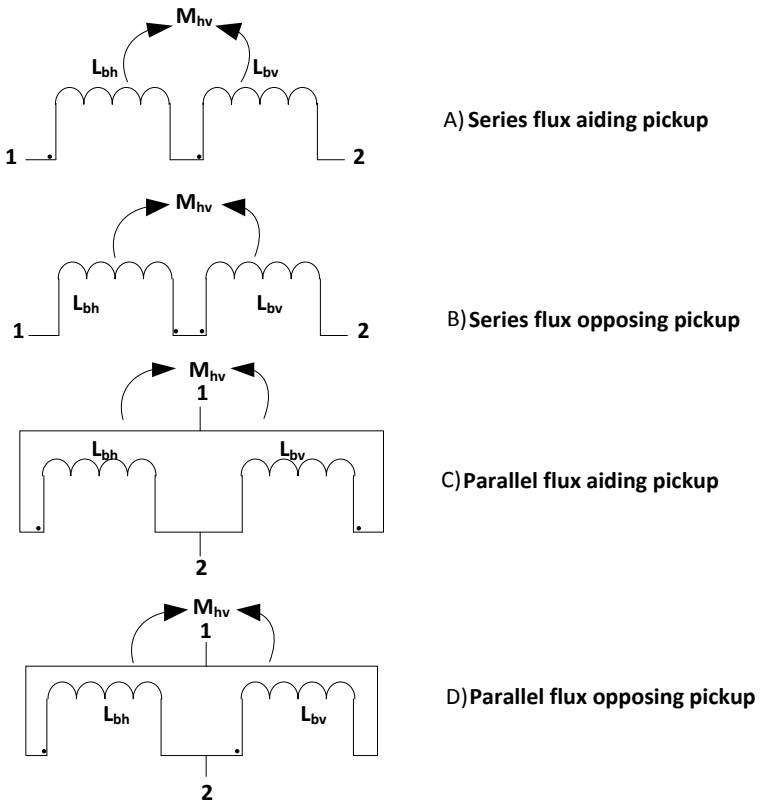

Figure 4-19 Interconnection between the windings of the pickup

The equivalent inductance obtained by interconnecting the primary with the secondary is tabulated in Table 10.

Table 10 Equivalent inductance of the secondary and its combination with primary

S/No	Type of configuration	Inductance (L_b=L_{12})	Equivalent Inductance on connection to the primary (L_{eq})
1.	A	$L_b = L_{bh} + L_{bv} + 2M_{hv}$	$L_{eq} = L_a + L_b \pm 2M$
2.	B	$L_b = L_{bh} + L_{bv} - 2M_{hv}$	$L_{eq} = L_a + L_b \pm 2M$
3.	C	$L_b = \frac{L_{bh}L_{bv} - M_{hv}^2}{L_{bh} + L_{bv} - 2M_{hv}}$	$L_{eq} = \frac{L_aL_b - M^2}{L_a + L_b \pm 2M}$
4.	D	$L_b = \frac{L_{bh}L_{bv} - M_{hv}^2}{L_{bh} + L_{bv} + 2M_{hv}}$	$L_{eq} = \frac{L_aL_b - M^2}{L_a + L_b \pm 2M}$

The mutual inductance as obtained for all the four configurations of the windings on the central limb of the E core when tested for lateral misalignment at the fag-end of the line (x=1m, as this would yield the worst case mutual inductance) with a primary coil having 5 turns.

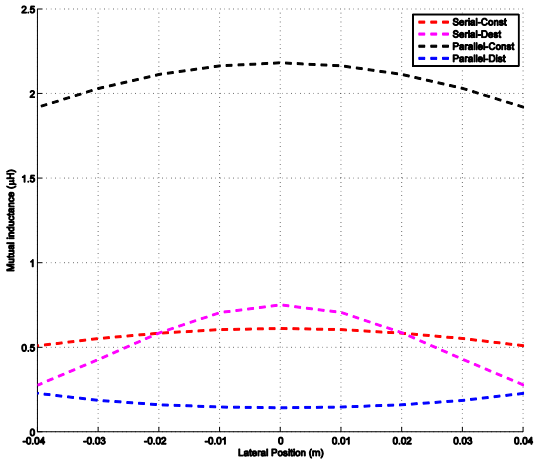

Figure 4-20 Variation of mutual inductance with lateral position

It was directly observed that the winding combination with flux construction seems to be the one in which the variation in mutual inductance as a function of lateral position is minimal. Out of the two possibilities for constructive flux addition, it is best to opt for parallel constructive addition as it shows higher mutual inductance with a much flatter variation in mutual inductance with lateral position.

4.6.8 Pickup with quadrature coil and study of longitudinal misalignment

In case of the quadrature coil, misalignment longitudinally would result in a more flatter power profile with characteristics intermediate between the case of longitudinal and lateral misalignment.

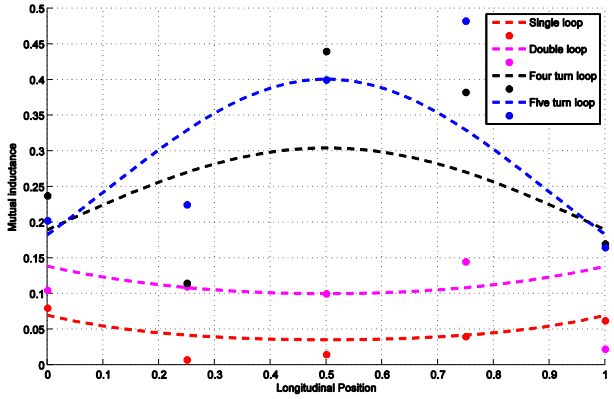

Figure 4-21 Variation of mutual inductance with longitudinal position for the quadrature coil

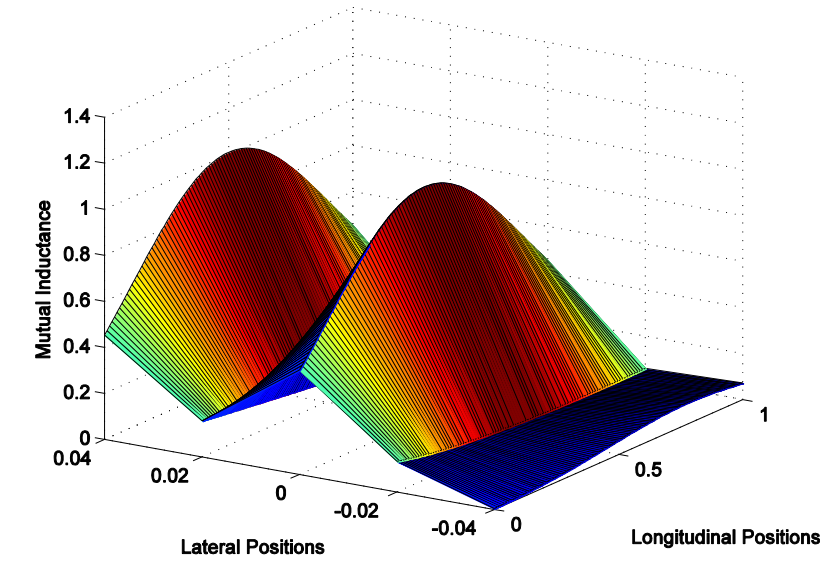
Mutual Inductance
1.4
1.2
1
0.8
0.6
0.4
0.2
0
0.04
0.02
0
-0.02
-0.04
Lateral Positions
0
0.5
1
Longitudinal Positions

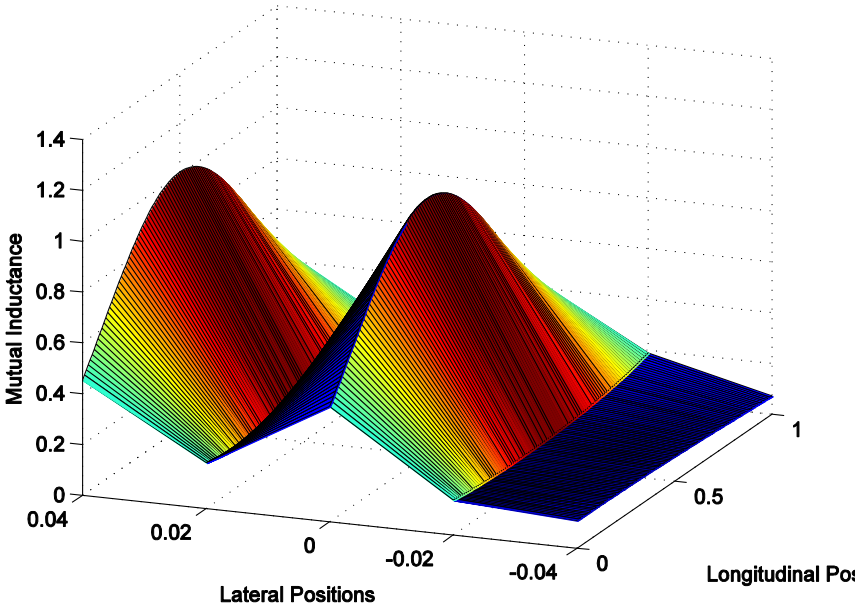
Mutual Inductance
1.4
1.2
1
0.8
0.6
0.4
0.2
0
0.04
0.02
0
-0.02
-0.04
Lateral Positions
0
0.5
1
Longitudinal Pos

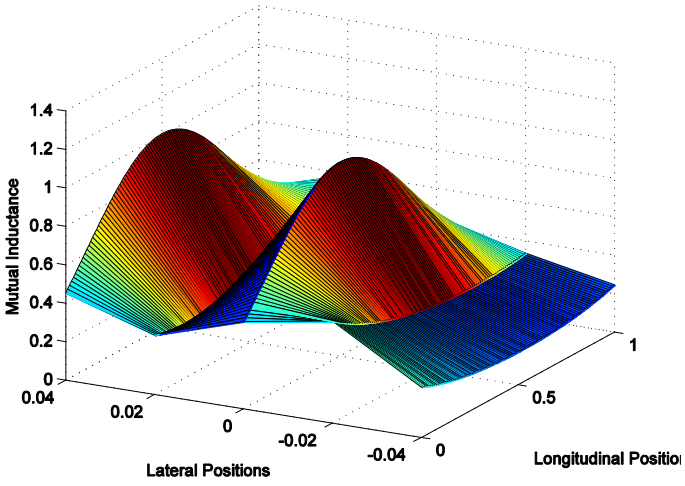

Figure 4-22 The variation in mutual inductance of the quadrature coil as a function of both lateral and longitudinal misalignment

It can be directly observed that the mutual inductance profile of the IPT system is improved as a result of addition of the quadrature coil.

4.7 Efficiency based optimization of the primary

In order to make a choice between the ideal number of turns of the primary for a fixed pickup, efficiency can be considered as the parameter to be optimized. It can be directly observed from Figure 4-6 that with an increased number of turns, the coil inductance increases. This would result in a better mutual inductance and hence power transfer. However, resistance of the circuit also increases as observed from Figure 4-7 and hence, the losses also increases. Therefore, an optimum can be observed for the number of turns for efficiency corresponding to a certain frequency of operation and for a fixed pickup.

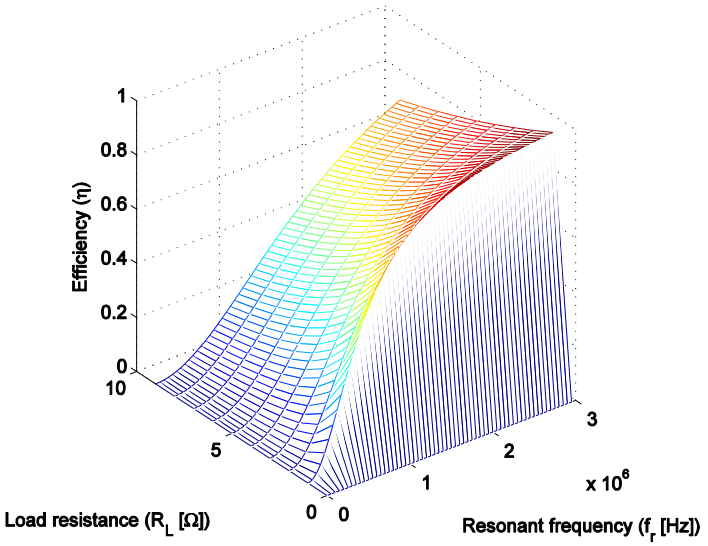

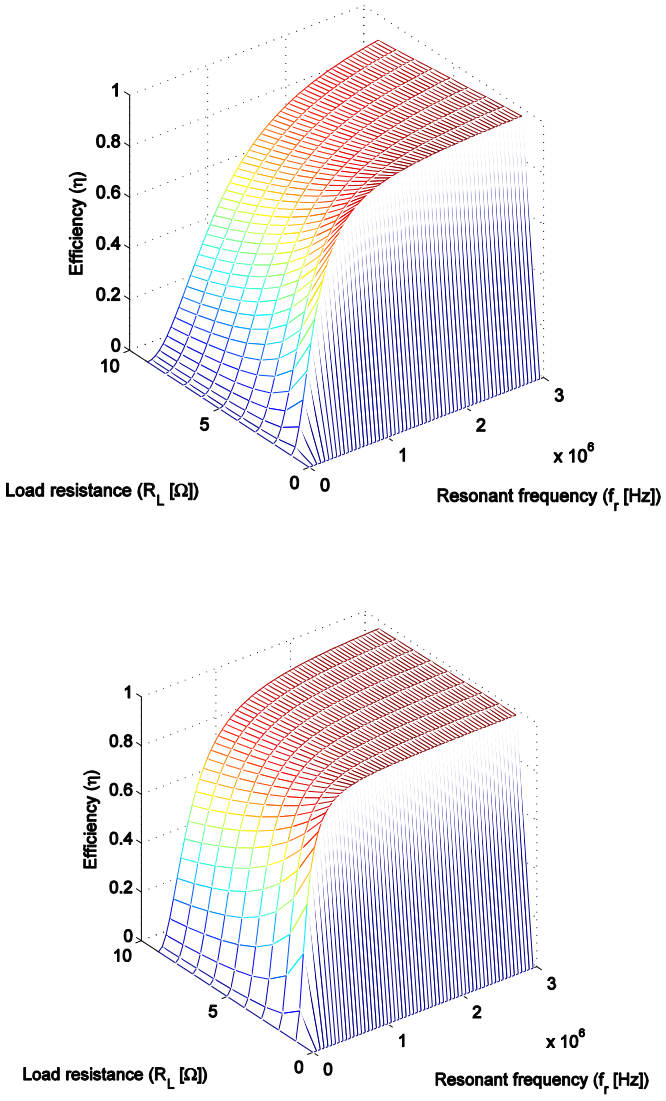

Figure 4-23 The variation in efficiency as a function of load resistance and resonant frequency for different turns of inductors (1, 2, 4)

A numerical listing of the essential parameters of the IPT transformer is tabulated in Table 11.

Table 11 Efficiency of the IPT transformer for different primaries

R_L=4Ω, f=1Mz, Quadrature coil in the pickup with 11 and 10 turns.		
S/No	Number of turns in the primary	Efficiency (%)
1.	1	37.95
2.	2	73.70
3.	4	92.95
4.	5	94.99

4.7.1 Choice of the primary for efficient power transfer

In order to make a choice, efficiency is considered keeping in mind very high levels of loading. This can be done by setting the load resistance to low values. A good choice for the load resistance in such a case can be R_L=0.01Ω. For this load, the efficiency is plotted as a function of resonant frequency for the various numbers of primary coils.

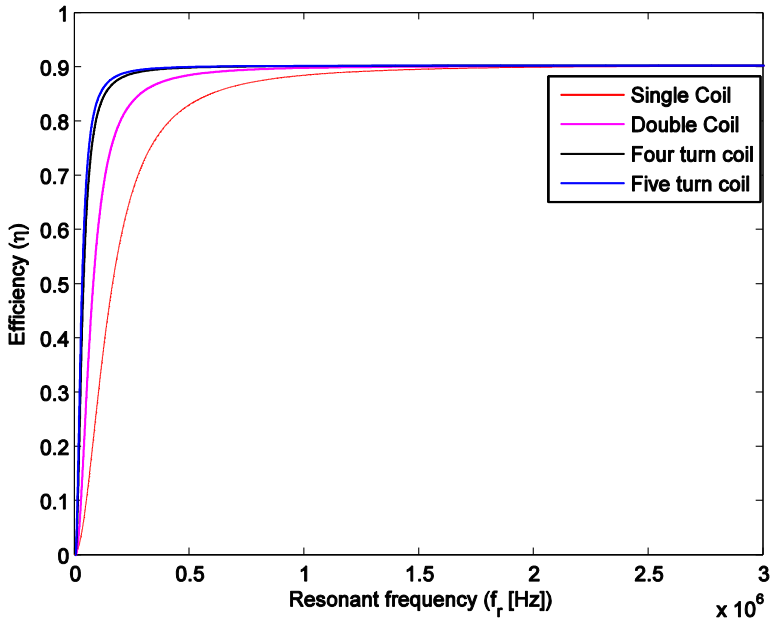

Figure 4-24 The variation in efficiency as a function of load resistance and resonant frequency

It can be directly observed that under high levels of loading (R_L=0.01) and at reasonably high frequencies (0.5-1.5 MHz), the two turn coil is as efficient as the single turn coil and hence, it would be advantageous to use the same. At higher frequencies (>2MHz), even the two turn coil is found to be as efficient as those with higher number of turns. However,

higher frequencies are restrictive in terms of the power electronic switches to be used at higher power levels, conducted EMI among other factors.

4.8 Conclusion

In order to study powering while driving, primary with different number of turns were constructed and a ferrite based pickup was constructed and misalignment was studied considering different positions both laterally as well as longitudinally. It was observed that the variation in mutual inductance due to lateral misalignment was different for the two types of coil used in the pickup. This would result in the fact that misalignment could be reduced by additive flux addition of the horizontal coil and the vertical coil of the pickup. An efficiency based optimization strategy was evolved so as to decide which primary coil could be used for efficient power transfer with minimal number of turns.

CHAPTER 5

MAGNETIC DESIGN OF THE PRIMARY

5.1 Introduction

In this chapter, the magnetic design aspects of an IPT system will be discussed. Conventional design of the primary consists of inductors with the pickup exposed to currents flowing in opposite directions. This configuration based on an E core would lead to maximum flux addition along the central limb. It is also possible to design inductors with currents flowing along the same direction and this would lead to flux cancellation along the central limb of the E core and flux addition in all other sections of the E core. These two configurations have been compared and investigated.

5.2 Magnetic design of the IPT system

In the design of the primary for the IPT, magnetic design and magnetic optimization plays a major role in deciding the type of core to be chosen and those sections where windings need to be housed. 2D Finite Element Method was used in order to compare two different configuration of inductors for the choice of a better solution for higher mutual inductance and hence the power transferred. The configuration of the coils and the direction of currents are shown in Figure 5-1.

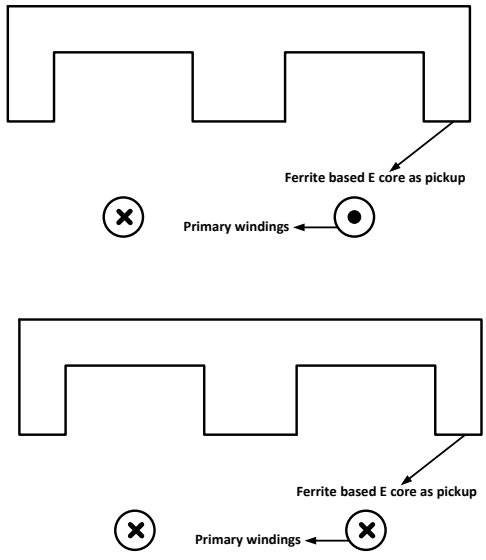

Figure 5-1 The two dimensional geometry of the primary and the core

5.3 Two dimensional FEM analysis

The two geometries of the model were simulated first in FEM using COMSOL Multiphysics 3.5a and the parameters as tabulated in Table 12 were used so as to simulate the real setup. The physical dimensions of the E core used were the same as described previously in Figure 4-2.

Table 12 Coil parameters and their magnitudes for the simulation

S/No.	Coil parameters	Magnitude
1.	Area (m^2)	3.795×10^{-6}
2.	Perimeter (m)	0.006909
3.	$J_{external}$(A/ m^2)	2.635×10^{6}

The differences can be obtained straightforwardly as indicated in Figure 5-2 and Figure 5-3. In case of currents flowing in the coil in the opposite direction, flux addition takes place at the central limb of the E-core. However, in case of currents flowing in the same direction, flux subtraction takes place at the central limb of the E-core.

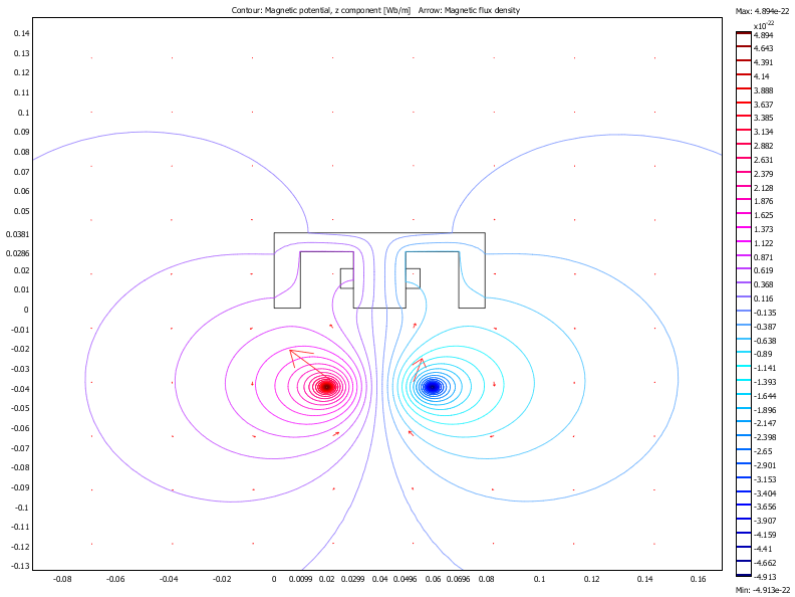

Figure 5-2 Flux lines for the case where coil currents are in the opposite direction

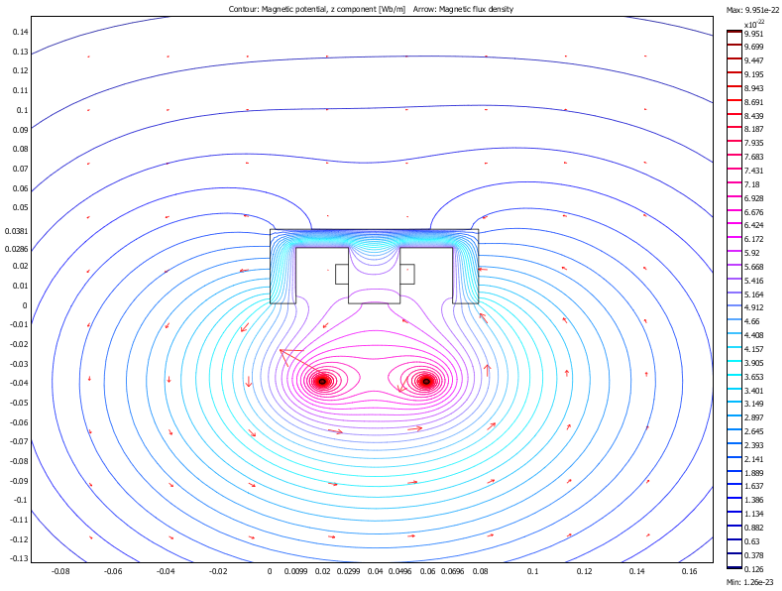

Figure 5-3 Flux lines for the case where coil currents are in the same direction

5.3.1 Replacing the E core with flat core for unidirectional currents

In case of unidirectional currents, a low reluctance path can be established by replacing the entire E core with a flat core placed at exactly the same displacement as the clearance between the bottom of the car and the ground. This setup is shown in Figure 5-4.

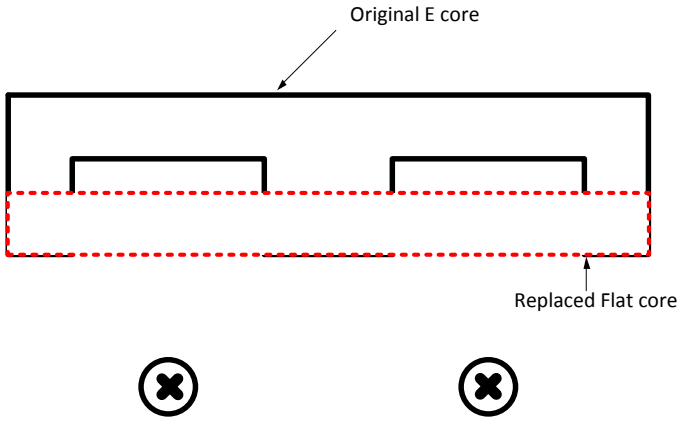

Figure 5-4 Arrangement in case of the replaced core

5.4 Simulation results from FEM Analysis

The geometry of the cores and the corresponding currents as in Table 12 is used to simulate the various possible configurations. A bar diagram representing the analyzed result is shown in Figure 5-5.

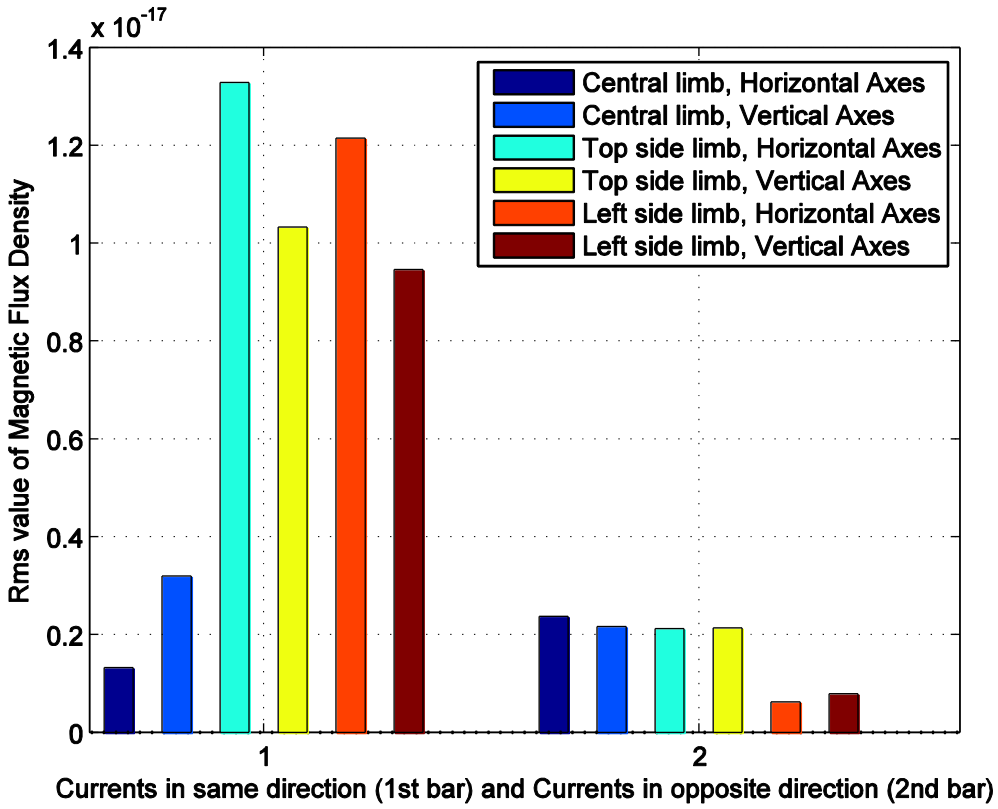

Figure 5-5 Bar diagram representation of the two configurations of inductors for E core

5.5 Experimental analysis of the inductor with unidirectional currents

For the experimentation, two novel inductors were designed with the parameters as tabulated in Table 13. This model is referred to as the "Double Lane Model". This is so because a single turn of the inductor so designed would yield two sections with unidirectional currents.

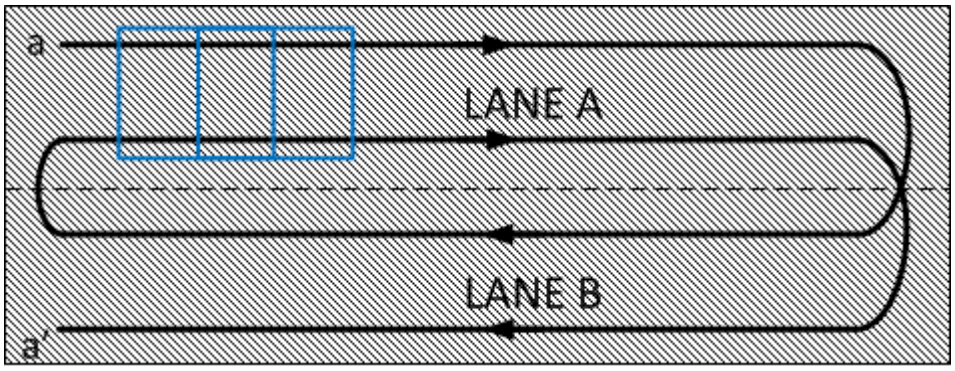

Figure 5-6 Double lane model of the IPT system

Table 13 Parameters of the novel unidirectional inductor

No. of turns	Resistance of the primary $(R_1, m\Omega)$	Inductance of the primary $(L_1, \mu H)$
1.	39.5	7.95
2.	73	25.59

5.6 Comparison of lateral misalignment

The variation in the Mutual Inductance with lateral position for the two inductor designs is as depicted in Figure 5-7. It is very clear that the absolute values of mutual inductances are higher in case of the novel primary inductor designed.

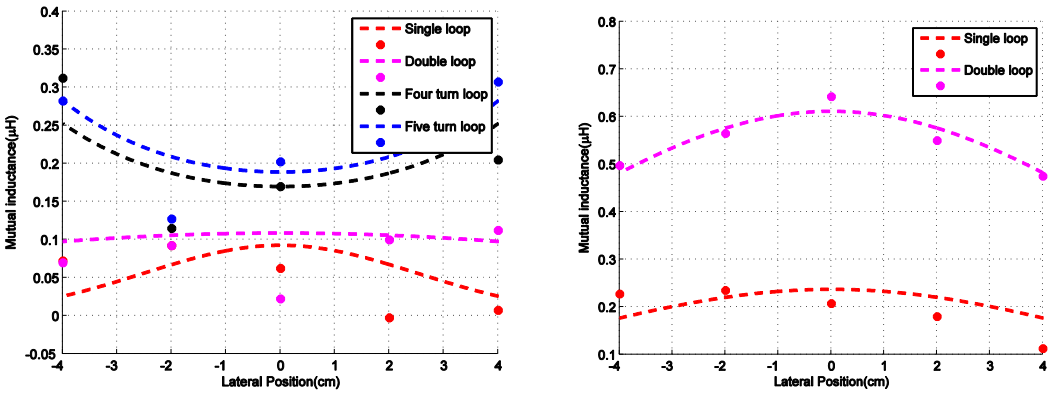

Figure 5-7 Mutual inductance variation as a function of lateral position (L-Opposing currents, R-Unidirectional currents)

5.6.1 Comparison of the two inductor configuration based on core utilization

In order to compare the two topologies, some of the parameters that are obtained from the FEM simulation are tabulated. A new parameter called core utilization factor, K_{core} defined in terms of the magnetic length of maximum flux lines (l_{mag}) and the total magnetic length of the core (l_{core}) is proposed in (44). The definition of core length is explained in Figure 5-8 and the the differences are tabulated in Table 14.

$$K_{core} = \frac{l_{mag}}{l_{core}} \tag{44}$$

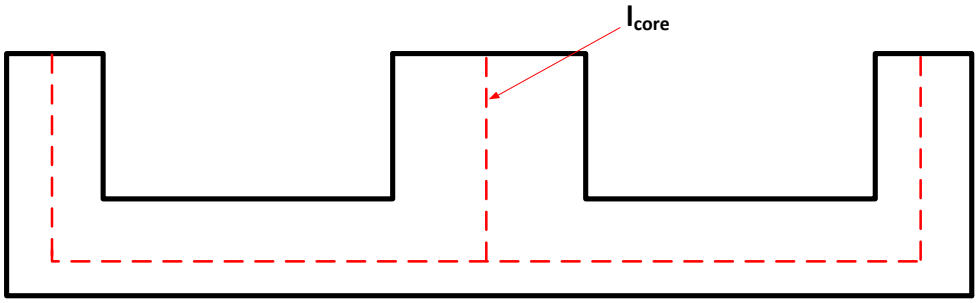

Figure 5-8 Definition of the core length for the Ecore

Table 14 Comparison of the two inductor configurations

S/No.	Current configuration - Ecore	K_{core}
1.	Same direction	0.1957
2.	Opposite direction	0.8042

5.7 Conclusion

FEM studies and experimental analysis on misalignment yield the result that in terms of mutual inductance and core utilization, the novel configuration of inductors proposed would fare much better compared to conventional inductors. This study proves that inductors designed with currents in the same direction would lead to a flux cancellation only at the center with the formation of a flux vortex or flux circulation and hence cores designed keeping in mind such a behavior would yield good power transfer results.

CHAPTER 6

CONCLUSIONS AND RECOMMENDATIONS

6.1 Conclusions

Electric mobility will see a rapid boost in popularity particularly due to the increasing social consciousness particularly related to the environment and also health. Also, the ever growing dependence on fossil fuels most of which are facing risk of complete depletion possibly in a few centuries adds to the list of problems.

The transition from HEVs to BEVs has already taken shape and a small number of fully electric cars are already available in the market – Mitsubishi i, Nissan Leaf, Tesla Roadster, Tesla Model S etc. This transition is quite important because a HEV still derives most of its power from petroleum and hence not the option as a sustainable mode of mobility. The development of BEVs have to be complemented by an increased penetration of renewable energy to form the solution to the global problem considering the fact that electricity largely remains "dirty" till date.

Within the domain of developments in EV technology, wireless power transfer is growing as an important technique owing particularly to the fact that it is safe, reliable and convenient. The elimination of messy cords and the fact that charging pads could be retrofitted below the chassis of existing cars also adds to an increased awareness in this domain.

This thesis was started keeping in mind various objectives mentioned in the introduction. This section would be a culmination of the various results that were obtained.

- A literature review of the different types of WPT was conducted and a discussion of the important types including IPT, CPT, MPT and LPT were discussed. Extensive research on IPT has been carried out.
- Design of an IPT system by looking into the transformer as an air-cored transformer and then appreciating the fact that resonant capacitive coupling can eliminate leakage and improve power transfer and efficiency. Efficiency based optimization of the transformer was undertaken so as to choose the frequency of operation that boosts efficiency. It can be generalized that an increase in frequency can lead to higher flux and hence better efficiency of power transfer. However, availability of switches at high power, switching losses of the inverter and EMC regulations affect the same conversely.

- Explained the effect that resonance has on the transferred power and the efficiency of power transfer. It can be generalized that resonances act in such a manner as to either increase or decrease the circuit impedance.
- It can also be generalized that the peak efficiency of secondary series topologies remain high and the power transferred by secondary parallel topologies is high.
- Dynamic charging / powering while driving with a number of distributed inductors were constructed and tested.
- Misalignment studies show that the variation in power can be drastic particularly when subjected to lateral misalignment.
- Longitudinal misalignment particularly in small sections can play a drastic role even if the pickup is well-aligned laterally. "Edge effect", referring to the unsymmetrical nature of mutual inductances at either ends of the inductor was studied and the reason for this behavior was investigated.
- Effect of quadrature coil on lateral misalignment was studied and it was observed that the parallel additive flux topology was the best in terms of both the absolute mutual inductances as well as for minimization of variation in mutual inductance laterally.
- A novel inductor configuration with currents flowing along the same direction was proposed. This configuration was tested experimentally as well as using FEM to compare with regular inductors.
- In case of opposing currents, the flux addition takes place at the central limb
- It was observed that when an E core is placed over currents flowing along the same direction, the flux assumes an oval circulation. This would imply that those sections of the core distinct from the central limb play an important role in the power transfer. In effect, a flat core would perform better than other cores.
- Core utilization factor would be a criterion to select the best core for such a dynamic charging scenario.

6.2 Recommendations and scope for future work

Over the course of research, a large number of domains were found that could be investigated particularly in relation to inductive power transfer. Some of the problems that could be identified for future research are listed in the following paragraphs.

Firstly, an algorithm and design flow for the entire system of IPT right from the selection of the coils to the inverter, compensation is essential.

Secondly, a self-tuning pickup which has only a single sensor that is proposed in this thesis could be constructed for different topologies and the theory could be verified.

Thirdly, in the domain of dynamic charging, extensive three dimensional FEM models could be used to study the magnetic fields and optimize the IPT transformer including the primary coil as well as the Ferrite.

Next, high power, high efficiency inverters switching at 100s of kHz need to be designed so as to transfer power efficiently particularly when coupling is poor such as the case with dynamic charging. The use of SiC and GaN switches can be looked into.

Finally, new converter topologies for minimizing THD and operation at upf can be looked into.

References

[1] W.C. Brown, "The history of wireless power transmission," *Solar Energy*, vol.56, no.1, pp. 3-21, Jan. 1996

[2] Chao Liu; Hu, A.P.; Nair, N.K.C.; Covic, G.A.; , "2-D alignment analysis of capacitively coupled contactless power transfer systems," *Energy Conversion Congress and Exposition (ECCE), 2010 IEEE* , vol., no., pp.652-657, 12-16 Sept. 2010

[3] Geoffrey A. Landis; , "RE-Evaluating Satellite Solar Power Systems for Earth," *Photovoltaic Energy Conversion, Conference Record of the 2006 IEEE 4th World Conference on* , vol.2, no., pp.1939-1942, May 2006

[4] PATH team, "Roadway Powered Electric Vehicle Project Parametric Studies: Phase 3D Final Report," California Partners for Advanced Transit and Highways Research Report, Oct. 1996

[5] Kobayashi, K.; Yoshida, N.; Kamiya, Y.; Daisho, Y.; Takahashi, S.; , "Development of a non-contact rapid charging inductive power supply system for electric-driven vehicles," *Vehicle Power and Propulsion Conference (VPPC), 2010 IEEE* , vol., no., pp.1-6, 1-3 Sept. 2010

[6] Sungwoo Lee; Jin Huh; Changbyung Park; Nam-Sup Choi; Gyu-Hyeoung Cho; Chun-Taek Rim; , "On-Line Electric Vehicle using inductive power transfer system," *Energy Conversion Congress and Exposition (ECCE), 2010 IEEE* , vol., no., pp.1598-1601, 12-16 Sept. 2010

[7] R. Balog, P. T. Krein, D. Hamill, "Coupled inductors -- a basic filter building block," in *Proc. Electrical Manufacturing and Coil Winding Ass'n.*, 2000, pp. 217-278

[8] N.G. Hingorani, L. Gyugyi, Understanding FACTS, Concepts and Technology of Flexible AC Transmission systems, IEEE Press 2000

[9] Chopra, S.; Bauer, P.; , "Analysis and design considerations for a contactless power transfer system," *Telecommunications Energy Conference (INTELEC), 2011 IEEE 33rd International* , vol., no., pp.1-6, 9-13 Oct. 2011

[10] Chopra, S.; "Contactless power transfer for electric vehicle charging application", TU Delft Institutional Repository, Aug. 2011

[11] Elliott, G.; Raabe, S.; Covic, G.A.; Boys, J.T.; , "Multiphase Pickups for Large Lateral Tolerance Contactless Power-Transfer Systems," *Industrial Electronics, IEEE Transactions on* , vol.57, no.5, pp.1590-1598, May 2010

[12] Stielau, O.H.; Covic, G.A.; , "Design of loosely coupled inductive power transfer systems," Power System Technology, 2000. Proceedings. PowerCon 2000. International Conference on , vol.1, no., pp.85-90 vol.1, 2000

[13] Chwei-Sen Wang; Stielau, O.H.; Covic, G.A.; , "Design considerations for a contactless electric vehicle battery charger," *Industrial Electronics, IEEE Transactions on* , vol.52, no.5, pp. 1308- 1314, Oct. 2005

[14] Sallan, J.; Villa, J.L.; Llombart, A.; Sanz, J.F.; , "Optimal Design of ICPT Systems Applied to Electric Vehicle Battery Charge," *Industrial Electronics, IEEE Transactions on* , vol.56, no.6, pp.2140-2149, June 2009

[15] Juan Luis Villa, Jesús Sallán, Andrés Llombart, José Fco Sanz, Design of a high frequency Inductively Coupled Power Transfer system for electric vehicle battery charge, Applied Energy, Volume 86, Issue 3, March 2009, Pages 355-363, ISSN 0306-2619, 10.1016/j.apenergy.2008.05.009.

[16] Villa, J.L.; Sallan, J.; Sanz Osorio, J.F.; Llombart, A.; , "High-Misalignment Tolerant Compensation Topology For ICPT Systems," *Industrial Electronics, IEEE Transactions on* , vol.59, no.2, pp.945-951, Feb. 2012

[17] Boys, J. T.; Elliott, G. A. J.; Covic, G. A.; , "An Appropriate Magnetic Coupling Co-Efficient for the Design and Comparison of ICPT Pickups," *Power Electronics, IEEE Transactions on* , vol.22, no.1, pp.333-335, Jan. 2007

[18] Li, H.L.; Hu, A.P.; Covic, G.A.; Tang, C.S.; , "Optimal coupling condition of IPT system for achieving maximum power transfer," *Electronics Letters* , vol.45, no.1, pp.76-77, January 1 2009

[19] Chwei-Sen Wang; Covic, G.A.; Stielau, O.H.; , "General stability criterions for zero phase angle controlled loosely coupled inductive power transfer systems," *Industrial Electronics Society, 2001. IECON '01. The 27th Annual Conference of the IEEE* , vol.2, no., pp.1049-1054 vol.2, 2001

[20] M. Sugimoto, "The past, present, and future of ferrites", *J. Amer. Ceram. Soc.*, vol. 82, no. 2, pp.269 - 277 1999

[21] Heeres, B.J.; Novotny, D.W.; Divan, D.M.; Lorenz, R.D.; , "Contactless underwater power delivery," *Power Electronics Specialists Conference, PESC '94 Record., 25th Annual IEEE* , vol., no., pp.418-423 vol.1, 20-25 Jun 1994

[22] Abe, H.; Sakamoto, H.; Harada, K.; , "A noncontact charger using a resonant converter with parallel capacitor of the secondary coil," *Industry Applications, IEEE Transactions on* , vol.36, no.2, pp.444-451, Mar/Apr 2000

[23] Yungtaek Jang; Jovanovic, M.M.; , "A contactless electrical energy transmission system for portable-telephone battery chargers," *Industrial Electronics, IEEE Transactions on* , vol.50, no.3, pp. 520- 527, June 2003

[24] Budhia, M.; Covic, G.A.; Boys, J.T.; , "Design and optimisation of magnetic structures for lumped Inductive Power Transfer systems," *Energy Conversion Congress and Exposition, 2009. ECCE 2009. IEEE* , vol., no., pp.2081-2088, 20-24 Sept. 200

[25] Covic, G.A.; Boys, J.T.; Kissin, M.L.G.; Lu, H.G.; , "A Three-Phase Inductive Power Transfer System for Roadway-Powered Vehicles," *Industrial Electronics, IEEE Transactions on* , vol.54, no.6, pp.3370-3378, Dec. 2007

[26] Budhia, M.; Covic, G.A.; Boys, J.T.; Chang-Yu Huang; , "Development and evaluation of single sided flux couplers for contactless electric vehicle charging," *Energy Conversion Congress and Exposition (ECCE), 2011 IEEE* , vol., no., pp.614-621, 17-22 Sept. 2011

[27] Keeling, N.; Covic, G.A.; Hao, F.; George, L.; Boys, J.T.; , "Variable tuning in LCL compensated contactless power transfer pickups," *Energy Conversion Congress and Exposition, 2009. ECCE 2009. IEEE* , vol., no., pp.1826-1832, 20-24 Sept. 2009

[28] Kacprzak, D.; , "A Novel S-Pickup for High Power Inductive Power Transfer Systems," *Magnetics Conference, 2006. INTERMAG 2006. IEEE International* , vol., no., pp.204, 8-12 May 2006 doi: 10.1109/INTMAG.2006.375786

[29] Budhia, M.; Covic, G.; Boys, J.; , "Magnetic design of a three-phase Inductive Power Transfer system for roadway powered Electric Vehicles," *Vehicle Power and Propulsion Conference (VPPC), 2010 IEEE* , vol., no., pp.1-6, 1-3 Sept. 2010

[30] Wu, H.H., Gilchrist, A., Sealy, K., Israelsen, P., Muhs, J., "A review on inductive charging for electric vehicles", *Electric Machines & Drives Conference (IEMDC), 2011 IEEE International,* On page(s): 143 – 147

[31] J. L. Villa, J. Sallán, A. Llombart and J. F. Sanz, "Design of a high frequency Inductively Coupled Power Transfer system for electric vehicle battery charge," Applied Energy, vol. 86, no. 3, pp. 355-363, 2009

[32] Kissin, M.L.G., Boys, J.T., Covic, G.A., "Interphase Mutual Inductance in Polyphase Inductive Power Transfer Systems", *Industrial Electronics, IEEE Transactions on,* On page(s): 2393 - 2400 Volume: 56, Issue: 7, July 2009

[33] Sibué, J.-R., Ferrieux, J.-P., Meunier, G., Périot, R., "Modeling of large air gap transformers using magnetic equivalent circuit for designing of high power application", *Electromagnetic Field Computation (CEFC), 2010 14th Biennial IEEE Conference on,* On page(s): 1 – 1

[34] Judek, S., Karwowski, K., "Analysis of inductive power transfer systems for variable air gap and voltage supply frequency", *Industrial Electronics (ISIE), 2011 IEEE International Symposium on,* On page(s): 1963 – 1968

[35] Chwei-Sen Wang; Covic, G.A.; Stielau, O.H.; , "Investigating an LCL load resonant inverter for inductive power transfer applications," *Power Electronics, IEEE Transactions on* , vol.19, no.4, pp. 995-1002, July 2004

[36] S. Dieckerhoff, M. J. Ruan, and R. W. De Doncker, "Design of an IGBT-based LCL-resonant inverter for high-frequency induction heating", *Proc. IEEE Industry Applications Conf.*, vol. 3, pp.2039 -2045 1999

[37] T. Bieler, M. Perrottet, V. Nguyen, and Y. Perriard, "Contactless power and information transmission", *Proc. IEEE Industry Applications Conf.*, vol. 1, pp.83 -88 2001

[38] Chwei-Sen Wang, Covic, G.A., Stielau, O.H., "Investigating an LCL load resonant inverter for inductive power transfer applications", *Power Electronics, IEEE Transactions on,* On page(s): 995 - 1002 Volume: 19, Issue: 4, July 2004

[39] Chwei-Sen Wang, Stielau, O.H., Covic, G.A., "Design considerations for a contactless electric vehicle battery charger", *Industrial Electronics, IEEE Transactions on,* On page(s): 1308 - 1314 Volume: 52, Issue: 5, Oct. 2005

[40] Raabe, S., Boys, J.T., Covic, G.A., "A high power coaxial inductive power transfer pickup", *Power Electronics Specialists Conference, 2008. PESC 2008. IEEE,* On page(s): 4320 – 4325

[41] Elliott, G.A.J., Covic, G.A., Kacprzak, D., Boys, J.T., "A New Concept: Asymmetrical Pick-Ups for Inductively Coupled Power Transfer Monorail Systems", *Magnetics, IEEE Transactions on,* On page(s): 3389 - 3391 Volume: 42, Issue: 10, Oct. 2006

Appendix A- IEEE Paper

Paper Title: Design of Inductive Power Transfer Systems – Study of Resonances

Authors: Venugopal Prasanth, Swagat Chopra, Pavol Bauer

Design of Inductive Power Transfer Systems – Study of Resonances

Venugopal Prasanth, Swagat Chopra, Pavol Bauer, *Senior Member IEEE*
Department of Electrical Sustainable Energy
Delft University of Technology, Mekelweg 4, 2628 CD
Delft, The Netherlands
P.Bauer@tudelft.nl

***Abstract*—Inductive Power Transfer (IPT) systems, that transfer power wirelessly from a primary coil onto a secondary coil, have been in study for several decades. However, the effect that resonance has on the various parameters of the coils has not been documented clearly. This paper tries to explain this effect by looking at the IPT system as an air-cored transformer . It then describes a novel method to decide the central parameter, the frequency of operation once an air cored transformer has been constructed. This is followed by a study on the effect that the various compensation topologies have on the transformer parameters. Finally, a comparison between the various basic topologies has been brought to light, so as to make a decision based on a number of possible criteria.**

Keywords-Inductive Power Transfer (IPT), wireless, resonance, basic topologies.

I. INTRODUCTION

IPT systems have seen a rapid increase in commercialization, particularly in the last two decades. Such systems have also seen an increased growth in the number of their applications such as clean room systems, material handling systems [1], compact electronic devices [2], mobile phones [3], biomedical implants [4], contactless under water power delivery [5] and electric mobility [6, 9] among many others.

An air cored transformer is characterized by a primary winding that has a resistance, R_1 and a self-inductance, L_1. Similarly, the secondary coil is characterized by a winding resistance, R_2 and a self-inductance, L_2. When such a primary is excited by a sinusoidal voltage source, V_1 of angular frequency, ω and brought closer to the secondary, a part of the primary current is used to set up the mutual flux, φ_m and the rest forms the leakage flux of the primary, φ_p. The mutual flux is that part of the flux that links both the primary and secondary and is produced by the combined effect of both the primary current I_p and secondary current I_s. Moreover, the secondary current is also subjected to leakage and is represented by the leakage flux of the secondary, φ_s. This has been represented diagrammatically in Figure 1. Thus, according to the theory of coupled inductors, when the primary is excited and the two coils are magnetically coupled, the self-inductance of the primary (L_1) results in a mutual inductance (M) and a series inductance (L_a). Also, the secondary self-inductance results in a series inductance (L_b) and the mutual inductance (M).

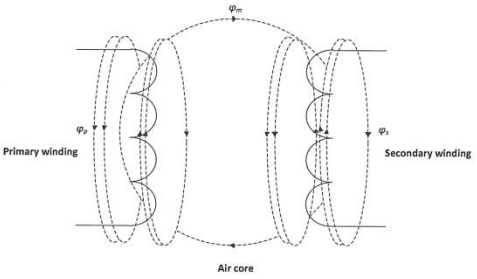

Figure 1. Flux linkage in an air cored transformer

This understanding can be transformed into an equivalent circuit by making use of the theory of coupled inductors [10]. This has been represented in Figure 2.

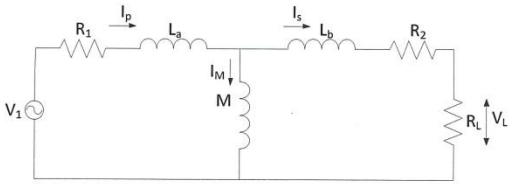

Figure 2. Equivalent circuit of an air cored transformer

A general description of the design of ICPT systems has been dealt with in [7]. A more detailed description of the design of IPT systems has been described in [8]. In [6], apart from a description of design, a comparison of topologies has been undertaken. However, in these descriptions, the effect of resonance on the system parameters have not been explained. This paper intends to look into the IPT system first as a simple air core transformer and then evolve a technique to compute the frequency of operation so as to maximize the power transferred (Section II, Section III). Then, the various compensation topologies and their parameters are derived and their effect at resonance is explained (Section IV). Next, efficiency is taken as a parameter for optimization of frequency and simulation of all the topologies has been carried out to

explain the resonance using the selected frequency (Section V). Finally, the compensation techniques are compared based on a number of criteria (Section VI).

II. Analysis of Air Cored Transformer

From the equivalent circuit in Figure 2, it can be directly obtained that the equivalent impedance of the air cored transformer is

$$Z_{eq} = R_1 + j\omega(L_a + M) + \left(\frac{\omega^2 M^2}{R_2 + R_L + j\omega(L_b + M)}\right) \quad (1)$$

The air cored transformer can be characterized by the current division ratio, k_c. This is given by :

$$k_c = \mathrm{Re}\left(\frac{I_s}{I_p}\right) = \mathrm{Re}\left(\frac{j\omega M}{R_2 + R_L + j\omega(L_b + M)}\right) \quad (2)$$

This current division ratio will begin to saturate after the frequency exceeds a threshold. The condition for this saturation can be derived as when $\omega M >> (R_2 + R_L)$. Also, the current division ratio on saturation is obtained as

$$k_{c(sat)} = \frac{M}{(L_b + M)} \quad (3)$$

Thus, it is possible to theorize that an air cored transformer will exhibit a threshold frequency at which it produces maximum secondary current for a given primary current obtained by fixing a primary voltage. This is taken as the first step in fixing the frequency of operation following the physical design of an air cored transformer.

III. Laboratory Test Setup

The laboratory test setup that was designed and constructed at the TU Delft [9] is shown in Figure 3. Further, the transformer was made of Litz wire, therefore, the measured physical parameters are tabulated in Table 1.

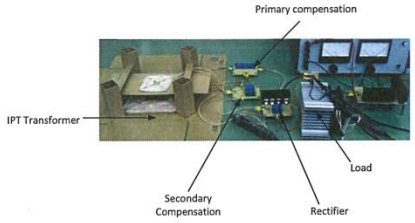

Figure 3. IPT system test setup for wireless power transfer

TABLE I. Physical parameters of the IPT system

Physical parameters	Measured values
Leakage inductance of primary	103.4 µH
Leakage inductance of secondary	12.67 µH
Mutual inductance	6.02 µH
DC resistance of primary	0.153 Ω
DC resistance of secondary	0.066 Ω

From the theory developed in Section II, and using the parameters in Table I, the variation of the current division ratio k_c as a function of frequency can be observed in Figure 4 and Figure 5.

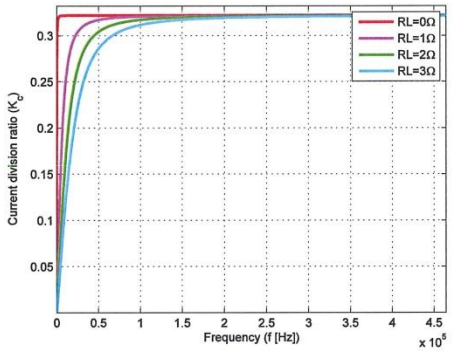

Figure 4. Variation of current division ratio as a function of frequency for different loads and M=6.02 µH

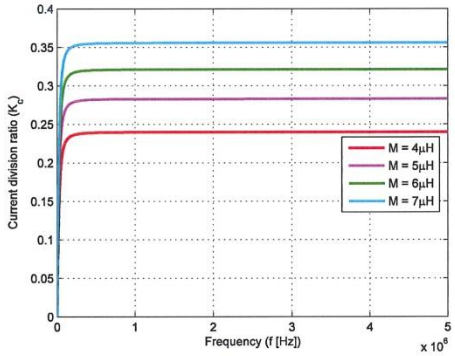

Figure 5. Variation of current division ratio as a function of frequency for different mutual inductances at $R_L = 3\Omega$

It can be observed from the above figures that the current division ratio, k_c increases with increase in frequency and saturates after reaching the knee-point frequency (threshold). For a given coil pair (M=a constant), the current division ratio is an indirect indication of coupling and hence efficiency. The various parameters calculated using (3) and its condition are tabulated in Table II.

TABLE II. CALCULATION OF THRESHOLD FREQUENCY

M = 6.02 µH, L_b = 12.67 µH, R_2 = 0.066 Ω			
S/No.	*R_L(Ω)*	*Threshold frequency (kHz)*	*$K_{c(sat)}$*
1.	0	1.745	0.3221
2.	1	28.183	
3.	2	54.62	
4.	3	81.058	

Table II gives a minimum frequency value beyond which the operation of the air-cored transformer would yield maximum power. Thus, the lower limit of the frequency can be fixed from the above analysis.

IV. ANALYSIS OF COMPENSATION TOPOLOGIES

Due to the large leakage inductances associated with both the primary and secondary, an air-cored transformer suffers from poor efficiency. An intelligent method to circumvent this problem is to compensate the reactive currents by using capacitors. The technique of compensation and the guidelines for the choice of capacitors are well explained in [6]. According to literature, the four basic topologies for IPT are :

- SS Topology (Primary Series, Secondary Series)
- SP Topology (Primary Series, Secondary Parallel)
- PS Topology (Primary Parallel, Secondary Series)
- PP Topology(Primary Parallel, Secondary Parallel)

Figure 6 shows the basic compensation topologies.

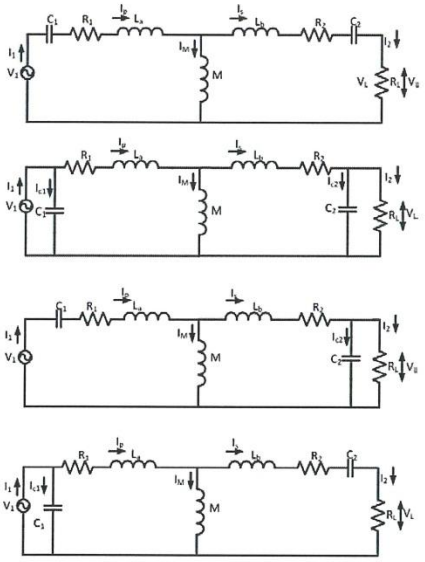

Figure 6. The basic compensation topologies - (SS, PP, SP and PS)

A detailed derivation of the various parameters have been conducted in [9]. It would however be interesting to also consider the impedance at resonance, knowing well that the circuit at resonance has an impedance with only the real part. This has been tabulated in Table III.

$$Z_{eq(topology,\ \omega=\omega_0)} = Re\left(Z_{eq(topology)}\right) \qquad (4)$$

TABLE III. EQUIVALENT IMPEDANCES AT RESONANCE FOR SERIES AND PARALLEL TOPOLOGIES

Topology type	Equivalent Impedance at Resonance
SS	$\left(\frac{M^2\omega^2}{R_2+R_L}\right)+R_1$
SP	$\left(\frac{M^2\omega^2\left(R_2+\frac{R_L}{1+(R_LC_2\omega)^2}\right)}{\left(R_2+\frac{R_L}{1+(R_LC_2\omega)^2}\right)^2+\left(\omega(L_b+M)-\frac{(R_L^2C_2\omega)}{1+(R_LC_2\omega)^2}\right)^2}\right)+R_1$

Topology type	Equivalent Impedance at Resonance
PS	$\frac{k_2\left(R_1+\frac{R_2+R_L}{k_1\left((R_2+R_L)^2+\left(\omega L_b-\frac{1}{\omega C_2}\right)^2\right)}\right)}{\left(R_1+\frac{R_2+R_L}{k_1\left((R_2+R_L)^2+\left(\omega L_b-\frac{1}{\omega C_2}\right)^2\right)}\right)^2+\left(\omega L_a-\omega C_1+\frac{\left(\omega L_b-\frac{1}{\omega C_2}\right)}{(R_2+R_L)^2+\left(\omega L_b-\frac{1}{\omega C_2}\right)^2}\right)^2}$ $k_2=\left(R_1+\frac{\left(\frac{R_2+R_L}{(R_2+R_L)^2+\left(\omega L_b-\frac{1}{\omega C_2}\right)^2}\right)}{k_1}\right)^2+\left(\omega L_a+\frac{\frac{1}{\omega M}+\frac{\left(\omega L_b-\frac{1}{\omega C_2}\right)}{(R_2+R_L)^2+\left(\omega L_b-\frac{1}{\omega C_2}\right)^2}}{k_1}\right)^2$ $k_1=\left[\left(\frac{R_2+R_L}{(R_2+R_L)^2+\left(\omega L_b-\frac{1}{\omega C_2}\right)^2}\right)^2+\left(\frac{1}{\omega M}+\frac{\left(\omega L_b-\frac{1}{\omega C_2}\right)}{(R_2+R_L)^2+\left(\omega L_b-\frac{1}{\omega C_2}\right)^2}\right)^2\right]$
PP	$\frac{\frac{R_1}{k_3}+\frac{R_2}{k_1k_2k_3}+\frac{\frac{1}{R_L}}{\left(\left(\frac{1}{R_L}\right)^2+(\omega C_2)^2\right)(k_1k_2k_3)}}{k_4}$ $k_4=\left(\frac{R_1}{k_3}+\frac{R_2}{k_1k_2k_3}+\frac{\frac{1}{R_L}}{\left(\left(\frac{1}{R_L}\right)^2+(\omega C_2)^2\right)(k_1k_2k_3)}\right)^2+\left(\frac{1}{\omega M(k_2k_3)}+\frac{\omega L_b}{(k_1k_2k_3)}-\frac{\omega C_2}{(k_1k_2k_3)\left(\left(\frac{1}{R_L}\right)^2+(\omega C_2)^2\right)}+\frac{\omega L_a}{k_3}-\omega C_1\right)^2$ $k_3=\left(R_1+\left(\frac{R_2+\frac{\frac{1}{R_L}}{\left(\frac{1}{R_L}\right)^2+(\omega C_2)^2}}{k_1k_2}\right)\right)^2+\left(\omega L_a+\frac{1}{k_2}\left(\frac{\omega L_b-\frac{\omega C_2}{\left(\frac{1}{R_L}\right)^2+(\omega C_2)^2}}{k_1}+\right.\right.$

$$\left.\left.\frac{1}{\omega M}\right)\right)^2$$

$$k_2 = \left(\frac{R_2+\frac{\frac{1}{R_L}}{\left(\left(\frac{1}{R_L}\right)^2+(\omega C_2)^2\right)}}{k_1}\right)^2 + \left(\frac{\left(\omega L_b-\frac{\omega C_2}{\left(\frac{1}{R_L}\right)^2+(\omega C_2)^2}\right)}{k_1}+\frac{1}{\omega M}\right)^2$$

$$k_1 = \left(R_2+\frac{\frac{1}{R_L}}{\left(\left(\frac{1}{R_L}\right)^2+(\omega C_2)^2\right)}\right)^2 + \left(\frac{\left(\omega L_b-\frac{1}{\omega C_2}\right)}{(R_2+R_L)^2+\left(\omega L_b-\frac{1}{\omega C_2}\right)^2}\right)^2$$

To understand the effect of resonance, the complex impedances were simulated in MATLAB and the results of the simulation are presented in Figures 7 and 8.

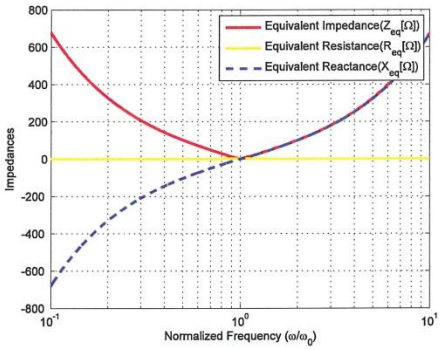

Figure 7. Effect of resonance on primary series topologies (SS and SP)

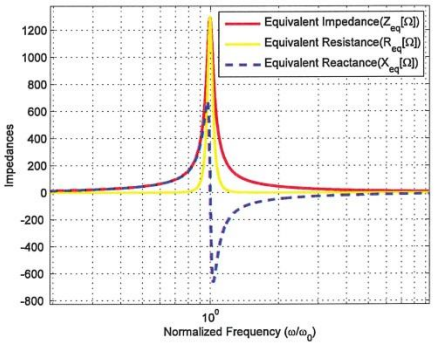

Figure 8. Effect of resonance on primary parallel topologies (PS and PP)

A. Discussion on the effect of resonance on the topologies

- In case of the Primary Series compensated topologies, the compensated air cored transformer shifts from a capacitive circuit at low frequencies to an inductive circuit at higher frequencies. Resonance occurs at the point where the capacitive and inductive reactance's become equal and cancel each other. A very peculiar feature that can be observed is the fact that the equivalent resistance for all variations in the frequency becomes independent of frequency.
- In case of primary parallel compensated topologies, the compensated air cored transformer shifts from an inductive circuit at lower frequencies to a capacitive circuit at higher frequencies. However, a major difference between the parallel and series compensated topologies is the fact that the equivalent resistance of the IPT transformer peaks at the resonant frequency and hence the impedance reaches a peak at the same frequency.

B. Discussion on a source change in the equivalent circuit

The difference in resonance between the Primary Series and Primary Parallel topologies makes it apparent that the PP and PS topologies need to be sourced by a current source in order to transfer power effectively. Hence, the authors wish to make the change as indicated in Figure 9 to the topology as used so far [6,9].

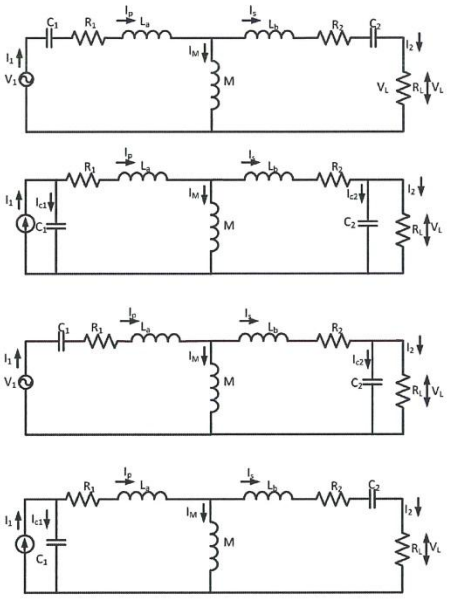

Figure 9. Proposed change in the equivalent circuit for IPT - (SS, PP, SP and PS)

V. Optimization of Compensation Topologies

The efficiency of an air-cored transformer with the equivalent circuit in Figure 2 is given by

$$\eta = \frac{R_L I_s^2}{R_L I_s^2 + R_2 I_s^2 + R_1 I_p^2} \quad (5)$$

Thus, it can be observed that

$$\eta = func(f, R_L) \quad (6)$$

The condition for optimization can be fixed by considering the frequency of operation at the point where the incremental change in efficiency with frequency for a particular load becomes small.

$$\left(\frac{\partial \eta}{\partial f}\right)_{R_L = const} \cong 0 \quad (7)$$

This being the case, simulation studies were carried out for all the basic topologies, in order to gain insight into the variation in the parameters during resonance. The parameters as tabulated in Table I were used to simulate the behavior of the various compensation topologies. Also, the following assumptions were considered while performing the simulation:

- Skin effect was considered at every frequency of operation.
- Proximity effect was not considered.
- For the Primary Series topologies, the transformer was assumed to be sourced by an ideal voltage source with $V_1 = 20$ V.
- For the Primary Parallel topologies, the transformer was assumed to be sourced by an ideal current source with $I_1 = 5$ A.
- In order to select an appropriate frequency for the comparison of all four topologies, (5), (6) and (7) were considered with the compensation topologies adapted such that they are resonant at all frequencies and the results for the Primary Series topologies are presented in Figures 10, 11.

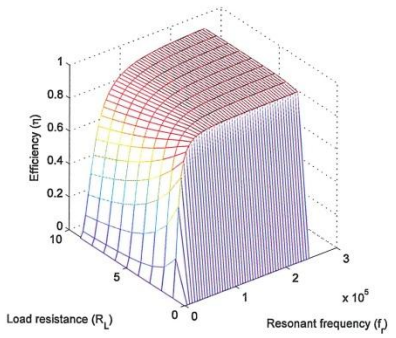

Figure 10. Three dimensional variation of efficiency of SS topology for various loads and variable resonant frequencies

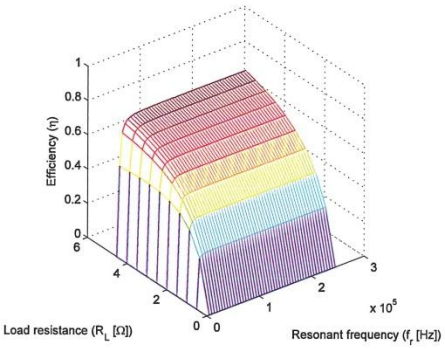

Figure 11. Three dimensional variation of efficiency of SP topology for various loads and variable resonant frequencies

The above results along with the study of efficiency for Primary Parallel topologies gave the result that a resonant frequency of 100 kHz was good enough for all the four topologies for a good variation in load resistance. This was hence fixed as the frequency for comparison. This is the second step in fixing the frequency of operation .

A. SS Topology

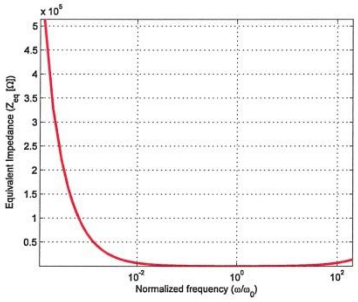

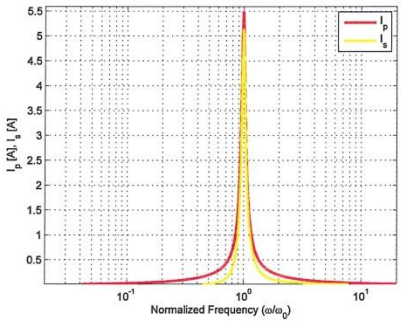

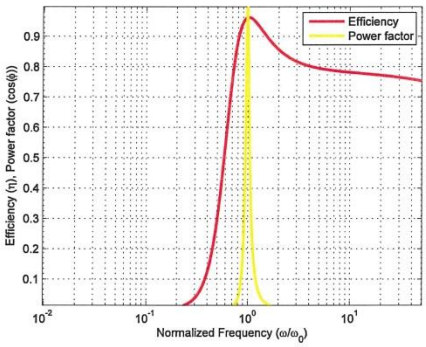

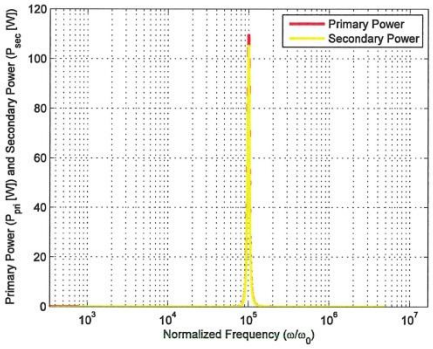

Figure 12. The variation in SS parameters with normalized frequency

Similar results were obtained for all the other topologies and are not reproduced. A more useful comparison would be between topologies of the Primary Series and that of Primary Parallel. Their results are presented in the following subsections.

1) SS and SP Comparison

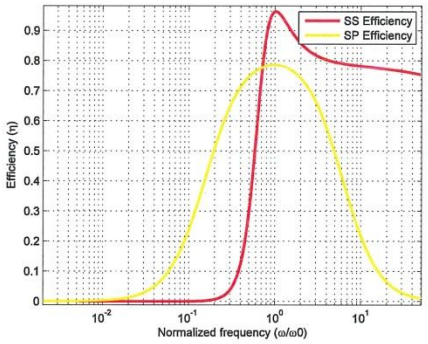

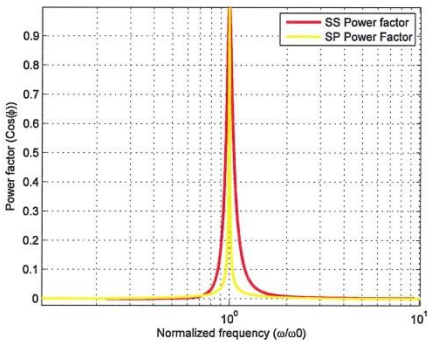

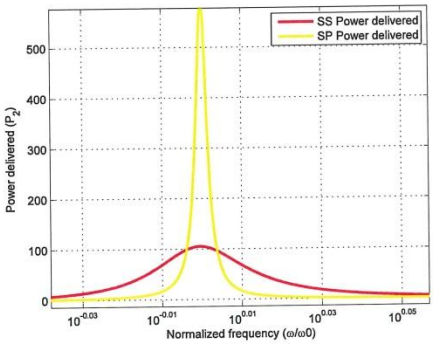

Figure 13. Parameter comparison of Primary Series topologies

A very important feature that the primary series compensation topologies possess is that the choice of their compensation capacitances is independent of the load which is a desirable property particularly when the loading profile is variable [8,9]. The choice between the two primary series compensation strategies would in turn depend on various factors such as efficiency and its tolerance to variable frequencies, the desired power levels of operation, power factor and its tolerance to variable frequencies and cost. It can be generally observed that for higher power levels, SP compensation can transfer high powers at low voltage and high current. In case of SS compensation, due to its comparatively large impedance at resonant frequency, the currents drawn at low voltages are not very high and hence high power transfer can take place only at high voltages. In case of variable frequency operations, it is desirable to go for SS topology as it has higher tolerance for power factor when frequency changes.

It can also be observed that the maximum efficiency for SS topology is much higher than that of SP topology. Hence, for fixed frequency systems, it would be better to opt for SS topology. However, frequency tolerance for efficiency is better in case of SS topology over SP topology particularly at super-resonant frequencies. For sub-resonant frequencies, the efficiencies in case of SP topology is higher than that of SS topology.

2) PS and PP Comparison

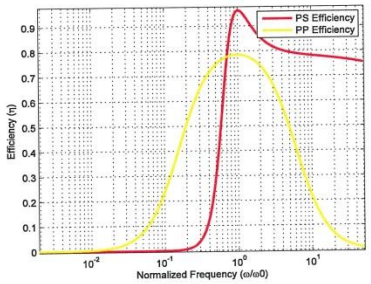

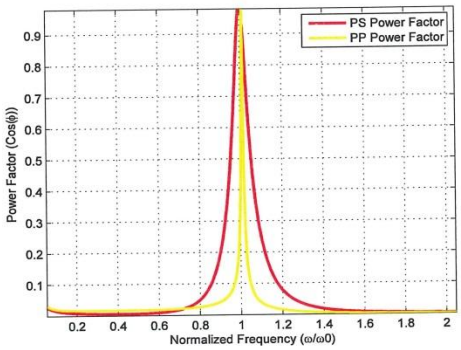

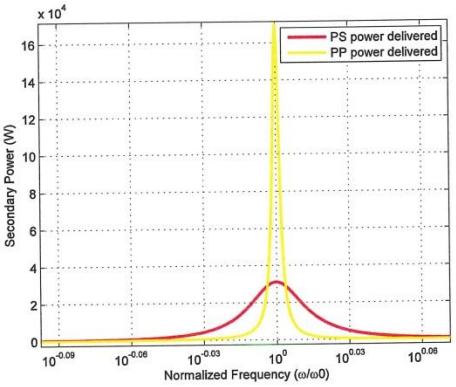

Figure 14. Parameter comparison of Primary Parallel topologies

A very unfavorable feature that the primary parallel topologies possess is the fact that the compensation capacitance varies with changing load. Hence, in applications where load changes are drastic, it would be better to prefer series primary compensation.

It can be readily observed that peak efficiency for the PS topology is higher than that of the PP topology. Also, the power factor tolerance for PS topology for super-resonant frequencies is much higher than that of PP topology. However, for sub-resonant frequencies, the efficiency of PP topology is higher than that of PS topology. Also, the frequency tolerance for PS topology is much higher than that of PP topology. In terms of the power transferred at a constant current level, PS topology can deliver much higher power at a given current level than PP topology.

VI. Results of Comparison

The results obtained are quantified and represented in Table IV and the general observations are presented in Table V.

TABLE IV. SIMULATED RESULTS OF THE VARIOUS TOPOLOGIES

Characteristic of the topology	SS Topology	SP Topology	PS Topology	PP Topology
V_1 /I_1	20V	20V	5A	5A
Circuit impedance at resonance (Ω)	3.65	0.53	1296.5	8654.4
Maximum power delivered (P_{mass},W)	105.36	596.53	31.18k	170.03k
Efficiency (η, %)	96.31	78.6	96.31	78.6

TABLE V. GENERAL OBSERVATIONS OF THE VARIOUS TOPOLOGIES

Characteristic of the topology	SS Topology	SP Topology	PS Topology	PP Topology
Dependence of the primary compensation capacitance on load	None	None	Dependent	Dependent
Circuit equivalent impedance at resonance	Minimum	Minimum	Maximum	Maximum
Type of ac source to be applied so as to transfer maximum power	Voltage source	Voltage source	Current source	Current source
Power transferred at constant source voltage (SS, SP)/ current (PS,PP)	Lower	Higher	Lower	Higher
Peak efficiency	Higher	Lower	Higher	Lower
Tolerance of efficiency to variable frequency	Lower	Higher	Lower	Higher
Tolerance of power factor to variable frequency	Higher	Lower	Higher	Lower

VII. CONCLUSION

A technique in order to estimate the rough frequency of operation of the air cored transformer is derived. This is followed by an efficiency based optimization technique to estimate the exact frequency of operation for a particular load. For the constructed air-cored transformer, a frequency of operation, f_0=100kHz (resonant frequency) is chosen based on the optimization technique as it proved rather efficient for all topologies for a loading of (R_L=0-10 Ω). A comparison between the various compensation techniques would yield that peak efficiency of the system remains high for Secondary Series topologies while the power transferred is higher for Secondary Parallel topologies.

REFERENCES

[1] Okuno, A.; Gamage, L.; Nakaoka, M.; , "Performance evaluations of high-frequency inverter-linked DC/DC converter with noncontact pickup coil," *Industrial Electronics, IEEE Transactions on* , vol.48, no.2, pp.475-477, Apr 2001

[2] Abe, H.; Sakamoto, H.; Harada, K.; , "A noncontact charger using a resonant converter with parallel capacitor of the secondary coil," *Industry Applications, IEEE Transactions on* , vol.36, no.2, pp.444-451, Mar/Apr 2000

[3] Yungtaek Jang; Jovanovic, M.M.; , "A contactless electrical energy transmission system for portable-telephone battery chargers," *Industrial Electronics, IEEE Transactions on* , vol.50, no.3, pp. 520- 527, June 2003

[4] Joung, G.B.; Cho, B.H.; , "An energy transmission system for an artificial heart using leakage inductance compensation of transcutaneous transformer," *Power Electronics Specialists Conference, 1996. PESC '96 Record., 27th Annual IEEE* , vol.1, no., pp.898-904 vol.1, 23-27 Jun 1996

[5] Heeres, B.J.; Novotny, D.W.; Divan, D.M.; Lorenz, R.D.; , "Contactless underwater power delivery," *Power Electronics Specialists Conference, PESC '94 Record., 25th Annual IEEE* , vol., no., pp.418-423 vol.1, 20-25 Jun 1994

[6] Sallan, J.; Villa, J.L.; Llombart, A.; Sanz, J.F.; , "Optimal Design of ICPT Systems Applied to Electric Vehicle Battery Charge," *Industrial Electronics, IEEE Transactions on* , vol.56, no.6, pp.2140-2149, June 2009

[7] Stielau, O.H.; Covic, G.A.; , "Design of loosely coupled inductive power transfer systems," *Power System Technology, 2000. Proceedings. PowerCon 2000. International Conference on* , vol.1, no., pp.85-90 vol.1, 2000

[8] Chwei-Sen Wang; Stielau, O.H.; Covic, G.A.; , "Design considerations for a contactless electric vehicle battery charger," *Industrial Electronics, IEEE Transactions on* , vol.52, no.5, pp. 1308- 1314, Oct. 2005

[9] Chopra, S.; Bauer, P.; , "Analysis and design considerations for a contactless power transfer system," *Telecommunications Energy Conference (INTELEC), 2011 IEEE 33rd International* , vol., no., pp.1-6, 9-13 Oct. 2011

[10] R. Balog, P. T. Krein, D. Hamill, "Coupled inductors -- a basic filter building block," in *Proc. Electrical Manufacturing and Coil Winding Ass'n.*, 2000, pp. 217-278.